GOETHE UNIVERSITÄT
FRANKFURT AM MAIN

DISSERTATION ZUR ERLANGUNG DES DOKTORGRADES DER NATURWISSENSCHAFTEN

CLIMATE MODELING OVER THE MEDITERRANEAN SEA: IMPACT OF ATMOSPHERE–OCEAN COUPLING AND ATMOSPHERIC GRID RESOLUTION ON SEA SURFACE HEAT FLUXES, MEDICANES, AND VB-CYCLONES

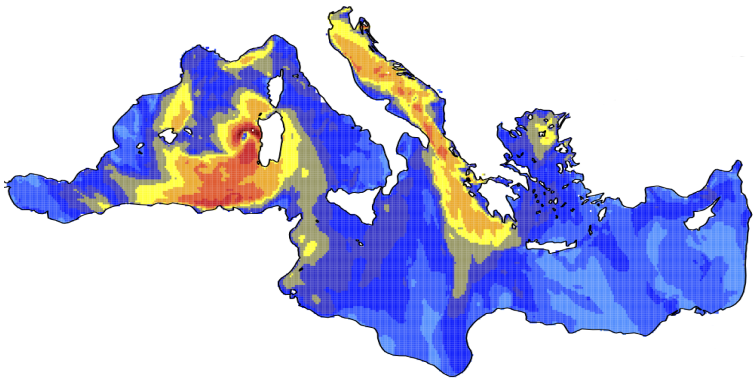

VORGELEGT BEIM FACHBEREICH GEOWISSENSCHAFTEN/GEOGRAPHIE DER JOHANN WOLFGANG GOETHE-UNIVERSITÄT IN FRANKFURT AM MAIN

von
NAVEED AKHTAR
aus Rawalpindi, Pakistan

Frankfurt (2019)
(D 30)

Vom Fachbereich 11 (Geowissenschaften/Geographie) der Johnann Wolfgang Goethe-Universität als Disseration angenommen

Dekan:
Prof. Dr. Georg Rümpker

Gutachter:
Prof. Dr. Bodo Ahrens
Dr. Habil. Stefan Hagemann

Datum der Disputation: **12.02.2019**

Abstract

Air-sea feedbacks between the Mediterranean Sea and the atmosphere on various temporal and spatial scales play a major role in the Mediterranean regional climate system and beyond. The Mediterranean Sea is a source of moisture due to excess evaporation and, on a long-term average, is associated with a warming of the lower atmosphere in contact with the sea surface due to heat loss at the air-sea interface. The complex air-sea interactions and feedbacks in the Mediterranean basin strongly modulate the sea surface fluxes and favor several cyclogenetic activities under certain meteorological conditions. Examples of such cyclonic activities are medicanes (Mediterranean hurricanes) and Vb-cyclones. Medicanes are mesoscale, marine, and warm-core Mediterranean cyclones that exhibit some similarities to tropical cyclones, while Vb-cyclones are extra-tropical cyclones, that propagate from the Western Mediterranean Sea and travel across the Eastern European Alps into the Central European region. Extremely strong winds and heavy precipitation associated with these cyclones can lead to severe destruction and flooding. Changes in the intensity and frequency of these cyclones are also projected under changing future climate conditions, where the Mediterranean region has been identified as a hotspot in terms of rising temperatures.

The development of high-resolution regional climate models (RCMs) has progressed our understanding of the processes characterizing the Mediterranean climate. However, large uncertainties still exist regarding the estimates of air-sea fluxes, which, in turn, affect the simulation of the Mediterranean climate. Several factors can be attributed to such discrepancies, such as data quality, temporal and spatial resolution, and the misrepresentation of physical processes. To overcome some of these inconsistencies and deficiencies of the existing climate simulations, a new high-resolution atmosphere-ocean regional coupled model (AORCM) has been developed to simulate the air-sea feedback mechanisms. This coupled model incorporates the coupling of RCM COSMO-CLM (CCLM) and the regional ocean model NEMO-MED12 for the Mediterranean Sea (MED) as well as NEMO-NORDIC for the North- and Baltic Sea (NORDIC). Several experiments were performed using both the coupled and uncoupled models to investigate the impact of air-sea interactions and feedbacks on sea surface heat fluxes, wind speed, and on the formation of Mediterranean cyclones (i.e., medicanes and Vb-cyclones). These experiments were performed using different horizontal atmospheric grid resolutions to analyze the effect of resolution on sea surface heat fluxes, wind speed, and the development of medicanes.

The results of the present study indicate that a finer atmospheric grid resolution ($\sim$9 vs. $\sim$50 km) improved the wind speed simulations (particularly near coastal areas) and subsequently improved the simulations of the turbulent heat fluxes. Both parameters were better simulated in the coupled simulations than in the uncoupled simulations, but coupling introduced a warm SST bias in winter. Radiation fluxes were slightly better represented in coarse-grid simulations

than in fine-grid simulations. However, the higher-resolution coupled model could reproduce the observed net outgoing total surface heat flux over the Mediterranean Sea. In addition to that sub-diurnal SST variations have a strong effect on sub-daily heat fluxes and wind speed but minor effects at longer timescales.

Regarding the impact of atmospheric grid resolution ($\sim$50, $\sim$25, and $\sim$9 km) and ocean coupling on medicanes, it was detected that the coupled model with a finer atmospheric grid ($\sim$9 km) was able to not only reproduce most medicane events, but also improved the track length, warm core, and wind speed compared to the uncoupled model. The coupled model with the coarse-grid ($\sim$50 and $\sim$25 km) did not show any improvement in simulating medicanes compared to the uncoupled model. The spectral nudging technique, applied on the wind components above 850 hPa in the interior domain to keep large-scale circulation close to the driving data (i.e., ERA-Interim reanalysis), improved the accuracy of the times and locations of generated medicanes, but no improvement was found in the track length and intensity.

Concerning the role of the Mediterranean Sea coupling on Vb-cyclones, the investigation showed that atmosphere-ocean coupling had an overall positive impact, although with a strong case-by-case variation, on the trajectories and intensity of Vb-cyclones as a result of the variation in moisture source for each event. In general, all model configurations could replicate Vb-cyclones, their trajectories, and associated precipitation fields. The average structure of the precipitation field was best represented in the coupled simulations. Coupling of the North- and Baltic Seas also showed an improvement in some of the simulated Vb-cyclones.

The atmosphere-ocean coupling showed an overall positive impact on the simulation of sea surface heat fluxes and Mediterranean cyclones (medicanes and Vb-cyclones). Moreover, the representation of sea surface heat fluxes, wind speed, and medicane features was more realistic when using a finer atmospheric grid resolution (less than 10 km). The present study suggests that the combination of a finer atmospheric grid resolution together with atmosphere-ocean coupling is advantageous in simulating the Mediterranean climate system.

Kurzfassung

Rückkopplungen zwischen dem Mittelmeer und der Atmosphäre spielen eine wichtige Rolle auf verschiedenen zeitlichen und räumlichen Skalen im regionalen Klimasystem des Mittelmeerraums und darüber hinaus. Das Mittelmeer ist eine Feuchtequelle aufgrund von exzessiver Verdunstung. Im langfristigen Durchschnitt bewirkt das Mittelmeer eine Erwärmung der unteren Atmosphäre infolge des Wärmeverlustes an der Grenzfläche zwischen Luft und Meer. Die komplexen Luft-Wasser-Wechselwirkungen und Rückkopplungen im Mittelmeerbecken regulieren stark die Flüsse an der Meeresoberfläche und begünstigen mehrere zyklogenetische Aktivitäten unter bestimmten meteorologischen Bedingungen. Beispiele sind die Medicanes (Mediterrane Hurrikane) und Vb-Zyklonen. Medicanes sind mesoskalige, marine Mittelmeer-Zyklonen mit warmen Kern, die einige Ähnlichkeiten mit tropischen Zyklonen aufweisen. Vb-Zyklonen sind extratropisch und wandern vom westlichen Mittelmeer aus über die osteuropäischen Alpen in die mitteleuropäische Region. Extrem starke Winde und Starkniederschläge stehen im Zusammenhang mit diesen Zyklonen und führen zu schweren schäden und Überschwemmungen. Änderungen in der Intensität und Häufigkeit von Wirbelstürmen werden auch im zukünftigen Klima projiziert, indem insbesondere die Mittelmeerregion nach jetzigem Erkenntnisstand ein Hotspot in Bezug auf steigende Temperaturen sein wird.

Die Entwicklung von hochauflösenden regionalen Klimamodellen (RCMs) hat unser Verständnis der Prozesse, die das Mittelmeerklima charakterisieren, vorangetrieben. Es bestehen jedoch nach wie vor große Unsicherheiten hinsichtlich der Flüsse zwischen Atmosphäre und Meer, die sich wiederum auf die Simulation des mediterranen Klimas auswirken. Die Unsicherheiten können verschiedenen Faktoren zugeschrieben werden, wie z. B. Datenqualität, zeitliche und räumliche Auflösung und fehlerhafte Darstellung physikalischer Prozesse. Um einige der Inkonsistenzen zu überwinden, wurde ein neues hochauflösendes, regional gekoppeltes Atmosphären-Ozean-Modell (AORCM) entwickelt, um die Rückkopplungs-Mechanismen zwischen Atmosphäre und Ozean zu simulieren. Dieses AORCM beinhaltet die Kopplung von COSMO-CLM (CCLM) und dem regionalen Ozeanmodell NEMO-MED12 für das Mittelmeer (MED) sowie NEMO-NORDIC für die Nord- und Ostsee (NORDIC). Mehrere Simulationen wurden durchgeführt, wobei sowohl die gekoppelten als auch nicht gekoppelte Modelle verwendet wurden, um den Einfluss von Atmosphäre-Wasser-Wechselwirkungen zu untersuchen und ebenso Rückkopplungen auf die Wärmeflüsse an der Meeresoberfläche, die Windgeschwindigkeit und auf die Bildung von Mittelmeerzyklonen (Medicanes und Vb-Zyklone). Die Modellsimulationen wurden unter Verwendung verschiedener horizontaler atmosphärischer Gitterauflösungen durchgeführt, um zusätzlich den Effekt der Auflösung auf die Wärmeflüsse der Meeresoberfläche, die Windgeschwindigkeit und die Entwicklung von Medicanes zu analysieren.

Die Ergebnisse der vorliegenden Studie zeigen, dass eine feinere atmosphärische Gitterau-

flösung (∼9 km vs. ∼50 km) die Simulation der Windgeschwindigkeit (insbesondere in der Nähe von Küstengebieten) verbessert sowie die Simulationen der turbulenten Wärmeströme. Auch wurden beide Parameter in den gekoppelten Simulationen besser simuliert als in den ungekoppelten Simulationen, jedoch führte die Kopplung im Winter zu einer zu warmen Meersoberflächen-Temperatur (SST). Die Strahlungsflüsse wurden in Grobgittersimulationen etwas besser dargestellt als in Feingittersimulationen. Jedoch konnte das hochaufgelöste, gekoppelte Modell den beobachteten bodennahen Nettowärmefluss über dem Mittelmeer wiedergeben. Darüber hinaus zeigen meine Ergebnisse, dass tageszeitliche SST-Variationen einen starken Einfluss auf die tageszeitlichen Wärmeflüsse und die Windgeschwindigkeit haben, wobei die Auswirkungen auf längeren Zeitskalen gering sind.

Bezüglich des Einflusses der Gitterauflösung (∼50, ∼25 und ∼9 km) und der Atmosphären-Ozean-Kopplung wurde festgestellt, dass das gekoppelte Modell mit einem sehr feinen atmosphärischen Gitter (∼9 km) die meisten Medicane reproduzieren konnte. Zusätzlich wurden die länge der Zugbahn, der warme Kern und die Windgeschwindigkeit besser erfasst als im nichtgekoppelten Modell. Das gekoppelte Modell mit einem groben Gitter (∼50 und ∼25 km) zeigte jedoch im Vergleich zum nichtgekoppelten Modell keine Verbesserung der Simulation von Medicanes. Die spektrale Nudging Technik, die auf die Windkomponenten oberhalb von 850 hPa innerhalb des Modellgebietes angewendet wurde und die die großräumige Zirkulation an die Antriebsdaten anpassen soll (d.h. ERA-Interim Reanalyse), verbesserte das Timing und die Positionen der Medicanes, aber die länge der Zugbahn und die Intensität wurden nicht verbessert.

Bezüglich der Atmosphäre-Ozean-Kopplung des Mittelmeeres zeigte sich bei den Untersuchungen der Vb-Zyklonen, dass die Kopplung zwischen Atmosphäre und Ozean insgesamt positive Auswirkungen hat, obwohl eine große Abhängigkeit vom Einzelfall besteht: Positive Auswirkungen wurden bei den Zugbahnen und der Intensität der Vb-Zyklonen festgestellt, was ein Resultat der Variabilität der Feuchtequellen ist. Im Allgemeinen konnten alle Modellkonfigurationen Vb-Zyklonen, ihre Zugbahnen und die zugehörigen Niederschlagsfelder reproduzieren. Die räumliche Struktur des Niederschlagsfeldes wurde am besten in den gekoppelten Simulationen dargestellt. Die Kopplung der Nord- und Ostsee zeigte ebenfalls eine Verbesserung bei der Simulation einiger Vb-Zyklonen.

Die Atmosphäre-Ozean-Kopplung zeigte insgesamt einen positiven Einfluss auf die Simulation von bodennahen Wärmeflüssen und Mittelmeer Tiefdruckgebieten. Darüber hinaus können die Modelle die Ozean Wärmeflüsse, die Windgeschwindigkeiten und die Charakteristika von Medicanes besser darstellen, wenn eine hohe Gitterauflösung (weniger als 10 km) verwendet wird. Dahingehend kann für die hier vorliegende Studie geschlussfolgert werden, dass eine Kombination von hoher räumlicher Auflösung und die Verwendung einer Kopplung zwischen Atmosphäre und Ozean vorteilhaft ist in Bezug auf die Simulation des Klimasystems im Mittelmeer.

Acknowledgements

All praise to Almighty ALLAH, the most benevolent and merciful, the creator of the universe, who enable me to complete this research work successfully. I offer Salaam to the Holy Prophet Muhammad (may peace be upon him) who is a blessing for the world.

First, I want to express my deepest gratitude to my respectable teacher and supervisor Prof. Dr. Bodo Ahrens for his invaluable guidance and support. He has stimulated my mind to give me the insight of research. His sympathetic attitude and encouraging discussions enabled me to broaden and improve my capabilities regarding atmospheric science and meteorology. My immense gratitude goes to Dr. Jennifer Brauch (DWD) who helped me a lot throughout my research work, especially in ocean modeling. I must also sincerely thank all the teachers of Institut für Atmosphäre und Umwelt (IAU), especially Dr. Ulrich Achatz and dean of the institute (Prof. Dr. Georg Rümpker) for providing a pleasant and motivating working environment. I am greatly thankful to Dr. Stefan Hagemann (HZG) for reviewing this thesis.

I am very thankful to JW Goethe University and IAU for providing a wonderful and studious environment for research and also to Centre for Scientific Computing (CSC) Frankfurt and Deutsches Klimarechenzentrum (DKRZ) for providing excellent computational facilities. I acknowledge support from the German Federal Ministry of Education and Research (BMBF) under grant MiKliP II (FKZ 01LP1518C), Senckenberg Biodiversity and Climate Research Centre (BiK–F), Frankfurt am Main and JW Goethe University Frankfurt am Main for financial support. I would also like to acknowledge Cindy Lebeaupin Brossier, Jonathan Beuvier, Thomas Arzouse, Samuel Somot and Philippe Drobinski for their help regarding NEMO-MED12 and French GIS and GMMC which have supported NEMO-MED12 model. This work is part of the Med-CORDEX initiative (www.medcordex.eu) supported by the HyMeX (www.hymex.org).

My cordial thanks to Shakeel Asharaf, and Erwan Brisson, Praveen Kumar, Amelie Krug and all others who helped me during my research work. A special thanks to Burkhart Rockel, Beate Geyer, Ronny Petrik and Ha Thi-Minh Ho-Hagemann for helping me with the thesis.

Finally, my deepest sense of acknowledgments goes to my, loving Father Muhammad Younas (late) and mother Zeenat Begum who always pray for my success in every aspect of life. My heartfelt gratitude goes to my elder brothers Tanveer Akhtar, Shahzad Akhtar and younger brother Nadeem Akhtar who always supported me. I also wish to record my deepest obligations to my sisters for their everlasting love, care, and moral support, especially to Rozina Kleem and brother in law Kleem Yousaf. Last but not least I want to thank my loving and caring wife Kiran Rasheed, who is always cooperative and encouraging in every aspect of life.

DEDICATED TO MY MOTHER

Contents

List of Figures

List of Tables

List of Contributing Peer-Reviewed Publications

1. Akhtar N, Brauch J, Dobler A, Bérenger K, Ahrens B (2014) Medicanes in an ocean-atmosphere coupled regional climate model. Nat Hazards Earth Syst Sci 14:2189–2201. doi:10.5194/nhess-14-2189-2014

2. Akthar N, Brauch J, Ahrens B (2018) Climate modeling over the Mediterranean Sea: Impact of resolution and ocean coupling. Clim Dyn 51:933–948. doi:10.1007/s00382-017-3570-8

3. Akthar N, Krug A, Brauch J, Arsouze T, Dieterich C, Ahrens B (submitted) European Marginal Seas in a regional atmosphere-ocean coupled model and their impact on Vb-cyclones and associated precipitation. Submitted to Clim Dyn

List of Abbreviations

AOGCM	Atmosphere-Ocean General Circulation Model
AORCM	Atmosphere-ocean Regional Coupled Model
BiK–F	Biodiversität und Klima Forschungszentrum
BMBF	Bundesministerium für Bildung und Forschung
COSMO	Consortium for Small-scale Modeling
COSMO-CLM	COSMO Climate Limited area Model
CCLM	COSMO-CLM
CORDEX	Coordinated Regional climate Downscaling Experiment
CSC	Center for Scientific Computing
DKRZ	Deutsches Klimarechenzentrum
DWD	Deutscher Wetterdienst
DFG	Deutsche Forschungsgemeinschaft
ECMWF	European Centre for Medium-Range Weather Forecasts
ECAD	European Climate Assessment and Dataset
ERA-Interim	European Reanalysis Interim
EOBS	ENSEMBLES Observations
ERA40	European Reanalysis 40
EU-FP	European Framewark Program
EURO-CORDEX	European CORDEX
E-HYPE	High-resolution Pan-European water model
GIS	Groupement d'Intéerêt Scientique
GMMC	Groupe de Mission Mercator Coriolis
HyMeX	Hydrological Cycle in the Mediterranean Experiment
HZG	Helmholtz-Zentrum Geesthacht Zentrum für Material- und Küstenforschung
IAU	Institut für Atmosphäre und Umwelt
LIM	Louvain-la-Neuve Ice Model
LH	Latent Heat flux
LOEWE-CSC	Landes-Offensive zur Entwicklung Scientific-economic excellence-CSC

LW	Long-wave radiation
MACC	Monitoring Atmospheric Composition and Climate
MD	Mean Difference
MED	NEMO-MED12 coupled with CCLM
MED+NORDIC	NEMO-MED12 and NEMO-NORDIC coupled with CCLM
Med-CORDEX	Mediterranean CORDEX
MERRA	Modern-Era Retrospective Analysis for Research and Applications
MiKliP	Mittelfristigen Klimaprognosen
NASA	National Aeronautics and Space Administration
NCEP	National Centers for Environmental Prediction
NCAR	National Center for Atmospheric Research
NEMO	Nucleus for European Modelling of the Ocean
NEMO-MED12	NEMO regional configuration for the Mediterranean Sea
NEMOMED12	NEMO regional configuration for the Mediterranean Sea
NEMO-NORDIC	NEMO regional configuration for the North- and Baltic Seas
NH	Net sea surface Heat flux
NOAA	National Oceanic and Atmospheric Administration
NORDIC	NEMO-NORDIC coupled with CCLM
OPA	Océan PArallélisé
ORAS	ECMWF's Ocean Reanalysis
OISST	Optimum Interpolation Sea Surface Temperature
OAFlux	Objectively Analyzed Air-sea Fluxes
RCM	Regional Climate Model
RMSE	Root Mean Square Error
SST	Sea Surface Temperature
SH	Sensible Heat flux
SW	Short-wave radiation
TOP	Tracer in the Ocean Paradigm
UOI	Unified OASIS3-MCT Interface
UTC	Universal Time Coordinated
WHOI	Woods Hole Oceanographic Institute
WRF	Weather Research and Forecasting

CHAPTER 1

Introduction

The Mediterranean climate is controlled by a variety of complex processes, particularly the interactions between mid-latitude and tropical processes, due to its geographical location, as well as the interactions between local processes as a result of the complex morphology of the Mediterranean region. These interactions of complex processes at a wide range of spatial and temporal scales in the Mediterranean region result in a large spatial variability and diversity of climate types (Lionello et al. 2006a). Among others, the tundra climate in the Alpine regions, the continental climate between Turkey and Greece, and the arid climate in northern Africa, are evidence of the large climatic diversity in the Mediterranean region (Peel et al. 2007; McKnight and Hess 2000). Moreover, the interactions between both the large-scale and the local processes often lead to the development of extreme weather conditions in the Mediterranean region, such as medicanes (Mediterranean hurricanes) and Vb-cyclones (pronounced five-b). These cyclones are major natural hazards for both coastal regions and several parts of Europe.

The Mediterranean region has been identified as a climate change "hotspot" due to substantial changes in the mean and interannual variability of temperature and precipitation (Giorgi 2006). Various studies show a decrease in the frequency and an increase in the intensity of medicanes (see for example, Cavicchia et al. 2014b; Walsh et al. 1996) and Vb-cyclones (Nissen et al. 2014; Fischer et al. 2014) under future climate conditions. These type of climate conditions may have large negative impacts on both the regional environment and the social-economical activities in the area.

Several studies have been carried out to improve the understanding of the processes characterizing the Mediterranean climate using surface measurements, satellite data, and model simulations. These studies increase the knowledge understanding of the Mediterranean climate, however, there are still issues that are open to debate; for example, uncertainties in various components of the sea surface heat fluxes as well as the misrepresentation or lack of information related to the air-sea interactions and feedbacks in simulating the Mediterranean cyclones (medicanes and Vb-cyclones).

This chapter describes the main factors as well as the remote and local processes that drive the Mediterranean climate. It also highlights the difficulties and deficiencies in traditional modeling systems. Additionally, several questions are raised and addressed in this study to advance the understanding of the Mediterranean climate.

1.1 The Mediterranean climate

The Mediterranean region features a semi-enclosed sea surrounded by high mountain ranges as well as extremely urbanized areas (see Fig. 1.1) and includes three continents (Asia, Europe, and Africa). The Mediterranean basin covers a total area of 2.5×10^6 km^2 that extends over 3×10^3 km in longitude and 15×10^2 km in latitude, shaping a 46×10^3 km long coastline. The Mediterranean Sea is composed of two smaller basins of almost similar size, namely the Eastern and the Western Mediterranean Sea, separated by the narrow and shallow Strait of Sicily. The Mediterranean Sea is connected to the Atlantic Ocean through the Strait of Gibraltar, and to the Black Sea through the Bosporus channel. The sea acts as a thermodynamic machine that exchanges heat and water with the Atlantic Ocean through the Strait of Gibraltar as well as with the atmosphere through its surface. It has an overall freshwater deficit due to excess evaporation

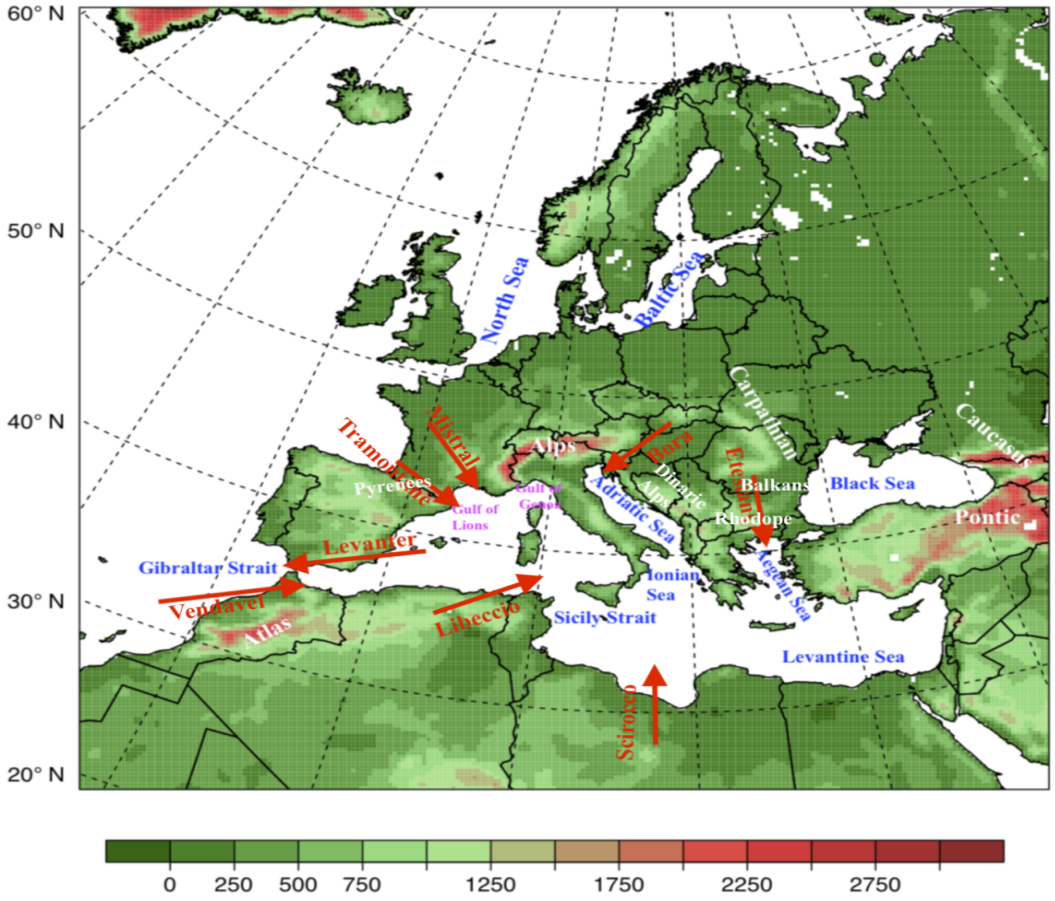

Figure 1.1: Model integration area, brown, white, blue and pink colors indicates the wind system, mountain ranges, seas/straits and gulfs respectively.

thereof in comparison to freshwater input (precipitation, river run-off, and the Black Sea input). The total heat budget of the Mediterranean Sea is negative, meaning that it loses more energy than it gains. However, the exchange between the Mediterranean Sea and the Atlantic Ocean at the Strait of Gibraltar compensates for these losses of heat and freshwater. This exchange

consists of a two-layered flow, namely, a relatively warm and fresh (15.4 °C; 36.2 psu) upper water inflow and a cooler and saltier (13 °C; 38.4 psu) deeper water outflow (Bryden 1994; Tsimplis et al. 2000). The Mediterranean water influences the global climate through saline and warm water outflows into the Atlantic Ocean, which enhances and stabilizes the meridional overturning circulation (Artale et al. 2006).

The morphology and geographical location of the Mediterranean region results in a strong weather regionality and a diverse climate. This region holds a transitional position not only from a geographical point of view but also from a climatological point of view. The climate and weather of the region are mainly controlled by two large-scale atmospheric circulation phenomena. To the north, a large part of the atmospheric variability is controlled by large-scale air masses driven by the Atlantic Jet Stream, and the subsidence of the Hadley Cell through the Azores High influences atmospheric variability in the south. In addition, the El Niño South Oscillations (ENSO) influences the atmospheric variability in the east (Rodwell and Hoskins 1996; Price et al. 1998; Xoplaki et al. 2003; Trigo et al. 2004; Alpert et al. 2006). The Atlantic Jet Stream transports water vapor in and out of the Mediterranean region while the subsidence of the Hadley Cell circulation reduces the air moisture (Gimeno et al. 2010; Schicker et al. 2010). Therefore, a relatively small change in the general circulation of mid-latitude (e.g., a shift in storm track location) or sub-tropical (e.g., a shift in high-pressure) systems can lead to a substantial change in the Mediterranean climate. Thus, Mediterranean climate variations are a direct consequence of the interannual variability of these large-scale circulations (Mariotti et al. 2002; Josey et al. 2011).

The climate of the Mediterranean region is known for its large contrast in seasonal temperature variation, strong winds, heavy precipitation, and cyclones. It has hot and dry summers and mild, wet winters. Köppen and Geiger (1936) classified the Mediterranean climate as a dry summer subtropical climate, where the winter rainfall is three times more than the summer rainfall. Importantly, in winter, precipitation is influenced by a high-Icelandic low regime called the North Atlantic Oscillations (NAO) over the western areas of the Mediterranean (e.g., Hurrell 1995; Sumner et al. 2001; Reale et al. 2001; Rodriguez-Fonseca and Castro 2002; Fernández et al. 2003). The East Atlantic can also affect the winter climate as well as precipitation variability over the northern and eastern areas of the Mediterranean region. Additionally, ENSO can significantly influence the winter precipitation variability over the eastern Mediterranean areas (Alpert et al. 2006).

The summer Mediterranean climate is mainly dominated by descending motions and high-pressure systems, leading to hot and dry conditions especially in the Southern Mediterranean region. It has been found that the Mediterranean summer climate variability is linked to the South Asian and African monsoons (Alpert et al. 2006) and with a strong geopotential blocking over Central Europe (Xoplaki et al. 2004; Trigo et al. 2006). Additionally, the seasonal distribution of heavy rain events (maximum in late summer and autumn) in the Western Mediterranean region suggests an active role of the Mediterranean Sea due to high evaporation during that time of the year.

In addition to the large-scale processes and teleconnections, local topographical features, such as high mountain ranges (the Pyrenees, Alps, Dinaric Alps, Balkan and Rhodope in the north, and Atlas mountains in the south), large islands (Balearic, Sicily, Sardinia, Corsica, Crete, and Cyprus), peninsulas (Italian and Hellenic), and complex coastlines in the presence of a large body of water (i.e., the Mediterranean Sea), strongly control the regional climate and weather regimes (Fig. 1.1; Giorgi 2006; Li 2006). Medium to high mountain ranges steer the air masses by deviating or channeling the wind flow through sea straits and valleys. Although the seasonality of the pressure system influences the inflow and outflow of wind currents, orography mainly drives the predominant wind currents. More specifically, an inflow stream occurs between the Alps and the Pyrenees mountain range channel and outflows take place at the Mesopotamia region, the plain between the highlands of Arabia and Iran, Dardanelles, over the Red Sea, and over the straits of Gibraltar (Schicker et al. 2010). Such morphological complexities lead to fine-scale spatial and temporal variability (Drobinski et al. 2014), which can develop strong weather phenomena (Tous and Romero 2013). Examples of such phenomena are intense wind systems such as the Vendaval and Levante in the Alboran Sea; the Mistral and Tramontane in the Gulf of Lions and the Ligurian Sea; the Bora in the Adriatic Sea, and the Libeccio in the Central Mediterranean Sea (Fig. 1.1). These intense offshore wind systems produce a strong moisture and heat exchange, representing a well-known effect of atmospheric forcing on oceanic circulation (Fernández et al. 2003).

The strong air-sea interactions associated with the Mediterranean also play an important role in the formation of intermediate and deep-water masses in the Southern Adriatic, Northeast Levantine basin, Aegean Sea, and in the Gulf of Lions (Roether et al. 1995; Ruti et al. 2016). The cold and intense winds largely increase the evaporation over the Mediterranean Sea, which then modifies the thermohaline characteristics by increasing the density of seawater in the surface layers (Marshall and Schott 1999; Lebeaupin and Drobinski 2009). In addition, the Mediterranean evaporation influences the land rainfall, which generally depends on the location of the area, season, as well as the atmospheric circulation and condition (Schicker et al. 2010). Regionally, the Mediterranean evaporation directly influences Europe, the Middle East, and northern Africa. Globally, it influences the precipitation in the whole Northern Hemisphere and has an effect on the global circulation (Li 2006; Gimeno et al. 2010). In addition to local wind systems, interactions between the complex coastline and sea surface temperature (SST) also create local weather regimes (Millán et al. 2005). The formation of intermediate and deep-water masses in the northwestern Mediterranean Sea is of fundamental importance for regional and global meridional overturning circulations (Calmanti et al. 2006; Josey 2003). Anomalies in net sea surface heat (NH) fluxes play a significant role in shaping the local climate (Roether et al. 1995; Theocharis et al. 1999).

1.2 Sea surface heat fluxes

Sea water gains or loses energy through radiative and turbulent fluxes at the air-sea interface. The temperature gradient between the air and the sea surface largely controls the NH. The energy gained by the sea through the atmosphere is then distributed to the deeper layers through turbulent diffusion and mixing. The energy is transferred from the sea to the air when the air

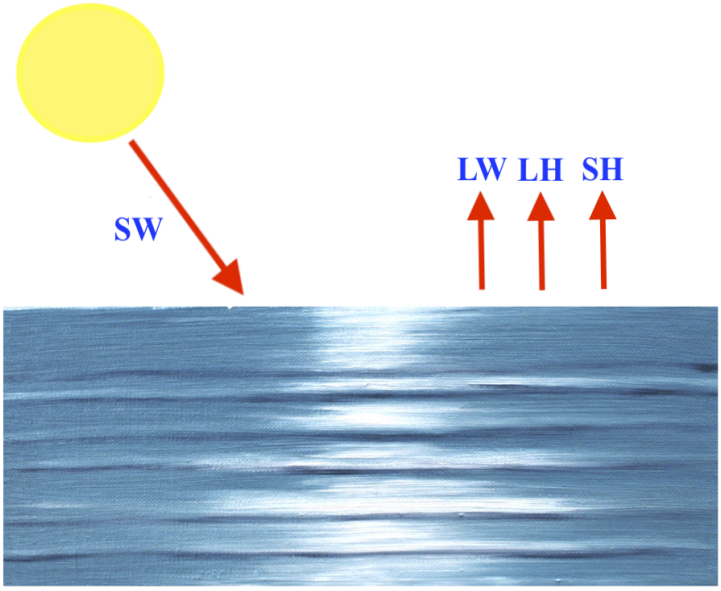

Figure 1.2: Different components of NH and their directions

temperature becomes colder than the SST. The sea water with greater thermal inertia (the heat capacity of sea water is approximately four times larger than that of the air) acts as a source or sink of heat that modifies the thermal characteristics of the atmosphere. The NH flux comprises of radiative (net short- and long-wave radiation) and turbulent (surface latent and sensible heat) fluxes. It is defined as follows:

$$NH = SW - LW - LH - SH, \tag{1.1}$$

where SW (positive downward) and LW (positive upward) represent net short- and long-wave radiation, respectively, and LH (positive upward) and SH (positive upward) are net surface latent and sensible heat flux, respectively (Fig. 1.2).

Incoming short-wave radiation is primarily determined by cloudiness, latitude, season, and time of day. More than half of the solar energy that reaches the earth is absorbed by the oceans and land, where it is temporarily stored near the surface and only about 5% of the available solar energy is absorbed by the atmosphere. The net short-wave radiation can be calculated as

$$SW = (1 - A)\, SW_{down}, \tag{1.2}$$

where A(0.065) is ocean albedo and SW_{down} is downward short-wave radiation. Most of the energy absorbed by the oceans and land is released through long-wave radiation and turbulent

fluxes. The net long-wave radiation can be calculated as

$$LW = \varepsilon_s \, (LW_{down} - \sigma T^4), \tag{1.3}$$

where $\varepsilon_s(0.97)$ is the surface emissivity, LW_{down} is downward long-wave radiation, $\sigma(5.67\times10^{-8}\,W^{-2}\,K^{-4})$ is the Stefan-Boltzmann constant, and T(K) is the surface temperature.

Turbulent fluxes can be calculated using bulk formulae, as they cannot be measured directly from observations. The LH can be calculated from relative humidity, water temperature, and wind speed using the bulk formula

$$LH = L_v \rho_a C_L U_{10} \, (Q_s - Q_a), \tag{1.4}$$

and the SH is calculated from the air-sea temperature differences as well as wind speed measurements using the bulk formula as

$$SH = L_v \rho_a C_S U_{10} \, (SST - T_a), \tag{1.5}$$

where $\rho_a(1.22\,kgm^{-3})$ is the density of the air, U_{10} is 10-meter wind speed, $C_p(1000.5\,JKg^{-1}\,K^{-1})$ is the air specific heat, T_a is the air temperature, $L_v(2.5\times10^6\,Jkg^{-1})$ is the latent heat of evaporation, and Q_s and Q_a are sea and air specific humidity, respectively. The transfer coefficients C_S and C_L mainly depend on sea surface roughness and the air-sea temperature difference.

The NH transport through the Gibraltar Strait has been estimated to be around $+5\,Wm^{-2}$ based on mooring measurements (McDonald et al. 1994; Sanchez–Gomez et al. 2011). The positive sign indicates the heat gain by the Mediterranean Sea, which should be compensated by an equivalent loss of heat through the Mediterranean Sea surface. Thus, the Mediterranean net surface heat flux is around $-5\,Wm^{-2}$. A better representation of sea surface fluxes can improve the representation of Mediterranean cyclones.

1.3 Mediterranean cyclones

In the presence of high mountain ranges, which can strongly modify the traveling synoptic and mesoscale systems, the evaporative Mediterranean Sea acts as an important source of moisture and energy for cyclogenesis (Lionello et al. 2006b). Such conditions make the Mediterranean region one of the main cyclogenetic regions in the world and, on average, a few thousand cyclones are reported per year (Pettersen 1956; Hoskins and Hodges 2002; Wernli and Schwierz 2006). Approximately 90% of the intense precipitation events in the Western Mediterranean are strongly linked to cyclones (Jansá et al. 2001). Several coastal locations of the Central (e.g., the Gulf of Genoa and the Adriatic Sea) and the Eastern Mediterranean (e.g., Cyprus) are the centers of topographically induced intense cyclogenesis (e.g., Alpert et al. 1995).

The complex air-sea interactions and orographic features play a prominent role in driving the Mediterranean climate on a range of spatial and temporal scales by modifying sea surface

heat fluxes. Mediterranean cyclones are extreme cases of air-sea interactions and a better representation of air-sea interactions and feedbacks can improve the estimates of sea surface heat fluxes, further improving the representation and predictability of extreme events. Although Mediterranean cyclones are known to occur from time to time, their frequency and intensity have increased during the last decades. The spatial and temporal distribution of these extreme events is irregular. Typical examples of such meteorological extremes in the region are medicanes (Mediterranean hurricane) and Vb-cyclones.

1.3.1 Medicanes

Medicanes are tropical-like hurricanes, that mainly develop at the leeward side of the Alps and the Atlas Mountains, with the primary maxima situated in the Genoa region and the secondary maxima in the Cyprus and Aegean regions. Other relative maxima are found in the Adriatic Sea, Algerian Sea, Balearic Sea, and in Gulf of Lions (Alpert et al. 1990; Jansá 1986; Romero 2008). These cyclones strongly affect the variability of the Mediterranean climate (Trigo et al. 2000; Gaertner et al. 2007; Zappa et al. 2015). Medicanes develop from a baroclinic cut-off low, evolving into a warm-core through a tropical transition (Emanuel 2005). They mainly develop during winter and autumn when the high Mediterranean SST and relatively cold air interactions during these seasons destabilize air masses and favor the release of latent heat during the development of cyclones. Under certain conditions, SSTs higher than 15 °C can favor

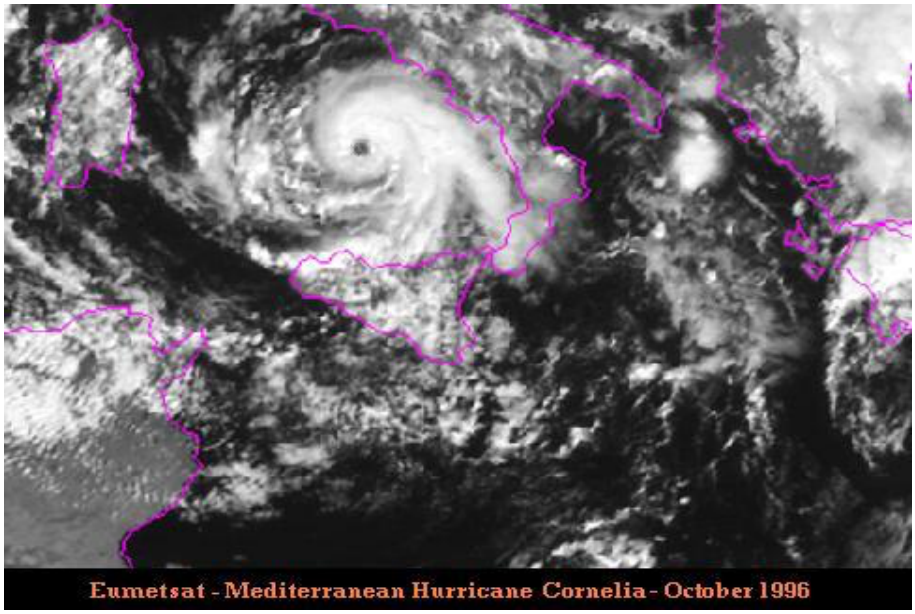

Figure 1.3: Satellite image of the October 1996 medicane event (source: Wikipedia)

the development of medicanes (Tous and Romero 2013). However, only a few medicanes are observed during summer (Gaertner et al. 2018). Similar to tropical cyclones, air-sea interactions and feedbacks play a fundamental role in the development and intensification of medicanes (Emanuel 1986; Emanuel and Rotunno 1987). Mediterranean cyclones are classified, depending

on the wind intensity, as Mediterranean tropical depressions (below 63 kmh^{-1}), Mediterranean tropical storms (64 to 111 kmh^{-1}), and medicanes (above 112 kmh^{-1}; www.srf.ch/meteo/meteo-news/medicane-der-wirbelsturm-ueber-dem-mittelmeer-2). The diameter of a medicane is typically less than 300 km and in general, the size and the intensity of medicanes is weaker than that of tropical hurricanes (Trigo et al. 2002; Moscatello et al. 2008; Flaounas et al. 2016); however, a few medicanes have reached the tropical hurricane classification of surface wind strength (118 kmh^{-1}; Fita et al. 2007; Moscatello et al. 2008). These warm-core surface flux driven cyclones can be potentially threatening for islands and coastal areas (Romero 2008). Modeling and observational studies agree on the warm-core and small-scale features of medicanes. Similar to hurricanes, clouds and rain bands swirl spirally around the eye in a counterclockwise direction (Fig. 1.3). See Chapter 4 for more details.

1.3.2 Vb-cylones

Another type of cyclone that develops over the Western Mediterranean Sea, typically over the Gulf of Genoa and travels across the Eastern European Alps toward the Baltic region, is the so-called Vb-cyclone (Van Bebber 1891; Messmer et al. 2015). In a typical Vb-type situation, an Icelandic low-pressure system moving eastwards encounters arctic air masses that divert it southward to the Mediterranean Sea, where it gains energy through the warm and moist air. It then moves toward the northeast and the air is lifted by the mountain ranges of Central Europe

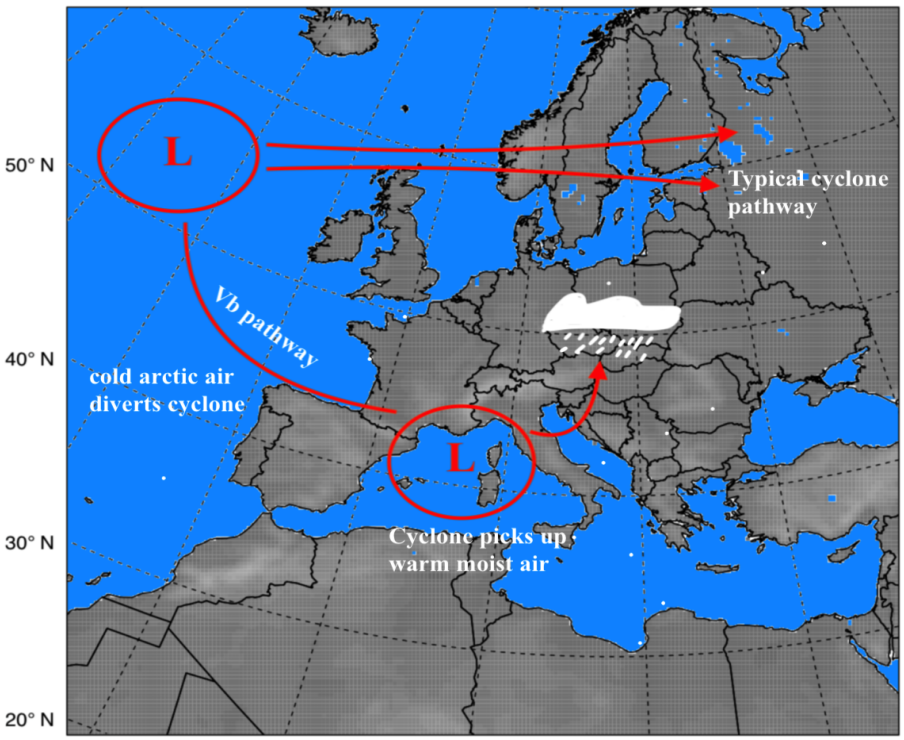

Figure 1.4: Typical pathways of cyclones over Europe and a characteristic Vb-cyclone track (modified from http://www.air-worldwide.com/Print-Preview/29239/)

(Fig. 1.4). These cyclones often transport a large amount of moisture to the northern side of the Alps and Central Europe that triggers intense and persistent precipitation leading to flash floods (Mudelsee et al. 2004; Nied et al. 2014). Most of the major floods in Central Europe have been caused by Vb-type weather conditions. In general, the occurrence of Vb-events is quite rare (3.5/year with a lifespan of 3.4 days) with the highest probability in April and autumn (Hofstätter and Chimani 2012). See Chapter 5 for more details.

1.4 Numerical Modeling: Challenges and scopes

Current efforts to assess air-sea fluxes in the Mediterranean Sea utilize observational or reanalysis data with a coarse spatial resolution (83–125 km) or conventional coarse (∼150 km) global Atmosphere–Ocean General Circulation Models (AOGCMs). Despite the fact that AOGCMs take into account the air-sea interactions, the Mediterranean region is generally not well represented, neither in the global atmospheric models, nor in global ocean models. In general, coarse-resolution AOGCMs cannot sufficiently resolve the local and mesoscale processes that characterize the Mediterranean region. On the other hand, high-resolution AOGCMs are not yet computationally feasible. A classical approach is to use Regional Climate Models (RCMs) to dynamically downscale the information on a regional scale from AOGCMs. Recent studies agree that an atmospheric grid resolution finer than 50 km is essential to better resolve the regional features (e.g., mountains, valleys, and local winds) of the Mediterranean area (Li 2006; Herrmann and Somot 2008; Elguindi et al. 2011). RCMs facilitate the investigation of extreme events, regional trends, and other important statistical properties related to the climate of a specific region. Several studies show that high-resolution RCMs improve the simulation of temperature, humidity, wind, and the exchange of other hydrological parameters (e.g., Ruti et al. 2008; Ruiz et al. 2008; Herrmann and Somot 2008; Dell'Aquila et al. 2012; Obermann et al. 2018). Despite a better representation of local features, high-resolution and high-frequency air-sea interactions and feedbacks are missing in RCMs, resulting in large uncertainties regarding air-sea fluxes (Dell'Aquila et al. 2012; Herrmann and Somot 2008; Herrmann et al. 2011). In a study based on a model ensemble, Sanchez–Gomez et al. (2011) found large uncertainties in the air-sea fluxes simulated in high-resolution (∼25 to 55 km) RCMs over the Mediterranean Sea. An RCM's SST is provided via reanalysis (e.g., ERA-Interim and NCEP/NCAR) or from AOGCM simulations. The spatial and temporal quality of the SSTs in these datasets is too coarse to resolve eddies (the internal Rossby radius of deformation is of the order of 15 km) and other high-frequency variations that characterize the Mediterranean Sea. NH with other processes (e.g., ocean mixing and transport) is important to calculate SST, which, in turn, modulates NH. Hence, a better representation of NH is essential for the better computation of SST and vice versa. Air-sea interactions and feedback processes are essential in understanding the Mediterranean circulations and climate (see e.g., Somot et al. 2008; Dell'Aquila et al. 2012).

When addressing the complex interactions between different components of the earth system a common approach is the coupling of numerical models (e.g., Will et al. 2017). In order to

resolve the two-way interactions at the atmosphere-ocean interface in the Mediterranean region a high-resolution atmosphere-ocean regional coupled model (AORCM) is required (Somot et al. 2008). The influence of atmosphere-ocean coupling on air-sea fluxes has been addressed in previous studies. It has been found that two-way, high-frequency interactions and a higher SST spatial resolution improves the representation of sea surface heat fluxes, hydrological parameters, and winds in the Mediterranean region (Lebeaupin and Drobinski 2009; Dubois et al. 2012; Lebeaupin et al. 2014; Sevault et al. 2014). Further, SSTs simulated with high-resolution ocean models can have a strong and beneficial effect on cyclogenesis and precipitation simulations (Sanna et al. 2013). Artale et al. (2010) show that a high-resolution AORCM can yield a more reliable estimate of air-sea fluxes than RCMs because of better SST simulations and wind fields. In another study, Sevault et al. (2014) show that ocean coupling improved the NH, but large errors occurred in individual components (particularly in LH and LW). Dubois et al. (2012) used an ensemble of five AORCMs and showed that the basin-wide average of the NH components differed significantly between the ensemble members. These studies show that even though the AORCMs improved the representation of air-sea fluxes over the Mediterranean Sea, large uncertainties persist. The uncertainties in the sea surface heat fluxes can strongly affect the simulations of the Mediterranean cyclones (medicanes and Vb-cyclones).

Most of the studies investigating medicanes (see e.g., Romero and Emanuel 2013; Cavicchia et al. 2014a; Walsh et al. 1996) and Vb-cyclones (see e.g., Hofstätter and Chimani 2012; Nissen et al. 2014; Grams 2014; Kelemen et al. 2016; Messmer et al. 2017) use RCMs simulations or reanalysis data. Therefore, fine-scale feedbacks associated with the air-sea interactions that strongly influence the temporal and spatial structure of Mediterranean cyclones are missing in these datasets. In a study, Flaounas et al. (2018) found that the atmosphere-ocean coupling only has a weak impact on the climatology and intensity of the Mediterranean cyclones, including medicanes (for more details see Appendix A). Concerning Vb-cyclones, the impact of air-sea interactions and feedbacks over the Mediterranean Sea on the characteristics of Vb-cyclones has not yet been investigated using an AORCM. Ho-Hagemann et al. (2015), demonstrated the importance of AORCM in simulating Vb-cyclones, who used an AORCM with a coupled North- and Baltic Seas model to investigate the July 1997 Oder flooding event. They identified the large-scale convergence of moisture from the Mediterranean Sea together with moisture coming from the North Atlantic Ocean via the North Sea and inland evaporation as responsible for heavy rainfall and floods in Central Europe. Their analysis found the use of a coupled North- and Baltic Seas model beneficial for simulating the event.

1.5 Objectives

A high-resolution AORCM was developed to overcome the deficiencies of the existing climate simulations and to fulfill the following objectives:

- Better representation of the fine-scale local process and SST patterns

- Better representation of sea surface fluxes through fine-scale air-sea interactions and feedbacks
- Better simulations of the Mediterranean cyclones (medicanes and Vb-cyclones)

In the context of this study, several experiments were performed with coupled and uncoupled models to address the following topics and their related questions:

- Investigation of sea surface heat fluxes and wind speed over the Mediterranean Sea to address the following questions:
  - What is the impact of fine-scale air-sea interactions and feedbacks on sea surface heat fluxes and wind speed?
  - How does horizontal atmospheric grid resolution affect sea surface heat fluxes and wind speed?
  - What is the impact of SST diurnal variation on sea surface heat fluxes and wind speed on sub-daily and longer timescales?
- Investigation of medicanes to address the following questions:
  - What is the impact of fine-scale air-sea interactions and feedbacks on the intensity and trajectories of medicanes?
  - Does a high-resolution horizontal atmospheric grid improve the representation of medicanes?
  - How does the spectral nudging method affect the simulation of medicanes?
- Investigation of Vb-cyclones to address the following questions:
  - What is the impact of fine-scale air-sea interactions and feedbacks over the Mediterranean Sea on the intensity and trajectories of Vb-cyclones?
  - How do the fine-scale air-sea interactions and feedbacks over the North- and Baltic Seas affect Vb-cyclones?

1.6 Outline

The content of the thesis is structured as follows:

1.6.1 Chapter 2: Modelling system and experimental setups

The following chapter presents a general description of the atmospheric and ocean models, as well as their coupling strategies. It also describes the datasets used as a reference in this study and the experimental setups.

1.6.2 Chapter 3: Climate modeling over the Mediterranean Sea: impact of resolution and ocean coupling

This chapter focuses on a detailed study investigating the impact of atmosphere-ocean feedbacks on various components of NH (equation 1.1) and wind speed over the Mediterranean Sea on seasonal and annual timescales. Additionally, the impact of horizontal atmospheric grid resolution and diurnal variations of SST on NH and wind speed was also analyzed in this study. For this purpose, uncoupled and coupled coarse (0.44°) and finer (0.08°) simulations were performed and analyzed.

The results indicate that the finer atmospheric grid improved the wind speed (mainly near the coastal areas) and subsequently the turbulent fluxes. The ocean coupling further improved the wind speed and turbulent fluxes. Radiation fluxes were slightly better represented in the coarse-grid simulations. Nevertheless, a coupled model with a finer atmospheric grid simulated a more realistic NH over the Mediterranean Sea. Diurnal variations of SST showed a strong effect on sub-daily sea surface heat fluxes and wind speed but minor effects on longer timescales.

1.6.3 Chapter 4: Medicanes in an ocean–atmosphere coupled regional climate model

In this chapter a study investigating the impact of ocean coupling on the trajectories and the intensity of medicanes is presented. Additionally, this study also investigates the impact of horizontal atmospheric grid resolution and spectral nudging on the representation of medicanes. Coupled and uncoupled simulations with three different atmospheric grid resolutions (0.44, 0.22, and 0.08°) were performed and analyzed in this study.

The results show that at resolutions of 0.44°and 0.22°, the coupled model did not show any improvement in simulating medicanes compared to the uncoupled model. However, the coupled model with the finer (0.08°) atmospheric grid had improved the track length, core temperature, and wind speed of the simulated medicanes compared to the uncoupled model. The results suggest that an atmospheric grid resolution higher than 0.22° is essential for a more realistic simulation of medicanes. Additionally, ocean coupling improves the simulation of medicanes.

1.6.4 Chapter 5: European Marginal Seas in a regional atmosphere–ocean coupled model and their impact on Vb-cyclones and associated precipitation

This chapter contains a study that analyzes the robustness of a coupled atmosphere-ocean model that includes models of two European marginal seas (Mediterranean and North- and Baltic) in reproducing the observed characteristics of selected Vb-cyclones and the impact of the air-sea coupling on the cyclones' trajectories and precipitation intensity. The Vb tracks were constructed using the method of Hofstätter and Chimani (2012). Furthermore, the characteristic of the

precipitation fields such as structure, amplitude, and location were investigated using the method of Wernli et al. (2008).

SST was evaluated to demonstrate the stability and reliability of the coupled configurations. Compared to observations, SSTs simulated using coupled configurations showed biases ($\sim$1 $^{\circ}$C) over the coupling regions, especially during winter and summer. In general, all model configurations could replicate Vb-cyclones, their trajectories, and associated precipitation fields. The atmosphere-ocean coupling had an overall positive impact, although with a strong case-by-case variation, on the trajectories and intensity of Vb-cyclones due to the variation in moisture source for each event. Furthermore, the average structure of the precipitation field was best represented in the coupled configurations including the coupling of the Mediterranean and North- and Baltic Seas.

1.6.5 Chapter 6: Conclusions

Chapter 6 describes a summary of the results and prospective future research.

1.6.6 Appendix

This section provides more details of the numerical tools (mainly focused on performance and methods) used in this study and a more detailed study on the Mediterranean cyclones.

- **A.1: The COSMO-CLM 4.8 regional climate model coupled to regional ocean, land surface, and global earth system models using OASIS3-MCT: description and performance**

  The study describes the coupling strategy and performance of the coupled regional climate system model based on CCLM that can couple two land surface models (the Community Land Model (CLM) and VEG3D), with the NEMO-MED12 regional ocean model for the Mediterranean Sea, two ocean models for the North and Baltic seas (NEMO-NORDIC and TRIMNP+CICE), and the MPI-ESM Earth system model. It presents different model components and the unified OASIS3-MCT interface (UOI) which handles all couplings in a consistent way, minimizing the model source code modifications and defining the physical and numerical aspects of the couplings. Additionally, this study also addresses the specific coupling issues like the handling of different domains, multiple usages of the MCT library, and exchange of 3-D field.

- **A.2: Assessment of an ensemble of ocean–atmosphere coupled and uncoupled regional climate models to reproduce the climatology of Mediterranean cyclones**

  This study assesses the ability of RCMs and AORCMs participating in the Med-CORDEX in reproducing the climatology of the Mediterranean cyclones including medicanes. The simulations were forced at the lateral boundaries by the ERA-Interim reanalysis framework for the period of 1989–2008.

In the end, the supplement contains a summary of the thesis in German.

Overview

Figure 1.5 shows the comprehensive overview of the thesis content.

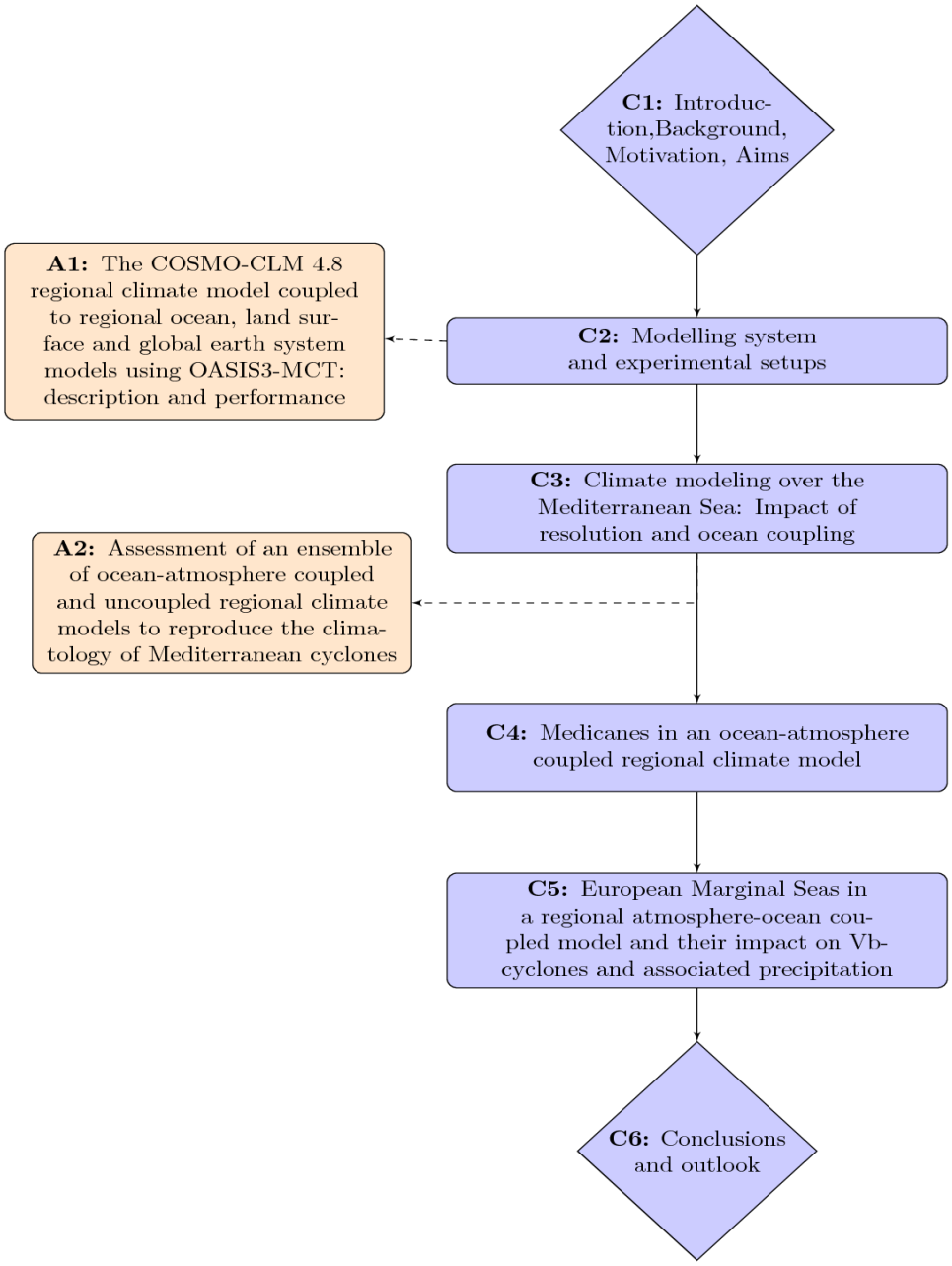

Figure 1.5: Flowchart for an overview of the thesis content. The characters (C1 – C6) and (A1, A2) represent Chapters and Appendices, respectively

CHAPTER 2

Modeling system and experimental setups

Chapter 1 describes the necessity of a high-resolution AORCM for a better representation of air-sea feedback processes and orographic features in the Mediterranean region. It also highlights several questions that are addressed in this thesis. The following chapter presents a general description of the numerical tools that were used to perform high-resolution coupled and uncoupled simulations involving the regional atmospheric and oceanic models and their coupling strategies. It also includes a short description of the data sets used as references throughout this work. More details related to the specific experiment are described in the relevant chapters. This chapter also includes an overview of my contributions to the model development throughout this work.

2.1 Numerical tools

Following atmospheric and ocean models and their coupling strategies were used in this work.

2.1.1 Atmospheric model

The state-of-the-art regional atmospheric model COSMO-CLM (CCLM), initially known as Lokall Modell, was developed by Deutscher Wetterdienst (DWD) in 1999 (Steppeler et al. 2003). It is one of the most widely used mesoscale atmospheric/climate models in various parts of the world and is maintained and supported by a highly vibrant CLM community (https://www.clm-community.eu/). This model has been intensively used for weather and climate related research over the Mediterranean and European region (e.g., Rockel et al. 2008; Rockel and Geyer 2008).

CCLM is a three-dimensional non-hydrostatic regional atmospheric circulation model, which solves the discretized primitive equations of atmospheric motion. It includes various physics– and dynamics–related options and a four-dimensional data assimilation technique. For horizontal discretization, CCLM uses a spherical Arakawa-C grid in which all variables are defined at the center of the grid, excluding wind components. The centers of the grid boxes are defined on a rotated latitude and longitude coordinate system and it can adopt a horizontal atmospheric grid resolution of up to 1 km. For vertical discretization, it uses the terrain-following height coordinate system. This model can be used for various applications including theoretical and

real-time studies.

Figure 1.1 shows the atmospheric model domain following the EURO-CORDEX extent (Giorgi 2006). As a limited area model, CCLM requires lateral boundary forcing data, which can be prepared using reanalysis data or outputs from global climate models. For lower boundary conditions, a multilayer soil model TERRA-ML can be used for soil hydrology treatment (Schrodin and Heise 2002), whereas SSTs over the ocean and seas can be prescribed or calculated using online coupling of an ocean component. In the present case, regional configurations of the following global ocean model are used to calculate SSTs over the coupling regions (see Fig. 1.1).

2.1.2 Ocean model

Nucleus for European Modelling of the Ocean (NEMO) is a widely used global ocean model and uses primitive equations to describe ocean fluid dynamics. The model includes a variety of different configurations, namely Océan PArallélisé (OPA) for ocean dynamics and thermodynamics, Louvain-la-Neuve Ice Model (LIM) for sea-ice dynamics and thermodynamics, and Tracer in the Ocean Paradigm (TOP) for biogeochemistry. These configurations can be used to study the ocean

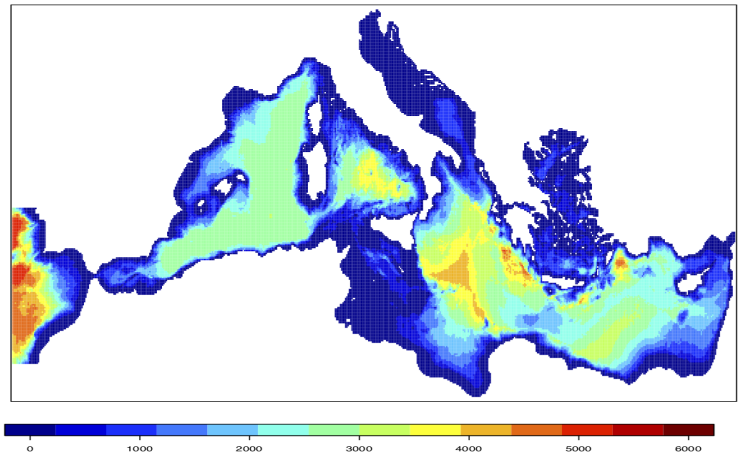

Figure 2.1: The Mediterranean Sea model (NEMO-MED12) bathymetry and model integration area

and its interactions with different components (atmosphere, sea-ice, and biogeochemical tracers) of the earth climate system over a wide range of spatial and temporal scales. Its one-dimensional configuration can be applied by setting the horizontal derivatives equal to zero. Several numerical schemes for momentum advection, pressure gradient, and advection tracers are offered in the model. For horizontal discretization, NEMO uses a staggered Arakawa-C grid with the land mask, while the vertical discretization depends on the representation of the bottom topography and the linearity or nonlinearity of the free surface. It uses the ORCA tripolar grid with a spherical north fold boundary condition. More information on different configurations can be found on the NEMO website (`https://www.nemo-ocean.eu/`).

The regional configurations of NEMO can be applied with closed basin geometries, periodic domains, and open boundary conditions. NEMO-MED12 (Beuvier et al. 2012; Lebeaupin et al.

2011) for the Mediterranean Sea and NEMO-NORDIC (Dieterich et al. 2013) for the North- and Baltic Seas are its two most widely used regional configurations. The NEMO-MED12 grid

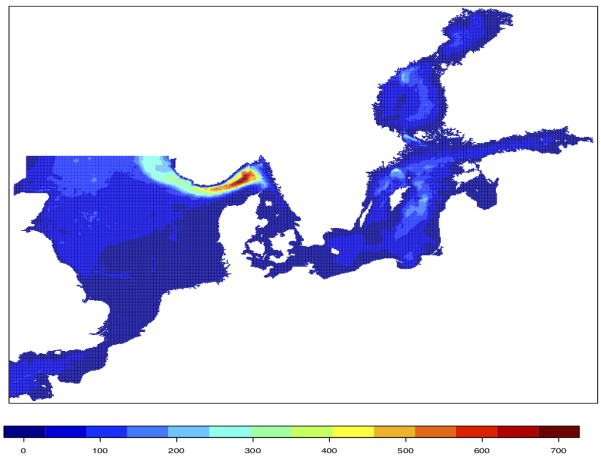

Figure 2.2: The North- and Baltic Seas (NEMO-NORDIC) bathymetry and model integration area

covers the whole Mediterranean Sea plus a small part of the Atlantic Ocean as a buffer zone for open boundary conditions (Fig. 2.1; Beuvier et al. 2012). It has the standard irregular ORCA grid with 1/12° resolution (∼6.5–8.0 km in latitude and ∼5.5–7.5 km in longitude; 567×264 grid points). In the vertical, 75 unevenly spaced z-levels are used with a layer thickness of 1 m at the surface increasing to 135 m at the bottom.

The NEMO-NORDIC grid covers the whole Baltic and the North Sea with two open boundaries in the Atlantic Ocean. The northern zonal boundary is the cross-section between the Hebrides and Norway and the southern meridional boundary lies in the English Channel (Fig. 2.2). It has a resolution of 2 nautical minutes (∼3.7 km; 619×523 grid points) and 56 stretched vertical levels with a thickness of 3 m at the surface and 22 m at the bottom of the Norwegian Sea. More details about the regional configurations of the ocean model are presented in the next chapters.

2.1.3 Coupling strategy

The coupling between RCM CCLM and ocean models NEMO-MED12 and/or NEMO-NORDIC is accomplished using the OASIS coupler developed at CERFACS (Craig et al. 2017). Figure 2.3 shows a systemic diagram of the coupling scheme. The OASIS coupler synchronizes not only the models, but also interpolates the coupling fields from one model grid to another. In the coupled setup, the ocean model sends SST to CCLM through OASIS and in turn receives solar energy, non-solar heat, momentum, and freshwater fluxes. In addition to that, NEMO-NORDIC sends the sea ice fraction to CCLM and receives sea level pressure. The coupling fields are exchanged every 1 or 3-h depending on the experiment.

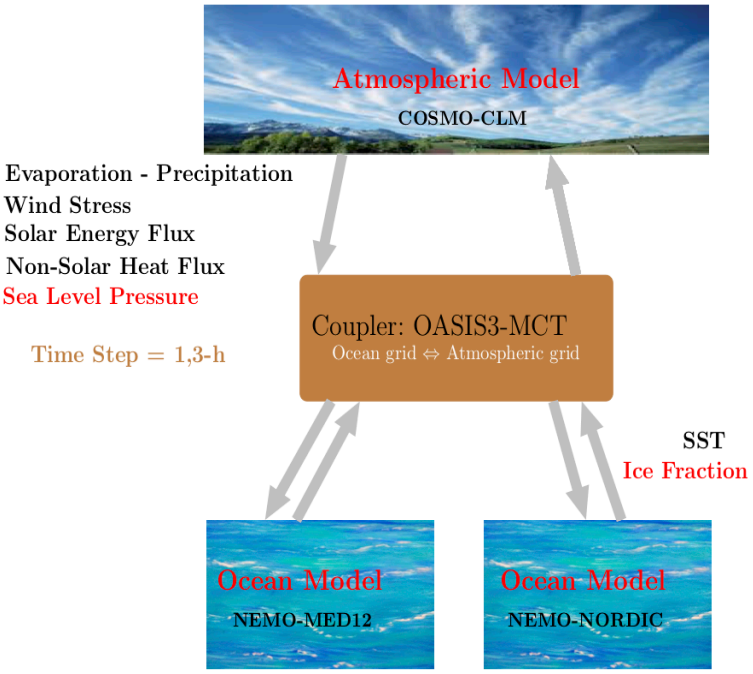

Figure 2.3: A systematic diagram for the coupling of CCLM to NEMO-MED12 and NEMO-NORDIC

2.2 Description of the experiments

Several simulations were conducted for this thesis, which are summarized in this section. To investigate the impact of horizontal atmospheric grid resolution and ocean coupling on sea surface heat fluxes and wind speed, five simulations were performed. Four simulations were performed at 0.44 and 0.08° atmospheric grid resolution, two uncoupled (CCLM) and two coupled (CCLM coupled to NEMO-MED12). The fifth simulation was done using CCLM (0.08°) with temporally smoothed (5 days averaged) Mediterranean SSTs to investigate the impact of sub-daily SST variations on sea surface heat fluxes and wind speed. In order to investigate the impact of horizontal atmospheric grid resolution and ocean coupling on medicanes, six simulations were performed, uncoupled (CCLM) and coupled (CCLM coupled to NEMO-MED12) at 0.44, 0.22, 0.08° horizontal atmospheric grid resolutions. To investigate the impact of ocean coupling on Vb-cyclones, four simulations were performed, one uncoupled (CCLM) and three coupled (CCLM coupled to NEMO-MED12, CCLM coupled to NEMO-NORDIC and CCLM simultaneously coupled to NEMO-MED12 and NEMO-NORDIC) at a horizontal atmospheric grid resolution of 0.22°. In all the coupled simulations, NEMO-MED12 and NEMO-NORDIC use the ocean grid resolution 1/12° and 2 nautical minutes, respectively. Table 2.1 presents a brief overview of the experimental setups including model versions, resolutions, and couplers.

2.2.1 Initial and boundary conditions

The initial and boundary conditions for CCLM were taken from the ECMWF's ERA-Interim reanalysis data (Dee et al. 2011). In the uncoupled simulations, SST was prescribed using the

Table 2.1: Name of the models their versions and resolution used in these studies

	Atmospheric model	Ocean model1	Ocean model2	Coupler
Study 1	CCLM v4.21 Res: 0.44, 0.08°	NEMO-MED12 v3.2 Res: 1/12°	– – – –	OASIS3-MCT
Study 2	CCLM v4.8 Res: 0.44, 0.22, 0.08°	NEMO-MED12 v3.2 Res: 1/12°	– – – –	OASIS3
Study 3	CCLM v5.7 Res: 0.22°	NEMO-MED12 v3.6 Res: 1/12°	NEMO-NORDIC v3.3 Res: 2 nautical minutes	OASIS3-MCT

ERA-Interim's daily SST. In the coupled simulations, SST was also prescribed from the ERA-Interim data except over the coupling regions, where it was calculated using the regional ocean models.

The initial conditions for three-dimensional potential temperature and salinity were provided by the MEDATLAS–II climatology in the Mediterranean Sea (Rixen 2012). Water exchange with the Atlantic Ocean was relaxed to the Levitus et al. (2005) climatology prescribed in the buffer zone. The Black Sea and runoff water input were prescribed from the climatological average of interannual data from (Ludwig et al. 2009).

For the North- and Baltic Seas, the initial conditions for three-dimensional potential temperature and salinity were provided by Janssen et al. (1999) and the lateral boundary conditions in the North Sea were prescribed from ORAS4 reanalysis data (Balmaseda et al. 2013). The tidal potential was prescribed at the open boundaries in the North Sea from the global tidal model of Egbert and Erofeeva (2002) and Egbert et al. (2010). The freshwater inflow of the rivers was provided from the daily time series of the E-HYPE model output (Lindström et al. 2010).

2.3 Model developments

The CCLM interface that includes the coupling of the regional ocean model NEMO was developed at the Institute for Atmospheric and Environmental Sciences (IAU), Goethe University Frankfurt. The following technical developments were made during the course of this study:

- Testing and operationalizing of CCLM and NEMO-MED12 coupling.
- Coupling of CCLM to the one-dimensional configuration of NEMO-MED12.
- Upgrading of the latest version of the atmospheric (CCLM version 4.8 to 5.7) and ocean model (NEMO-MED12 version 3.2 to 3.6).
- Upgrading the OASIS coupler from a single processor-based version to its latest fully parallel Model Coupling Toolkit (OASIS3-MCT) version.
- Addition of the North- and Baltic Seas (NEMO-NORDIC) model to the existing AORCM that allowed CCLM to couple two main European marginal seas simultaneously.

Coupling of CCLM and NEMO-NORDIC was implemented and tested by Trang von Pham (Van Pham et al. 2014). These developments are also a part of the unified OASIS interface (UOI) version of CCLM. For a more detailed description and performance of the CCLM UOI, I refer the reader to our technical paper (Will et al. 2017). The developments of the coupled system model emerged into several scientific peer-reviewed papers listed in the appendix.

2.4 Data

The following data sets are used as a reference in this work.

ERA-Interim European Reanalysis Interim by ECMWF. The data is available from 1979 to present on a 0.75° global grid at 6-h interval (Dee et al. 2011).

MERRA-1 Modern-Era Retrospective Analysis for Research and Applications version 1 by NASA. A period from 1 of January 1979 to 30 September 2013 is available on a 0.5° grid at 6-h interval (Rienecker et al. 2011).

MERRA-2 Modern-Era Retrospective Analysis for Research and Applications version 2 by NASA. A period from 1 of January 1980 to present is available on a 0.5°×0.625° grid at 6-h interval (Gelaro et al. 2017).

SeaWinds by National Oceanic and Atmospheric Administration (NOAA). The data is generated on 0.25° grid at 6-h interval by blending observations from multiple satellites. It is available from 9 July 1987 (Zhang et al. 2006).

OISST Daily Optimum Interpolation SST by NOAA. The data contains observations from different platforms (satellites, ships, and buoys). It is available from September 1981 to present on a 0.25° grid every 6-h (Reynolds et al. 2007).

EOBS ENSEMBLES Observations version 15.0 by European Climate Assessment and Dataset (ECAD). Station-based observations mainly over Europe are available from 1950 to present interpolated on a regular and rotated grid at 0.44, 0.25, and 0.22° horizontal resolutions (Haylock et al. 2008).

OAFlux Objectively Analyzed Air-sea Fluxes by WHOI. This data is available on a 1° grid and provides monthly means for the period of 1958 to present and daily means for the period 1985 to present. This product integrates satellite observations with mooring and ships reports and reanalyzed surface meteorology from atmospheric models (Yu et al. 2008).

CHAPTER 3

Climate modeling over the Mediterranean Sea: impact of resolution and ocean coupling[1]

Abstract

Feedback between the Mediterranean Sea and the atmosphere on various temporal and spatial scales plays a major role in the regional climate system. We studied the impact of horizontal atmospheric grid resolution (grid spacing of ∼9 vs. ∼50 km) and dynamic ocean coupling (the ocean model NEMO-MED12) in simulations with the regional climate model COSMO-CLM. The evaluation focused on sea surface heat fluxes, 10-m wind speed, and sea surface temperature (SST) parameters on both seasonal and annual timescales. The finer grid improved the wind speed (particularly near coastal areas) and subsequently the turbulent heat flux simulations. Both parameters were better simulated with the interactive ocean model NEMO-MED12 than with prescribed daily ocean SSTs (using near-observation ERA-Interim reanalysis based SSTs), but coupling introduced a warm SST bias in winter. Radiation fluxes were slightly better represented in coarse-grid simulations. Still, only the higher-resolution coupled simulations could reproduce the observed net outgoing total heat flux over the Mediterranean Sea. Investigation of the impact of subdiurnal SST variations showed a strong effect on sub-daily heat fluxes and wind speed but minor effects at longer time scales. Therefore, a coupled atmosphere–ocean climate model should be preferred for studying the Mediterranean Sea climate system. Higher-resolution models should be preferred, but they are not yet able to perform better than their coarse-resolution predecessors in all aspects.

3.1 Introduction

The semi-enclosed Mediterranean Sea, with its intricate coastline and topographic features, functions as a source of moisture and heat and has a substantial impact on local and remote climate conditions (Artale et al. 2010). A wide range of oceanic processes and air-sea interactions

[1]**Published as:** Akhtar N, Brauch J, Ahrens B (2018) Climate Modeling over the Mediterranean Sea: Impact of Resolution and Ocean Coupling. Clim Dyn 51:933–948. doi:10.1007/s00382-017-3570-8

of global and regional interest occur in the Mediterranean basin. The Mediterranean climate is known for its large seasonal temperature variations, strong winds (e.g., Mistral, Tramontane, and Bora winds), heavy precipitation, and cyclones (e.g., Medicanes). This region is also known as a "hot spot" in future climate change projections because of a substantial decrease in mean precipitation and increase in precipitation variability during warm and dry seasons (Giorgi 2006). The formation of intermediate and deepwater masses in the northwestern Mediterranean Sea is of fundamental importance for regional and global meridional overturning circulations (Calmanti et al. 2006; Josey 2003). Net sea surface heat flux (NH) anomalies play a significant role in the local climate (Roether et al. 1995; Theocharis et al. 1999). Therefore, an accurate representation of the ocean and atmosphere, especially the air-sea interactions, is crucial for accurate modeling of the Mediterranean climate. The NH is defined as:

$$NH = SW - LW - LH - SH, \tag{3.1}$$

where SW and LW are short-wave and long-wave radiation, respectively, and LH and SH are latent and sensible heat flux, respectively.

In general, coarse-resolution global models cannot sufficiently resolve the local and mesoscale processes that characterize the Mediterranean region. Therefore, these global models cannot correctly describe air-sea exchanges and their variability (Elguindi et al. 2011). On the other hand, high-resolution global models for studying regional processes are not yet feasible from a computational standpoint. This issue can be resolved by downscaling using uncoupled regional climate models (RCMs), which can have grid spacing finer than 50 km with a more realistic representation of regional features (see for example Gao et al. 2006; Herrmann and Somot 2008; Elguindi et al. 2011). The relatively high resolution of RCMs directly impacts the air-sea exchange and improves the representation of temperature, wind, humidity, and the exchange of other hydrological parameters (e.g., Ruti et al. 2008; Ruiz et al. 2008; Herrmann and Somot 2008; Dell'Aquila et al. 2012; Obermann et al. 2018).

However, the high-resolution and high-frequency interactions between the ocean and the atmosphere are missing in RCMs, which results in large uncertainties in airsea fluxes (Dell'Aquila et al. 2012; Herrmann and Somot 2008; Herrmann et al. 2011). An RCM's sea-surface temperature (SST) is provided via reanalysis (e.g., ERA-Interim and NCEP/NCAR) or from atmosphere–ocean coupled general circulation model (AOGCM) simulations. The spatial and temporal quality of the SSTs in these datasets is too coarse to resolve eddies (the internal Rossby radius of deformation is of the order of 15 km) and other high-frequency variations that characterize the Mediterranean Sea. Another important feature of the SST is its diurnal variation, which is missing or not well represented in the reanalysis and the majority of the AOGCM datasets as a result of coarse spatial and temporal resolution (e.g., ERA-Interim has daily values over the ocean). The SST diurnal variations affect the atmospheric conditions and in turn exert feedback on the SST. They can increase surface heat fluxes by roughly $10\,\mathrm{W\,m^{-2}}$ (Fairall et al. 1996), which can influence the atmospheric variability on sub-daily to intra-seasonal time scales (e.g., Kawai et al. 2007). In general, SST diurnal variations are small but have important effects on the physical and

biological processes in seas and oceans (Kawai et al. 2007). Therefore, an atmosphere–ocean regional coupled climate model (AORCM) with high-resolution and high-frequency (e.g., hourly) air-sea exchanges appears to be important for a good representation of Mediterranean climate characteristics.

Several modeling studies have investigated the impact of atmosphere–ocean coupling over the Mediterranean Sea. These studies have shown that two-way, high-frequency interactions and higher SST spatial resolution improve the representation of surface heat fluxes, hydrological parameters, winds, and extremes events (e.g., cyclogenesis, medicanes, and heavy precipitation events) in the Mediterranean region (Lebeaupin and Drobinski 2009; Sanna et al. 2013; Lebeaupin et al. 2014; Akhtar et al. 2014). In a recent study, Panthou et al. (2018) show that high-resolution regional atmospheric models coupled with Mediterranean Sea models improve the representation of hot days and droughts more than heavy precipitation events. Somot et al. (2008) show that a high-resolution AORCM amplifies the climate change signal compared to an RCM in future projections in the Euro-Mediterranean region. They explained this result based on better consistency among the SST, airsea fluxes, and vertical structure of the atmosphere in the AORCM. Artale et al. (2010) show that high-resolution AORCMs can yield a more reliable estimate of air-sea fluxes than RCMs because of better SST simulations and wind fields. In another study, Sevault et al. (2014) show that ocean coupling improved the NH, but large errors occurred in individual components (particularly in latent heat flux and long wave radiation). Dubois et al. (2012) used an ensemble of five AORCMs and showed that the basin-wide average of the NH components differed significantly between the ensemble members.

All the studies noted above used an atmospheric grid resolution in the range of 20–50 km to investigate the added value of ocean coupling over different timescales. These studies show that even though the AORCMs improved the representation of air-sea fluxes over the Mediterranean Sea, large uncertainties still persist. In this study, we investigated the spatial patterns and basin-wide averages of all of the components of NH, 10-m wind speed, and SST on seasonal and annual timescales to address the following questions:

1. Does ocean–atmosphere coupling improve the simulation of sea surface heat flux and 10-m wind speed over the Mediterranean Sea?

2. Does horizontal atmospheric grid resolution affect the sea surface heat flux and 10-m wind speed over the Mediterranean Sea?

3. Are certain areas and seasons more sensitive than others to the ocean coupling and atmospheric grid resolution?

4. What is the impact of SST diurnal variation on air-sea fluxes of heat and wind speed on sub-daily and longer timescales?

The paper is organized as follow. Section 3.2 explains the modeling system and experimental setup of our simulations. The results are presented and discussed in Sect. 3.3. The paper concludes in Sect. 3.4 with a summary of results and prospective future research.

3.2 Modeling system and experiment setups

In this study, we employ the RCM COSMO-CLM v4.21 (CCLM), based on non-hydrostatic equations (Rockel et al. 2008) in uncoupled and coupled (atmosphere– ocean) configurations. For the coupled ocean–atmosphere model, CCLM is coupled to the regional ocean model NEMO-MED12. We used an atmospheric grid resolution of 0.44° (∼50 km; 118×79 grid points and 32 σ levels) and a finer atmospheric grid resolution of 0.088° (∼9 km; 596×386 grid points and 32 σ levels) in both the uncoupled and coupled configurations. The initial and boundary conditions for CCLM were taken from the ECWMF's ERA-Interim reanalysis data (Dee et al. 2011), except the soil temperature and water content values for initialization. Here, the climatological values (2000–2010) of soil temperature and water content were taken from uncoupled CCLM simulations for a better soil initialization following the suggestion of Kothe et al. (2014). In the uncoupled configuration, SST is prescribed using the ERA-Interim's daily SST. In the coupled configuration, SST is also prescribed from the ERA-Interim data except over the Mediterranean Sea, where it is calculated using the regional ocean model NEMO-MED12. The aerosol optical depth data from MACC (Monitoring Atmospheric Composition and Climate), which is a global reanalysis product of the ECWMF (`atmosphere.copernicus.eu`), are used in CCLM. For both the uncoupled and coupled configurations, CCLM uses numerical time steps of 150 s and 40 s for the coarse and high-resolution simulations, respectively, with a third-order Runge–Kutta numerical integration scheme. In CCLM, we used the onedimensional prognostic turbulent kinetic energy scheme for vertical turbulent diffusion parameterization and a delta-two-stream radiation scheme proposed by Ritter and Geleyn (1992). The simulation domain follows the Med-CORDEX requirements indicated in Fig. 1 of Ruti et al. (2016).

NEMO-MED12 is a regional configuration of the ocean circulation model (OGCM) NEMO (Madec and the NEMO Team 2008) for the Mediterranean Sea (Lebeaupin et al. 2011, 2012). It has a horizontal resolution of 1/12° (∼6–8.0 km in latitude and ∼5.5–7.5 km in longitude; 567×264 grid points) and 50 vertical levels The changes in horizontal grid resolution are due to the use of the standard three-polar ORCA grid of NEMO (Beuvier et al. 2012). The NEMO-MED12 grid encompasses the entire Mediterranean Sea and a small part of the near Atlantic Ocean as a buffer zone; it does not include the Black Sea. The vertical levels were defined in z–coordinates using the partial step formulation. We adopted a numerical time step of 720 s in this configuration. NEMO-MED12 was initialized using the MEDATLAS–II (Rixen 2012) monthly mean seasonal climatology (1945–2002) in the Mediterranean Sea and in the Atlantic buffer zone using the climatology of Levitus et al. (2005). To obtain an initial equilibrium state of the Mediterranean Sea, NEMO-MED12 coupled with the coarse-grid CCLM was spun-up for 25 years. The ERA-Interim data (1979–1985) were used to drive the CCLM with a random-year strategy. To model the river discharge of fresh water into the Mediterranean Sea, the climatological average of the inter-annual data of Ludwig et al. (2009) was used to compute the monthly river discharge values (Beuvier et al. 2012). For a more detailed discussion of the NEMO-MED12 configuration, we refer the reader to Beuvier et al. (2012).

The CCLM and NEMO-MED12 models are coupled via OASIS3-MCT (Valcke 2013) with a 3-h coupling time step. The NEMO-MED12 sends SST to CCLM through OASIS3-MCT and in turn receives solar energy, non-solar heat, momentum, and freshwater fluxes. OASIS3-MCT uses a bi-cubic scheme to interpolate the fields from one grid to another.

We conducted the coupled and uncoupled model evaluation runs for the periods of 1979–2011 and 2000–2003 with the coarse and fine atmospheric grids, respectively. The coarse-coupled simulations were initialized with the ocean spun-up state of 1979 (the first year is used as an adjustment period for the ocean and atmosphere). The sea state of 2000 from the coarse-coupled simulations was then used to initialize the high-resolution coupled simulations from 2000 to 2003; a 1 year spin-up was used to adjust to the high-resolution atmospheric forcing.

Additionally, we performed a sensitivity experiment to analyze the effects of coupling and SST diurnal variations of sea surface heat fluxes on seasonal and sub-daily timescales. Hence, we averaged the SST over the Mediterranean Sea calculated by NEMO-MED12 in the high-resolution coupled simulations over periods of 5 days. These simulations were designed to include the same climatology and sub-monthly variations without the diurnal SST variations, short-term extreme variability and two-way active interaction of the Mediterranean Sea and the atmosphere. The temporally smoothed SSTs over the Mediterranean Sea combined with the ERA-Interim boundary conditions were then used to drive the high-resolution uncoupled CCLM simulations for the period of 2000–2003. This allowed for a fair investigation of SST diurnal variations and ocean coupling impacts.

Hereafter, we use the abbreviations "CPLxx" for the coupled simulations, "CCLMxx" for the uncoupled simulations, and "CCLMxx_SSTavg" for simulations with averaged SSTs, where "xx" refers to atmospheric grid resolution (i.e., "44" for 0.44° and "08" for 0.08°).

For the evaluation of the simulations, we used the following datasets:

- The NOAA Daily Optimum Interpolation SST (OISST), available from 1981 to present. This dataset contains global ocean SST data at 6-h intervals on a 0.25° grid. Observations from different platforms (satellites, ships, and buoys) were used to construct the OISST dataset (Reynolds et al. 2007).

- NOAA (SeaWinds), available from July 9, 1987 to present. This dataset contains global ocean 10-m winds and wind stresses at 6-h intervals on a 0.25° grid. Observations from multiple satellites were combined to generate the dataset (Zhang et al. 2006).

- Objectively Analyzed Air-sea Fluxes (OAFlux). This dataset of sea surface fluxes of heat, SST, and 10-m wind speed for the global oceans is available on a 1° grid and provides monthly means for the period of 1958 to present and daily means for 1985 to present. This product integrates satellite observations with mooring and ships reports and reanalyzed surface meteorology from atmospheric models (Yu et al. 2008).

3.3 Results and discussion

Here, we discuss the impact of ocean coupling and horizontal atmospheric grid resolution on simulated SST, 10-m wind speed, and NH and its components. Our discussion focuses on simulations for the period 2001–2003. The differences between coarse-coupled and -uncoupled simulations (CPL44 vs. CCLM44) for the periods 1980–2011 and 2001–2003 are systematic. Therefore, the choice of a shorter period (2001–2003) does not affect the results of our study. However, for the sake of completeness, further comparisons of long-term simulations for the period of 1980–2011 are presented in the supplementary information (SI). It is worth noting here that we have explicitly analyzed the impact of the European 2003 heat-wave in our results. We found that ocean coupling does not change the intensity of heat-waves, which is also shown by Tomassini and Elizalde (2012). The total mean difference (MD) and root mean square error (RMSE) of daily values of the respective seasons are used as simple statistical measures in the following discussions.

3.3.1 SST

Figure 3.1 illustrates the effect of ocean coupling and of a finer atmospheric grid resolution on the mean seasonal simulated SST. The first row of Fig. 3.1 compares the SST simulated with the high-resolution uncoupled CCLM08 with the observed OISST. The differences are small, as expected, because analyzed SST observations are applied in the ERA-Interim SST, thus forcing the CCLM08 simulation. The differences are larger near the coastal areas (RMSE ranges from 0.5 to 1.1 °C), mainly due to interpolation artifacts in preparing ERA-Interim SSTs as forcing data.

The second and third rows of Fig. 3.1 compare the CPL08 SST simulation with observations and with the CCLM08 simulation, respectively. The CPL08 is warmer in winter (MD = 1.3 °C) and colder in summer (MD = -1.0 °C). Locally, these differences are up to ± 3 °C (RMSE is 1.8 °C in winter and 1.2 °C in summer). This finding can partly be explained by the calculation method of SST in the coupled model: the SST is the mean temperature of the uppermost ocean layer, which is 1 m thick in NEMO-MED12 (Lebeaupin et al. 2014). The observed SSTs are derived from satellite radiometer data representative of the uppermost few millimeters of the ocean. The annual mean value of CPL08 over the simulated period is 0.3 °C higher than CCLM08. Similar differences can be seen in the coarse-coupled (CPL44) simulation for the period of 1980–2011 (Fig. S1). A comparison of CPL08 and CPL44 reveals that the atmospheric grid resolution also impacts the simulated SST (Fig. 3.1, last row). The CPL08 is colder than CPL44 in all seasons except summer. The winter warm bias in the coarser CPL44 simulation is stronger (1.8 vs. 1.3 °C) than CPL08, which might be due to better near-coastal simulation of 10-m wind speed in the finer atmospheric grid in CPL08 (discussed in detail in the next subsection) and in return better SST in CPL08. Higher wind speed increases the latent heat release and hence lowers the SST. The local differences in summer between coarse and fine simulations are almost as large as they are in winter (RMSE values of 0.8 and 1.0 °C, respectively). This disappearing

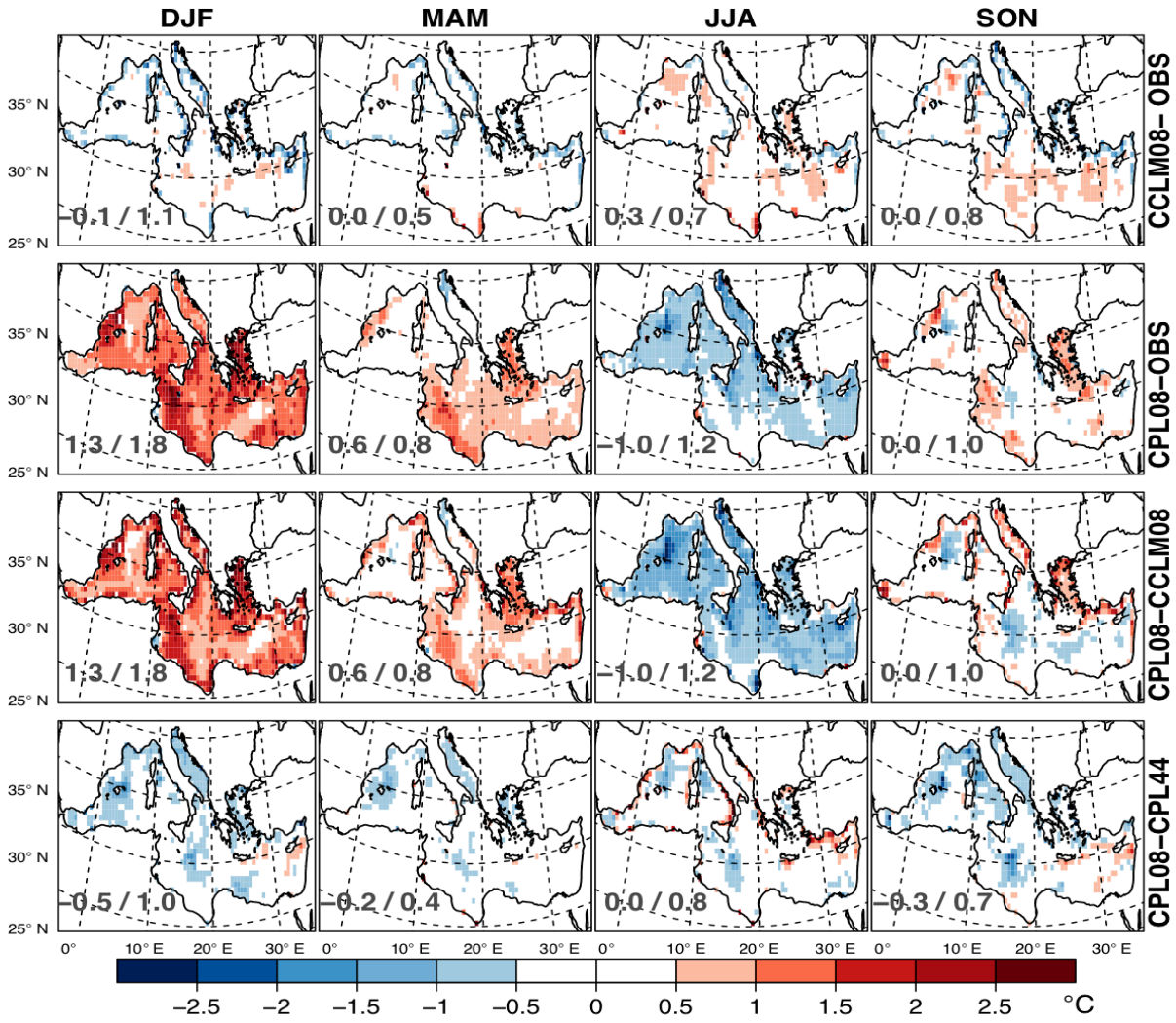

Figure 3.1: Mean differences in sea surface temperatures (in °C) for winter, spring, summer, and autumn (*columns*) in the period 2001–2003. The *rows* show the differences between CCLM08 and observations OISST, between CPL08 and observations OISST, between CPL08 and CCLM08, and CPL08 and CPL44, respectively. The *numbers* given in the *panels* are the total mean differences (MD) and the mean RMSEs as MD/RMSE

systematic effect correlates with the smaller wind speeds in summer in the Mediterranean basin.

Figure 3.2 shows the annual cycles of basin-averaged SSTs of the different simulations and the observation data. As noted above, the SSTs of the uncoupled simulation are similar to the observational data. The SSTs calculated in the coupled simulations reveal a warm bias in winter and a smaller cold bias in summer. The high-resolution simulation improves this bias slightly.

3.3.2 10-m wind speed

Figure 3.3 illustrates the effect of ocean coupling and of a finer atmospheric grid resolution on simulated seasonal 10-m wind speed. The comparison of simulated and observed 10-m wind speed reveals that the differences are particularly large in near-coastal areas, especially in areas that are associated with intense wind systems (e.g., Vendaval and Levante winds in the Alboran

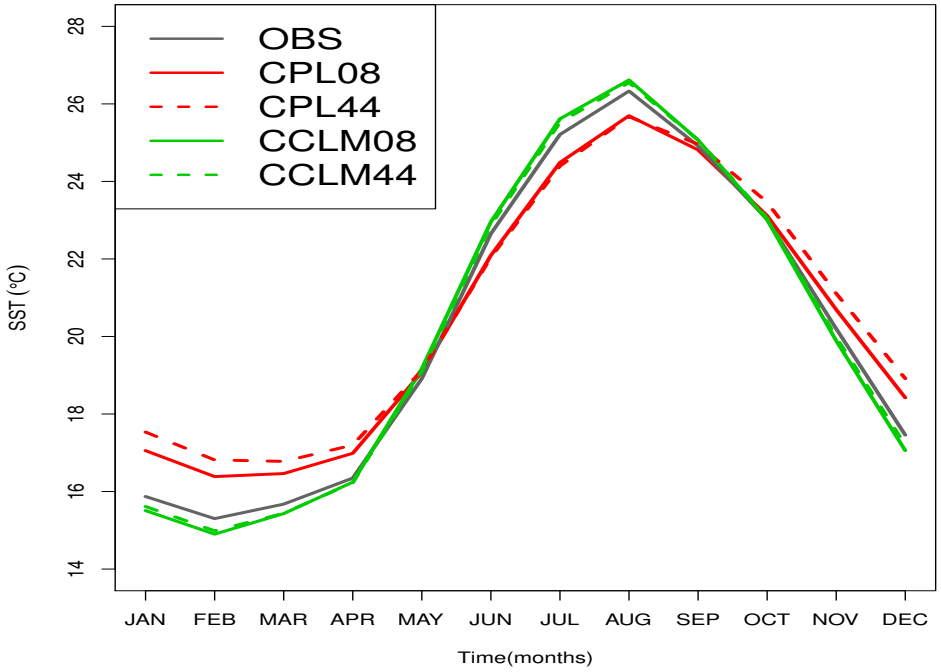

Figure 3.2: Annual cycle of SST (°C)

Sea; Mistral and Tramontane in the Gulf of Lions and Ligurian Sea; Bora winds in the Adriatic Sea; Libeccio winds in the central Mediterranean Sea). These wind systems are generally more intense in winter and autumn (Perry et al. 2001).

The first row of Fig. 3.3 compares the 10-m wind speed simulated in high-resolution uncoupled CCLM08 with the NOAA observations. The CCLM08 underestimates the mean 10-m wind speed with MD = 1.2 $\mathrm{m\,s^{-1}}$ in winter (observed mean 8.1 $\mathrm{m\,s^{-1}}$) and 0.2 $\mathrm{m\,s^{-1}}$ in summer (observed mean 4.5 $\mathrm{m\,s^{-1}}$). Locally, CCLM08 underestimates the 10-m wind speed by up to 3 $\mathrm{m\,s^{-1}}$ in winter and autumn (RMSEs, 1.4 and 1.0 $\mathrm{m\,s^{-1}}$, respectively). These differences are slightly reduced in CPL08 (winter: MD = 0.8 $\mathrm{m\,s^{-1}}$, RMSE = 1.1 $\mathrm{m\,s^{-1}}$), except in summer (MD = 0.5 $\mathrm{m\,s^{-1}}$, RMSE = 0.7 $\mathrm{m\,s^{-1}}$; Fig. 3.3, row 2). Figure 3.3, row 3 shows a comparison of 10-m wind speed in the CPL08 and CCLM08 simulations. The ocean coupling improves the 10-m wind speed simulation by about 1% over the simulated period; the largest improvement (about 5%) occurs in the winter (Fig. 3.3, row 4). This correlates with a deepening of the surface pressure in CPL08 (0.5–1.0 hPa) compared to CCLM08, yielding increased pressure gradients in winter and vice versa in summer (Fig. S4).

The last row of Fig. 3.3 shows that the impact of atmospheric grid resolution is more pronounced than the impact of coupling in the simulation experiment set-up that we tested. The high-resolution coupled CPL08 revealed an improvement over the coarse-coupled CPL44 of about 2–3 $\mathrm{m\,s^{-1}}$ (RMSE = 0.6–1.0 $\mathrm{m\,s^{-1}}$), mostly in near-coastal areas. The use of a fine atmospheric grid improved the simulation of fine-scale orography-related local and regional processes (such as in Louka et al. 2008; Obermann et al. 2018). The high resolution simulation revealed an

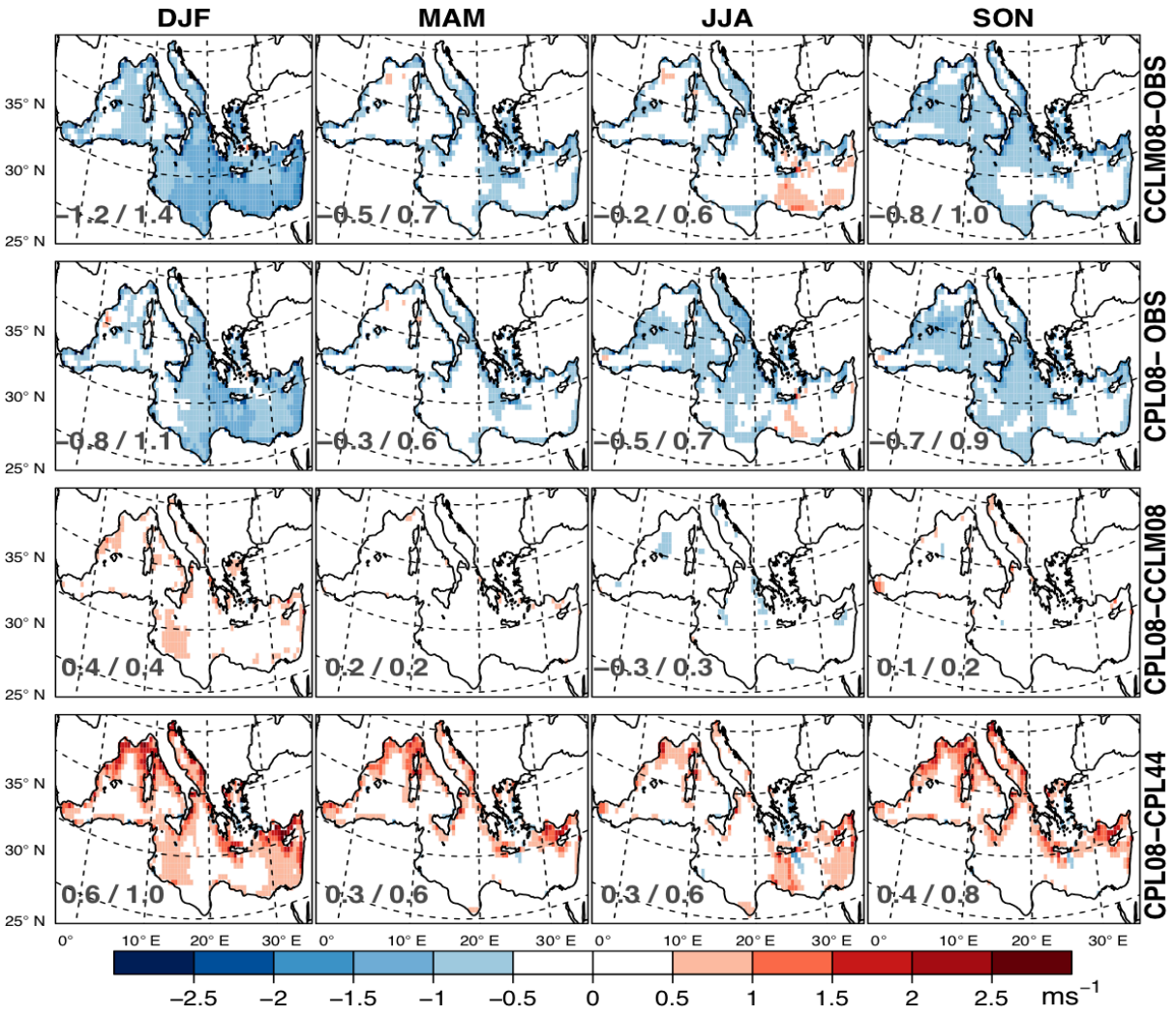

Figure 3.3: As in Fig. 3.1, but for 10-m wind speed (in $\mathrm{m\,s^{-1}}$)

added value of 4–7%, with the minimum in spring and maximum in winter. The comparison of the high-resolution uncoupled CCLM08 to the coarse-resolution uncoupled CCLM44 exhibited similar patterns (not shown here). Additionally, the higher-resolution simulations showed lower sea level pressure (1.5–2 hPa) and higher pressure gradients (Fig. S5), resulting in higher wind speeds during the winter half of the year.

Figure 3.4 shows the annual cycle of basin-averaged 10-m wind speeds of different simulations and observation data. The simulated and observed wind fields attained their maximums during winter and their minimums in summer. With a fine atmospheric grid and ocean coupling, the simulated 10-m wind speeds were closest to the observation data, although coupling has an adverse impact in summer (consistent with a negative bias in SST and higher sea level pressure than without coupling).

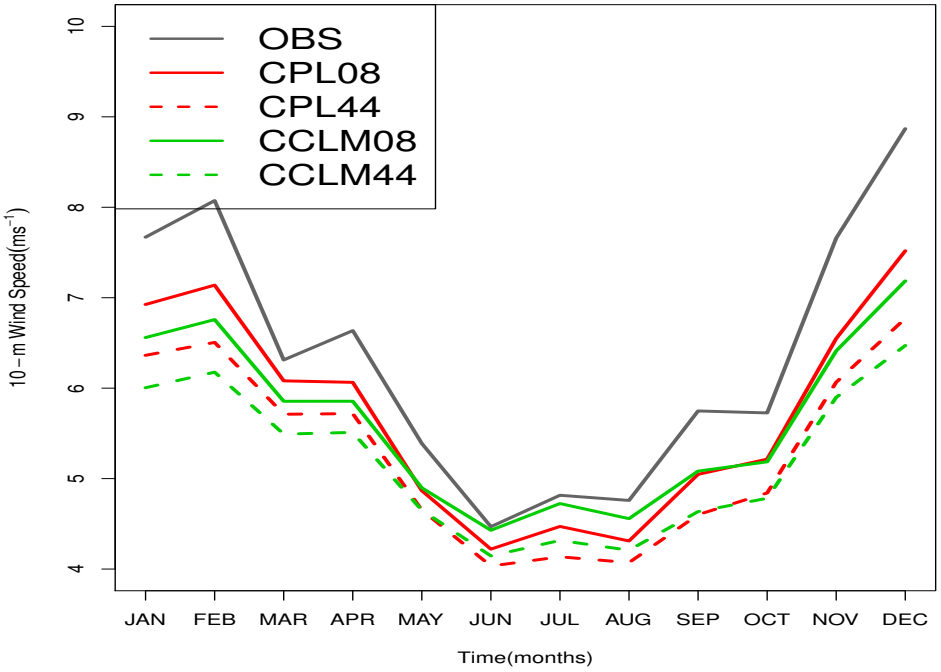

Figure 3.4: Annual cycle of 10-m wind speed ($\mathrm{m\,s^{-1}}$)

3.3.3 Sea surface heat fluxes

The Mediterranean Sea exchanges energy with the atmosphere through turbulent and radiative fluxes (Eq. 3.1). Here, we compare the NH and its components simulated in coupled CPL08 and uncoupled CCLM08 models with the OAFlux observations. Conversely, a detailed comparison of high-resolution CPL08 and coarse CPL44 is provided in the SI (Fig. S3). Additionally, the mean values for the periods 2001–2003 and 1980–2011 over the Mediterranean Sea for all the simulations are summarized in Table 1. The heat loss terms, LH, SH, and LW, are positive upward and the heat gain terms, SW and NH, are positive downward.

Figure 3.5 compares the turbulent fluxes LH and SH–as simulated with the high-resolution uncoupled CCLM08 and coupled CPL08–with the OAFlux observations. The high-resolution uncoupled CCLM08 underestimates LH in winter (MD = 31 $\mathrm{W\,m^{-2}}$) and autumn (MD = 21 $\mathrm{W\,m^{-2}}$), and it overestimates LH in summer (MD = 14 $\mathrm{W\,m^{-2}}$) and slightly overestimates LH in spring. The annual mean LH is approximately 10% smaller than the observational data (Table 3.1). The spatial patterns reveal that the differences are largest in the Gulf of Lions, the Ionian Sea, and the eastern basin of the Mediterranean Sea. The ratios of RMSE and mean observation values are 0.26, 0.11, 0.28, and 0.20 for winter, spring, summer, and autumn, respectively. The LH values in CPL08 are better; the ratios have values of 0.14, 0.19, 0.17, and 0.18, respectively. The annual mean value is approximately 5% smaller than the observational data (Table 3.1).

The SH flux is smaller than the observational data in absolute value (Table 3.1; Fig. 3.5) but larger near the northern coastlines (where the wind speed differences are large as well) compared

to other areas of the Mediterranean Sea. On average, the coupled CPL08 (20% underestimation) is better than CCLM08 (33% underestimation; Table 3.1). Table 3.1 shows that the high-resolution simulations represent the turbulent fluxes better than the coarser-resolution simulations. Turbulent fluxes are less well simulated in the coarse simulations (Table 3.1; Fig. S3).

Figure 3.6 compares the LW and SW surface radiation fluxes simulated in CCLM08 and CPL08 with the observations. Long-wave radiation is generally overestimated in winter (MD = 17–19 $W m^{-2}$; mean absolute value 73 $W m^{-2}$) and underestimated in the eastern Mediterranean Sea in summer. Short-wave radiation is overestimated by 17 and 18 $W m^{-2}$ in spring, with mean differences below 10 $W m^{-2}$ in the other seasons. Therefore, the impact of coupling is minor; there is about a 10% average error in LW and a 4% average error in SW, errors in SW and LW compensating each other. The coarser CPL44 and CCLM44 simulations are better (4 and 1% errors in LW and SW, respectively; Table 3.1) than the finer CPL08 and CCLM08 simulations (for seasonal mean comparison see S3). It should be noted that the LW observational data exhibit large inconsistencies (Sevault et al. 2014).

A comparison of simulated NHs with observation data is given in Fig. 3.7. This figure shows that CCLM08 largely overestimates NH in winter and autumn and underestimates NH in summer; smaller errors are present in spring. This situation largely occurs because of the errors in LH, which is better simulated in the coupled CPL08 (except in autumn). In absolute numbers, winter NHs are modeled most poorly because of the large errors in LH simulation. In relative numbers, the autumn NH values are worse in CCLM08 and CPL08 compared to the observations (errors of 30%). Overall, the coupled NH simulations performed better than the uncoupled, and the finer resolution simulations improve upon the coupled NH simulations.

Table 3.1 shows that there are compensating errors in the simulated SW and LW fluxes. This error compensation explains why NH is better simulated in the high-resolution models despite worse scores in radiation fluxes. This finding is also detectable in the annual cycle of NH (Fig. 3.8). Generally, in open oceans, LH controls the variability of NH when SW becomes less important (Alexander et al. 2002), which also applies to the Mediterranean Se (Josey et al. 2011; Papadopoulos et al. 2012) and is confirmed here. A better representation of LH due to the inclusion of ocean coupling results in a better representation of NH.

Table 3.1: Mean values of LH, SH, LW, SW, and NH in $W m^{-2}$ over the Mediterranean Sea of observations (OAFlux) and simulated by CPL08, CCLM08, CPL44, and CCLM44

	LH	SH	LW	SW	NH
OAFLUX (2001–2003)	100	15	79	184	-10
CPL08 (2001–2003)	95	12	86	192	-1
CPL44 (2001–2003)	94	10	82	186	0
CPL44 (1980–2011)	92	10	82	185	1
CCLM08 (2001–2003)	90	10	85	192	7
CCLM44 (2001–2003)	87	8	82	187	11
CCLM44 (1980–2011)	84	7	82	186	14

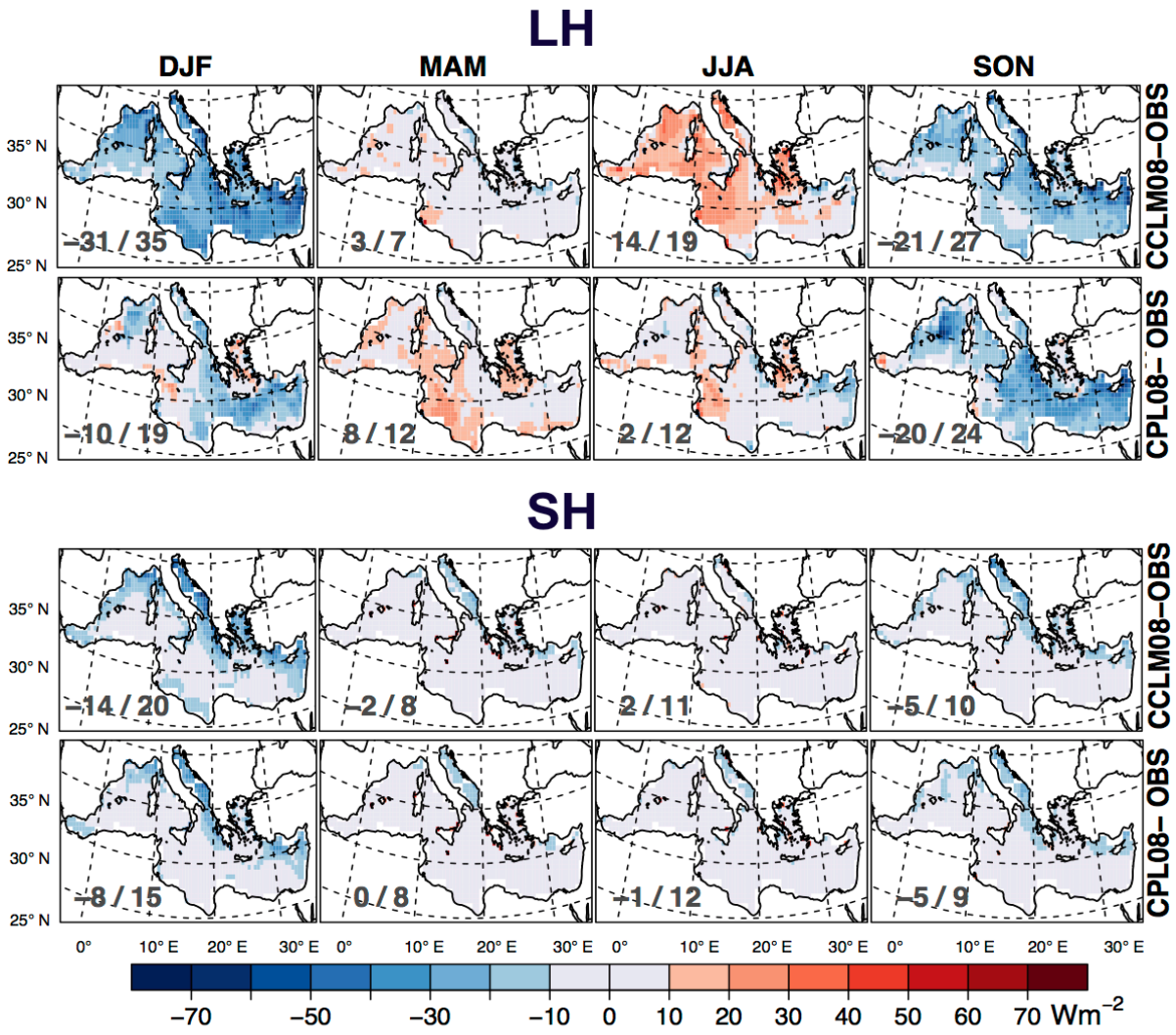

Figure 3.5: Mean differences of latent heat and sensible heat (in $\mathrm{W\,m^{-2}}$; positive upward) between uncoupled CCLM08 (*upper rows*) and coupled CPL08 (*lower rows*) with OAFlux observations for winter, spring, summer, and autumn (*columns*) in the period 2001–2003. The *numbers* given in the *panels* are the total mean differences (MD) and the mean RMSEs as MD/RMSE

The NH is balanced by the net heat through the Strait of Gibraltar, which is also known as the closure hypothesis. Using this hypothesis, Sanchez–Gomez et al. (2011) estimated NH = $-1\pm8\,\mathrm{W\,m^{-2}}$ using observational data. Given this estimate, the OAFlux value of $-10\,\mathrm{W\,m^{-2}}$ might be too negative. The mean NH values of our uncoupled simulations are probably too positive, with $7\,\mathrm{W\,m^{-2}}$ (CCLM08) and $14\,\mathrm{W\,m^{-2}}$ (CCLM44). However, the coupled simulations have mean NH values of -1 and $1\,\mathrm{W\,m^{-2}}$ in CPL08 and CPL44, respectively, and fit very well. Given the utmost importance of the sign of the NH value for the interplay between the inflow to the Strait of Gibraltar and the Mediterranean overturning circulation, the high-resolution coupled CPL08 simulation shows the most realistic estimate of NH. This finding confirms that ocean–atmosphere coupling is important for physically consistent simulations of the Mediterranean climate (e.g., Somot et al. 2008; Sevault et al. 2014).

Because the results showed the primary impact of errors in the LH simulations, we further

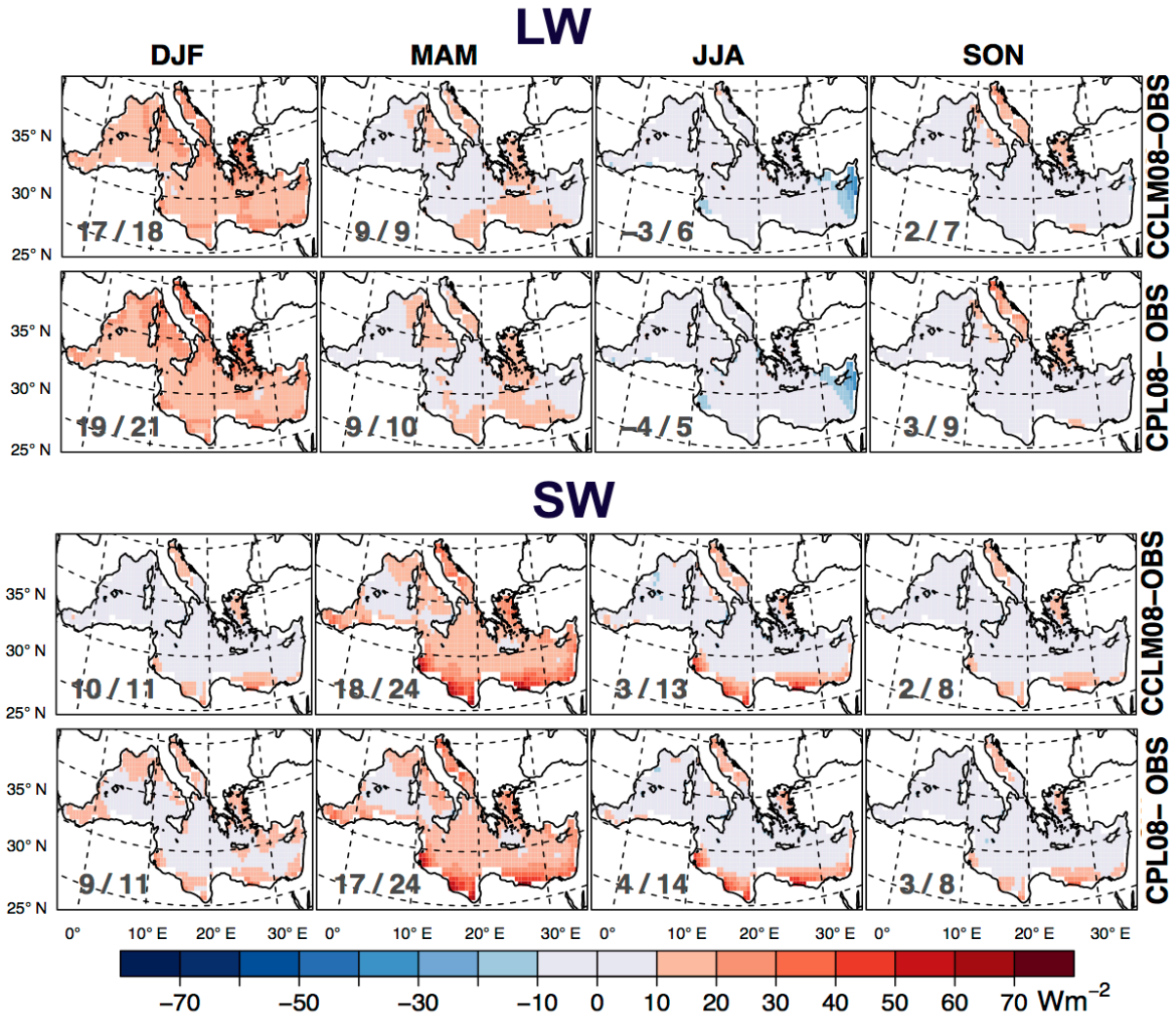

Figure 3.6: As in Fig. 3.5 but for longwave (in W m^{-2}; positive upward) and shortwave radiations (in W m^{-2}; positive downward)

investigated the important variables for its parameterization. LH largely depends on the difference between the sea surface specific humidity (Q_s) and the air specific humidity (Q_a), along with the 10-m wind speed. As discussed above, the wind speed was underestimated in all the simulations, and the best results were obtained by the high-resolution CPL08 and CCLM08. This explains why LH was better simulated in the higher-resolution setups (Table 3.1). Figure 3.9 shows that the specific humidity difference was larger (smaller) in winter (summer) in CPL08 than in CCLM08, which is consistent with warmer/colder SSTs (compare Fig. 3.1). This finding explains why CPL08 performs better than CCLM08 (Fig. 3.3; Table 3.1).

Sensible heat flux mainly depends on the difference between SST and air temperature (T_a), along with 10-m wind speed. Better wind speed simulations with high-resolution CPL08 and CCLM08 than with the coarse-resolution setups are consistent with better SH simulations (Table 3.1). Figure 3.9, row 2 shows that coupling had an impact on the temperature difference, which is larger (smaller) in winter (summer) in CPL08 than in CCLM08, which in turn influenced

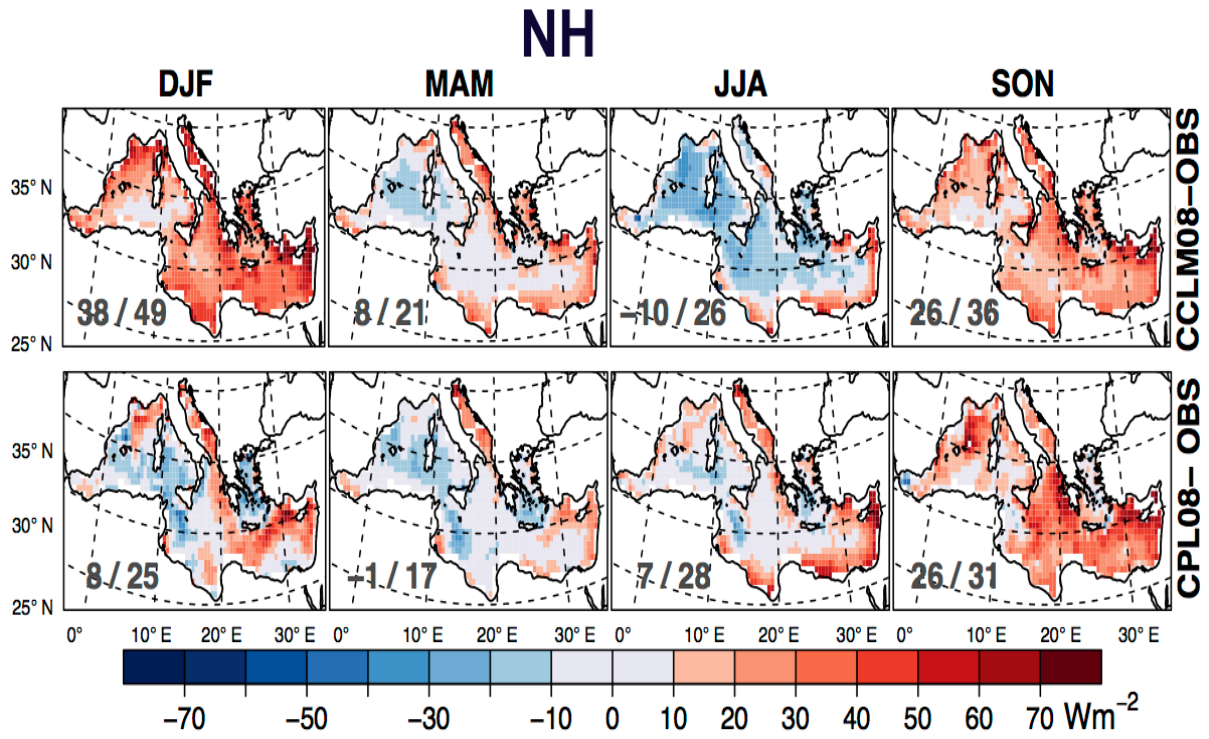

Figure 3.7: As in Fig. 3.5 but for neat heat flux (in $\mathrm{W\,m^{-2}}$; positive downward)

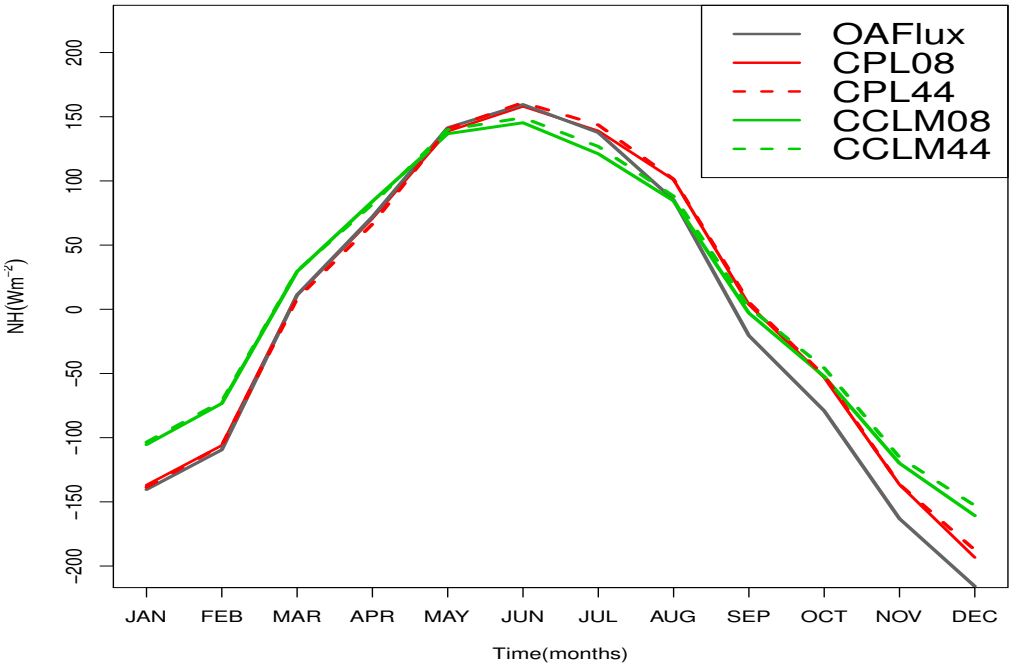

Figure 3.8: Annual cycle of neat heat flux ($\mathrm{W\,m^{-2}}$; positive downward)

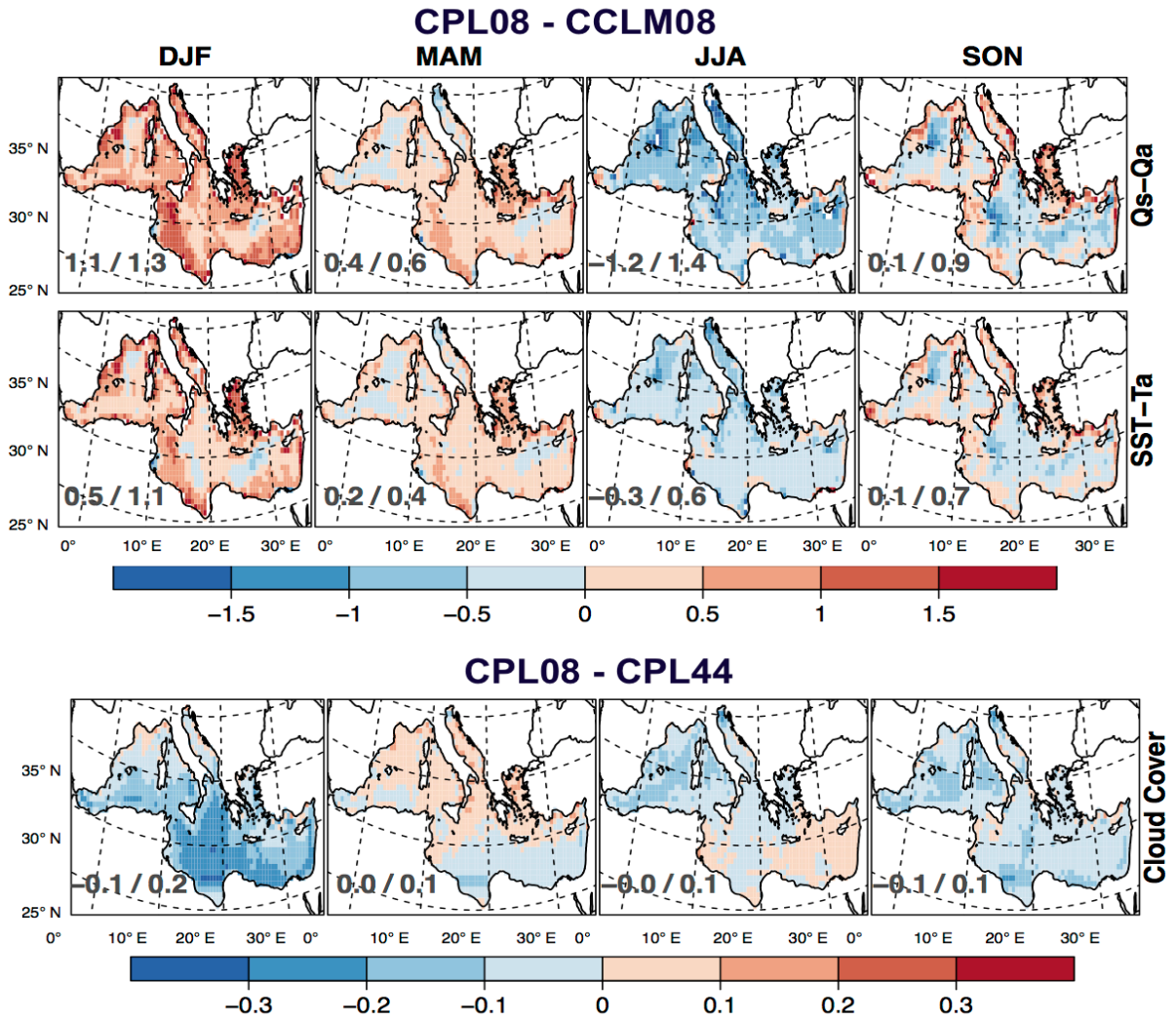

Figure 3.9: Seasonal mean differences between model set-ups of Q_s- Q_a (g/kg), SST-T_a (°C) and total cloud cover (1)

SH (Fig. 3.5; Table 3.1); CPL08 simulates the winter and annual-mean SH slightly better than CCLM08.

Ocean coupling had a minor impact on the LW and SW radiation fluxes. However, the performances of CPL08 and CCLM08 are worse than those of the coarse experiments with respect to radiative fluxes: outgoing LWs and incoming SWs are overestimated. The final row of Fig. 3.9 shows that winter cloud cover is 10% smaller in CPL08 than in CPL44. This result is remarkably consistent with the overestimated LWs in winter (Fig. 3.6). Short-wave radiation is overestimated in CPL08 and CCLM08, mainly in the spring and mainly in the southern part of the sea (Fig. 3.6). These results fit well with the cloud cover difference pattern (Fig. 3.9). Therefore, a higher resolution seems to have an adverse impact on the parameterization of clouds in COSMO-CLM.

3.3.4 SST diurnal variations

In CCLM44 and CCLM08, daily constant SST values were provided by ERA-Interim. Consequently, there was no diurnal variation in CCLM SST, except by interpolation in time and space (surface variations over land have an impact on near-coastal SSTs).

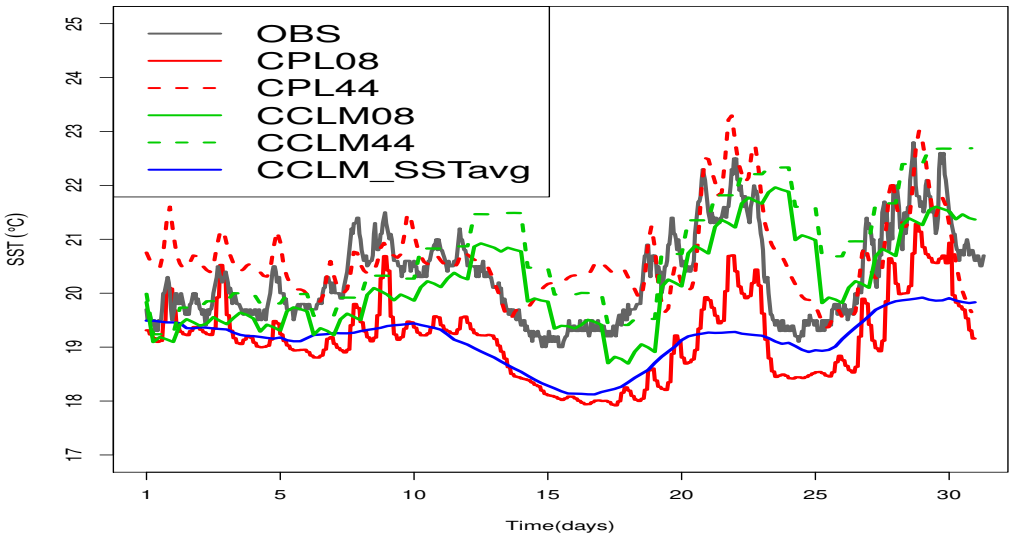

Figure 3.10: SSTs (°C) of July 2002 at Lion buoy location as simulated and observed by the buoy

This is shown in Fig. 3.10, with a clear diurnal variation in the observation data (SST measured at the Lion buoy) and in the coupled simulations. Not surprisingly, the mean SSTs of the CCLM simulation fit better than those of the CPL simulations (the bias of CPL08 and

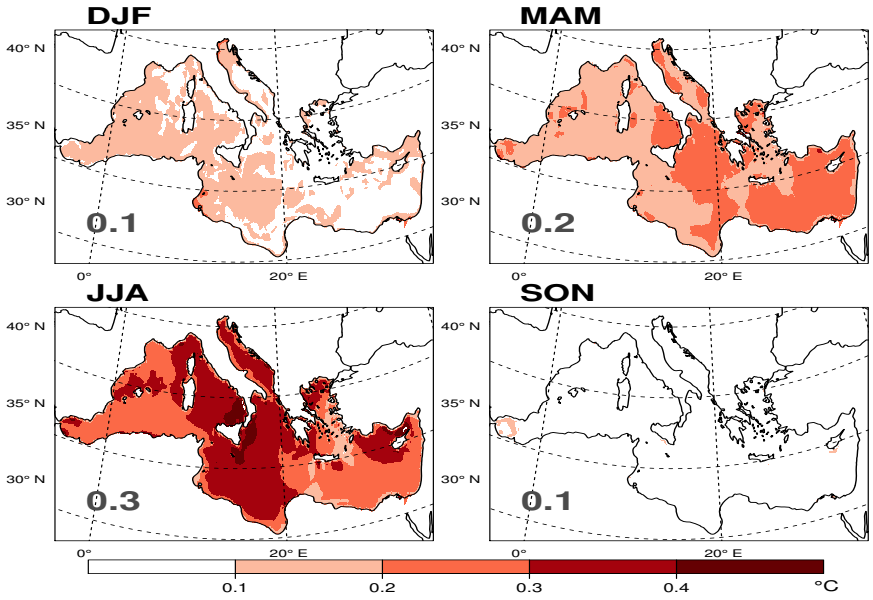

Figure 3.11: Mean SST (°C) amplitude difference between CPL08 and CCLM08_SSTavg

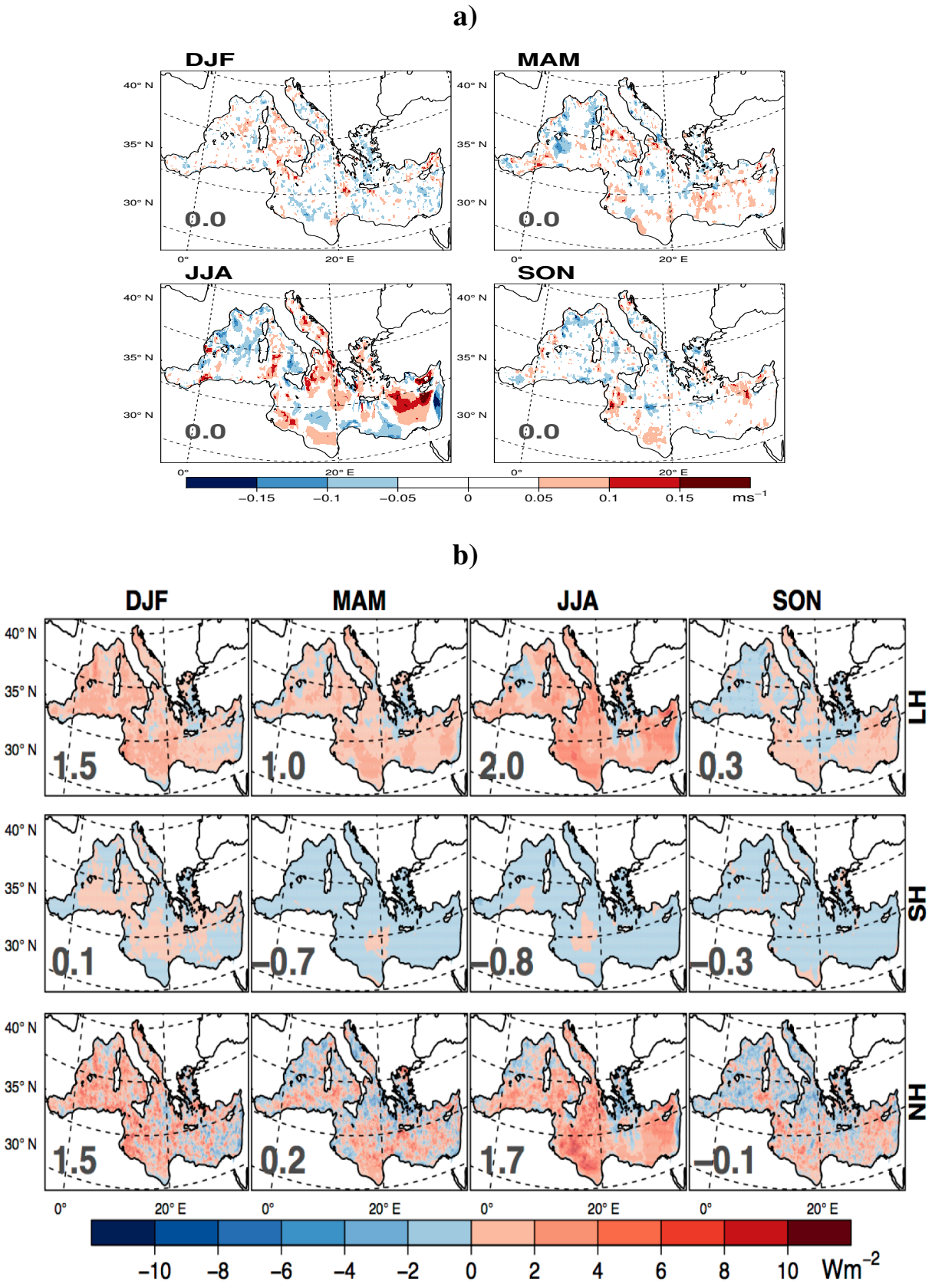

Figure 3.12: **(a)** Mean 10-m wind speed ($m\,s^{-1}$) amplitude difference between CPL08 and CCLM08_SSTavg. **(b)** Summer mean amplitude difference between CPL08 and CCLM08_SSTavg of LH, SH and NH ($W\,m^{-2}$)

CCLM08 compared with the Lion buoy data is −1.2 and −0.1 °C, respectively); this is not true, however, for the temporal variation of SST. Figure 3.11 shows the SST amplitude differences simulated by CPL08 and CCLM08_ SSTavg. The mean amplitude was highest in spring and summer seasons with 0.2 and 0.3 °C, respectively (the seasons with the largest amplitudes in NH and the smallest vertical mixing in the sea); the largest values occurred in the central Mediterranean. The minimum/maximum SST occurred at approximately 09:00/18:00 UTC. These amplitudes were on the same order of magnitude as the summer differences between the CPL08 and CCLM08 SSTs.

Therefore, we investigated the impact of sub-daily variability of SST. To this end, we smoothed the CPL08 SSTs over time (5-day block average; Fig. 3.10) and conducted an additional simulation CCLM08_SSTavg with prescribed smoothed SSTs. The diurnal variations were stronger during summer when SW radiations are higher and the ocean mixing layer depth is shallow. Figure 3.12 shows the impact of SST diurnal variations (largest during summer) on 10-m wind speed, LH, SH, and NH amplitudes. The impact on LW and SW was approximately zero (not shown here). Also, the impact on seasonal means was negligible (the summer mean differential for LH and SH between CPL08 and CCLM08_SSTavg is −0.6 and 0.6 $\mathrm{W\,m^{-2}}$ compared with a difference between CPL08 and CCLM08 of 12 and 3 $\mathrm{W\,m^{-2}}$, respectively). Therefore, SST diurnal variations were of minor importance for the mean seasonal state of the atmosphere. However, they modified the turbulent fluxes on a sub-daily timescale.

3.4 Conclusions

We have discussed the impacts of different grid-spacing (∼50 vs. ∼9 km) of the atmospheric RCM COSMO-CLM and the coupling of an ocean model (NEMO-MED12) on simulations in the Mediterranean Sea area. Our primary goal was to achieve an optimum performance of the simulations in terms of ocean–atmosphere fluxes and therefore 10-m wind speed and net heat flux components.

Our results revealed that the fine-grid simulations represent the winds better (especially near the coastlines, as also found in Obermann et al. (2018) in the western Mediterranean Sea) than the coarse-grid simulations. This fact had a positive impact on the simulation of turbulent fluxes. Coupling an active ocean model further improved the turbulent fluxes despite a simulated SST bias against available observations. Radiative fluxes were slightly better simulated using the coarser grid-spacing. This is due to the slightly worse representation of cloud cover in the high-resolution simulations. In terms of the turbulent flux simulations, both the coupled fine-grid CPL08 and coarsegrid CPL44 performed better than their uncoupled counterparts. However, CPL08 obtained the most realistic estimate of net heat flux, with a negative value consistent with observations.

With the coupled COSMO-CLM/NEMO-MED12 modeling system, we were able to simulate sub-daily SST variations. A sensitivity experiment revealed that the longterm means were only slightly affected if the daily mean SSTs were prescribed (as with using ERA-Interim SSTs) in

regional climate modeling. As shown previously in the literature, sub-daily variations are essential for extreme events such as medicanes (Akhtar et al. 2014), but given the results presented here they are of minor importance for the mean atmospheric state in the Mediterranean.

The results presented show that the cloud cover parameterization in the COSMO-CLM should be reassessed. Given the uncertainties in the radiation fluxes shown and the findings in the literature (Nabat et al. 2013), the prescription of aerosol optical depths should be investigated as well. Also, model inter-comparison within the Med-CORDEX (http://www.medcordex.eu) project could be useful for assessing the source of uncertainty and different model physics/parameterizations, but it is also necessary to have high-resolution coupled simulations over longer time periods ($\sim$30 years) to obtain robust model climatologies. Further, this study could be extended to investigate the impact of sub-daily variations in SST on extreme events such as heavy precipitation and medicane events. Finally, a highresolution coupled system, such as the one presented here, could be useful for studying the impact of climate change in the Mediterranean region.

Acknowledgements

The authors would like to thank the Center for Scientific Computing (CSC) of the Goethe University Frankfurt am Main and the Deutsches Klimarechenzentrum (DKRZ) for providing computational facilities. B. Ahrens acknowledges support by Senckenberg Biodiversity and Climate Research Centre (BiK–F), Frankfurt am Main. We acknowledge Cindy Lebeaupin Brossier, Jonathan Beuvier, Thomas Arzouse, Samuel Somot and Philippe Drobinski for their help regarding NEMO-MED12 and French GIS and GMMC which have supported NEMO-MED12 model. B. Ahrens and N. Akhtar acknowledge the support from the German Federal Ministry of Education and Research (BMBF) under grant MiKliP II (FKZ 01LP1518C). This work is part of the Med-CORDEX initiative (http://www.medcordex.eu) supported by the HyMeX (https://www.hymex.org/).

Supplementary Information (SI)

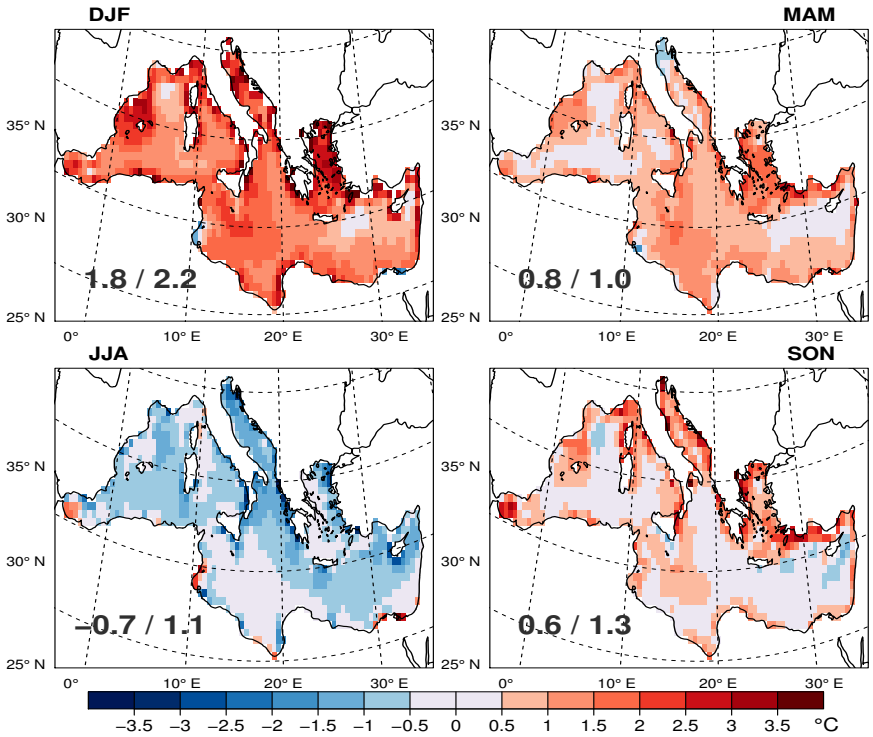

Figure S1: Seasonal mean difference of SST (°C) between CPL44 and CCLM44 in the period 1980–2011

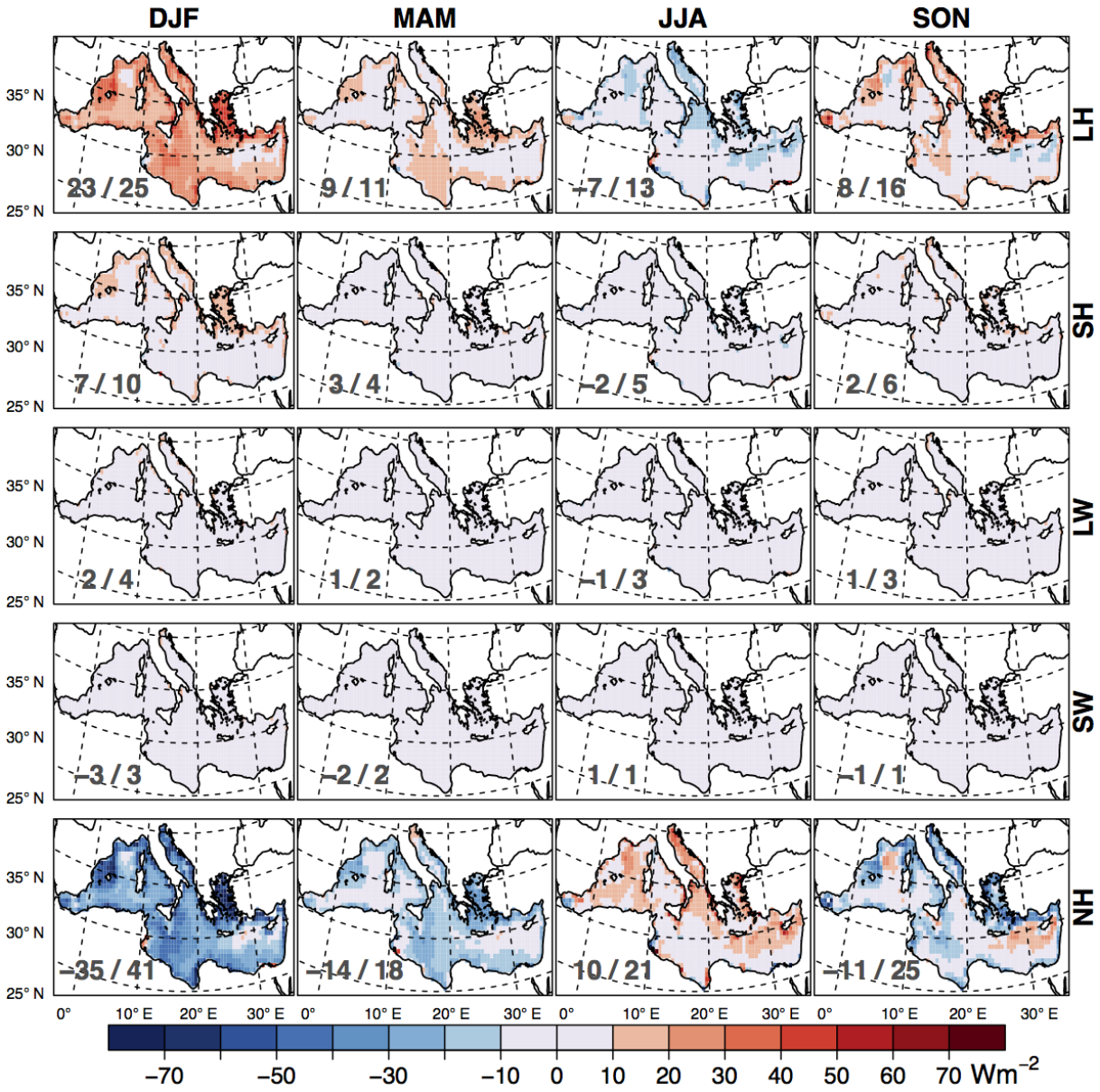

Figure S2: Mean differences in NH and its components (in $\mathrm{W\,m^{-2}}$) between CPL44 CCLM44 for winter, spring, summer, and autumn (*columns*) in the period 1980–2011. The rows show the differences of LH, SH, LW (positive upward), SW and NH (positive downward) respectively. The *numbers* given in the *panels* are the total mean differences/the spatial RMSEs

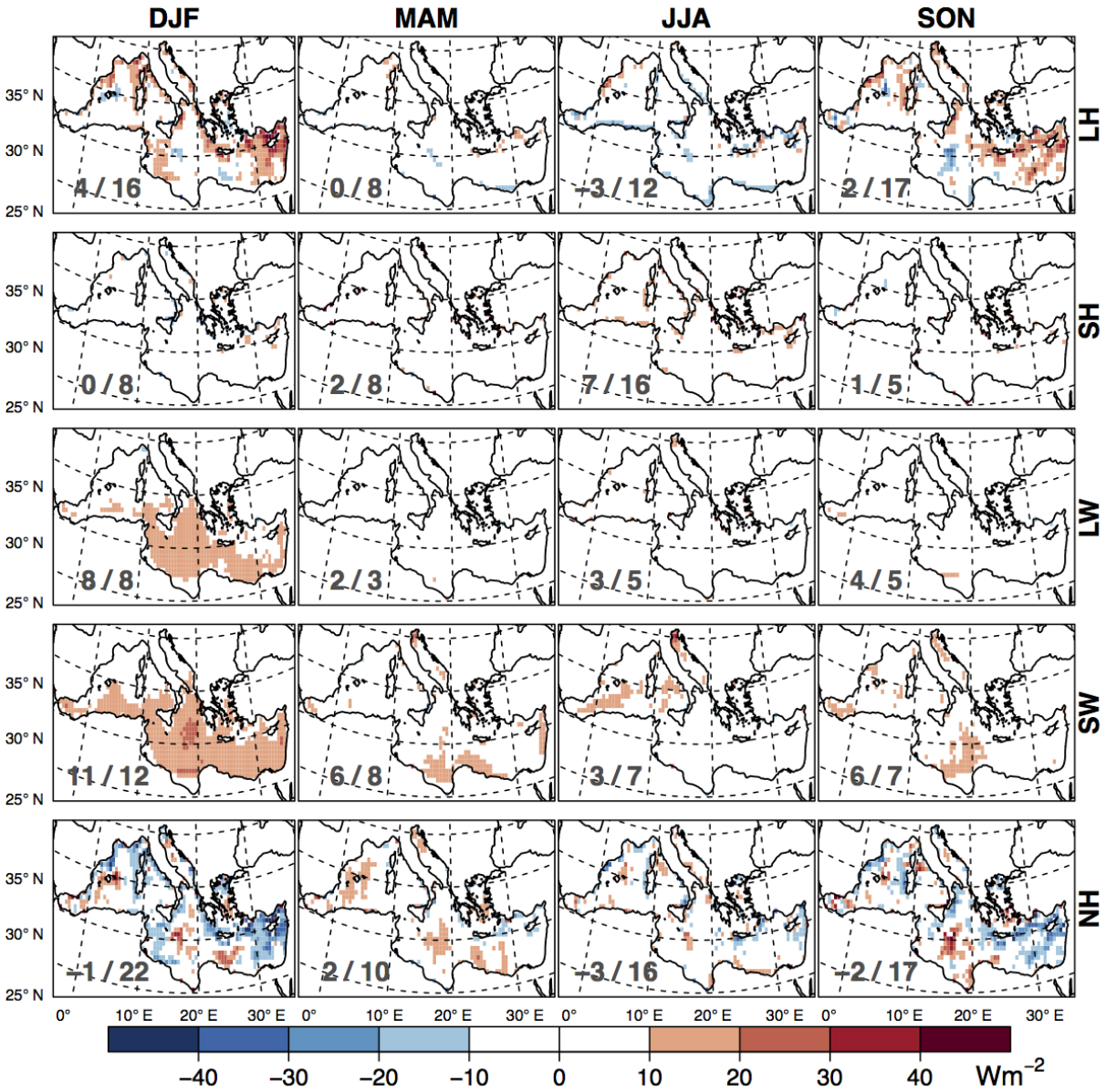

Figure S3: Mean differences in NH and its components (in $\mathrm{W\,m^{-2}}$) between CPL08 and CPL44 for winter, spring, summer, and autumn (*columns*) in the period 2001-2003. The rows show the differences of LH, SH, LW, SW and NH (positive downward) respectively. The *numbers* given in the *panels* are the total mean differences/the spatial RMSEs

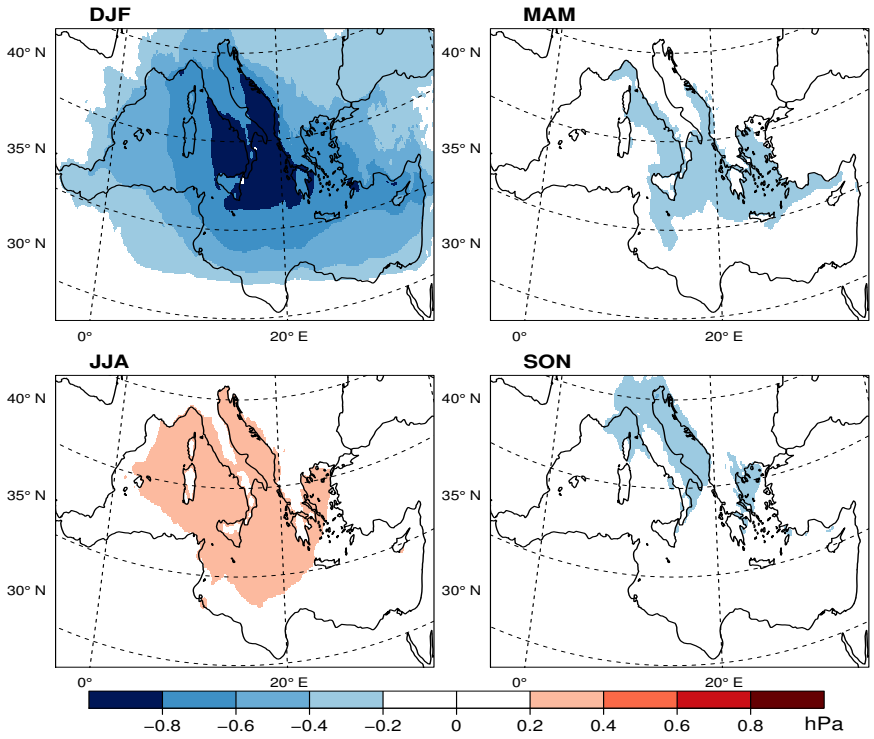

Figure S4: Seasonal mean difference of mean sea level pressure (hPa) between CPL08 and CCLM08 for the period 2001–2003

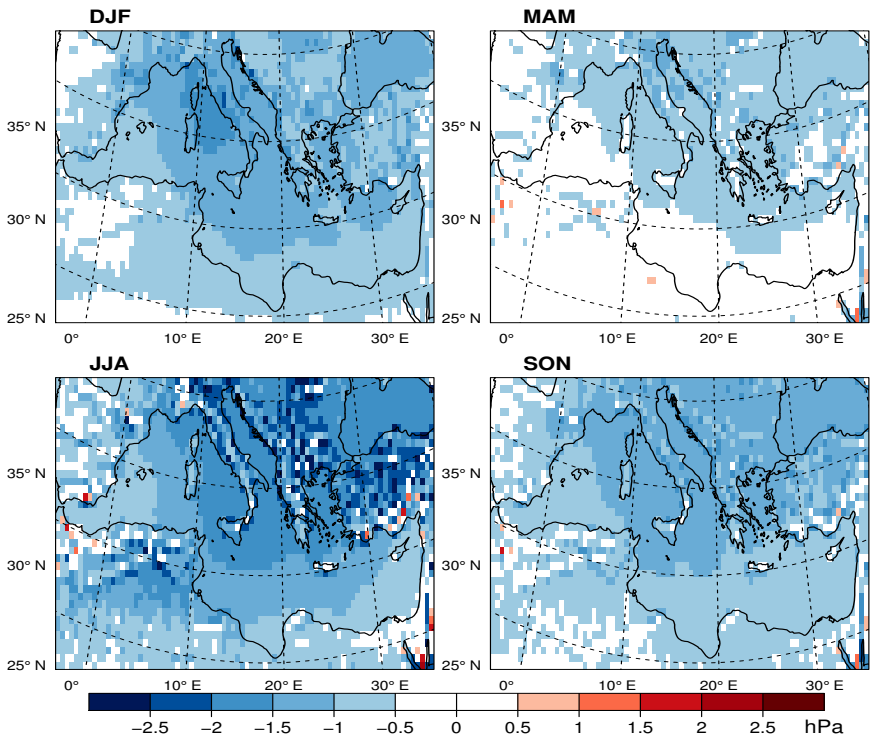

Figure S5: Seasonal mean difference of mean sea level pressure (hPa) between CPL08 and CPL44 for the period 2001–2003

CHAPTER 4

Medicanes in an ocean–atmosphere coupled regional climate model[1]

Abstract

So-called medicanes (Mediterranean hurricanes) are meso-scale, marine, and warm-core Mediterranean cyclones that exhibit some similarities to tropical cyclones. The strong cyclonic winds associated with medicanes threaten the highly populated coastal areas around the Mediterranean basin. To reduce the risk of casualties and overall negative impacts, it is important to improve the understanding of medicanes with the use of numerical models. In this study, we employ an atmospheric limited-area model (COSMO-CLM) coupled with a one-dimensional ocean model (1-D NEMO-MED12) to simulate medicanes. The aim of this study is to assess the robustness of the coupled model in simulating these extreme events. For this purpose, 11 historical medicane events are simulated using the atmosphere-only model, COSMO-CLM, and coupled model, with different setups (horizontal atmospheric grid spacings of 0.44, 0.22, and 0.08°; with/without spectral nudging, and an ocean grid spacing of 1/12°). The results show that at high-resolution, the coupled model is able to not only simulate most of medicane events but also improve the track length, core temperature, and wind speed of simulated medicanes compared to the atmosphere-only simulations. The results suggest that the coupled model is more proficient for systemic and detailed studies of historical medicane events, and that this model can be an effective tool for future projections.

4.1 Introduction

The Mediterranean Sea is known to be one of the main cyclogenetic regions in the world (Pettersen 1956; Hoskins and Hodges 2002; Wernli and Schwierz 2006). A certain type of cyclone in the Mediterranean Sea with physical and structural similarities to tropical cyclones is known as a medicane (Mediterranean hurricane). Medicanes are meso-scale cyclones (the diameter is usually less than 300 km), with a rounded structure and a cloudless area at the center. Other features include a warm core and intense low sea level pressure, combined with strong cyclonic

[1] **Published as:** Akhtar N, Brauch J, Dobler A, Béranger K, Ahrens B (2014) Medicanes in an ocean–atmosphere coupled regional climate model. Nat Hazards Earth Syst Sci 14:2189–2201. doi:10.5194/nhess-14–2189–2014

winds and heavy rainfall (Businger and Reed 1989). In general, the intensity of medicanes is much weaker than tropical hurricanes (Moscatello et al. 2008); however, a few medicanes have reached tropical hurricane strengths ($33\,\mathrm{m\,s^{-1}}$). Strong surface heat fluxes and deep convection are important initial conditions in the formation of medicanes. The triggering mechanisms involved in this development are the presence of cold anomalies in the high troposphere, surface heat fluxes (latent and sensible), low wind shear, and high low-level vorticity (Cavicchia et al. 2014a). According to Trenberth (2005), the minimum value of sea surface temperature (SST) to develop a tropical hurricane is 26 °C. However, in 2005 hurricane Vince developed on 24 °C SST (www.nhc.noaa.gov/archive/2005/dis/al232005.discus.001.shtml). Studies show that the SST has to be higher than 15 °C for medicanes (Tous and Romero 2013). As with tropical hurricanes, the air-sea temperature difference plays an important role in the development of medicanes (Palmen 1948; Miglietta et al. 2011). In the case of tropical hurricanes, SST creates the conditions of thermodynamical disequilibrium that trigger the development of a vortex, whereas in the case of medicanes, the interplay between the temperature at the surface and upper atmospheric layer plays a key role in their development (Cavicchia et al. 2014a). The ocean also plays an important role in the intensity of tropical cyclones (Emanuel 1986; Emanuel and Rotunno 1987); similarly, the ocean feedback is also crucial in the development of medicanes. Table 4.1 shows a list of medicane events from 1983 to 2003, their approximate times of mature phase, sizes and geographical positions (Tous and Romero 2013). Spatially, the central and western parts of the Mediterranean Sea are the main genesis regions of medicanes. Most of the events occurred during autumn and winter, but some were observed during the spring season.

Medicanes have a high potential for destruction in the densely populated coastal areas around the Mediterranean Sea. To reduce the risk of casualties and overall negative impacts, better knowledge of medicanes is essential for potential prediction. Due to their meso-scale and marine characteristics, medicanes are not well represented in automatic detection methods. The lack of dense observations over sea, and the occasional occurrence of medicanes make it more difficult to recognize meteorological features associated with them (Tous and Romero 2013). Surface observations of such storms are limited to ships crossing nearby; in situ weather reports are generally poor. One of the main sources of observations of medicanes with full coverage are satellite images available since 1980. Several studies have been carried out based on the observational evidence (e.g., Ernst and Matson 1983; Rasmussen and Zick 1987; Luque et al. 2007; Moscatello et al. 2008) and combined, model and observations (e.g., Miglietta et al. 2013; Conte et al. 2011). Most of the contemporary modeling studies on medicanes are done by dynamical downscaling using regional atmosphere-only models (e.g., Homar et al. 2003; Fita et al. 2007; Miglietta et al. 2011; Cavicchia et al. 2014a).

Coarse global climate models cannot fully resolve the complex orography and other important local processes such as the bora, mistral, and Etesian winds, and the deep-water formations that characterize the Mediterranean region. Therefore, the air-sea fluxes over this region are not correctly represented in a coarse global climate model (Elguindi et al. 2011). Recent studies show that high-resolution coupled models over the Euro-Mediterranean region significantly

Table 4.1: Code, date, approximate time of mature phase and geographical coordinates of medicane centers from 1983 to 2003 (Tous and Romero 2013)

Code	Date	Time (UTC)	Lat (° N)	Lon (° E)	Maximum diameter (km)	Lifetime (h)
ME01	29 Sep 1983	12:00	41.1	6.8	220	90
ME02	7 Apr 1984	06:00	36.4	19.2	230	36
ME03	29 Dec 1984	06:00	35.4	11.6	220	60
ME04	14 Dec 1985	12:00	35.5	17.6	290	54
ME05	5 Dec 1991	12:00	36.2	16.7	320	30
ME06	15 Jan 1995	18:00	36.4	19.1	300	78
ME07	12 Sep 1996	12:00	39.4	2.8	170	12
ME08	6 Oct 1996	18:00	37.2	3.9	240	90
ME09	10 Dec 1996	00:00	40.3	3.7	230	48
ME10	26 Jan 1998	12:00	36.7	17.9	250	30
ME11	19 Mar 1999	06:00	38.5	19.6	250	30
ME12	27 May 2003	00:00	40.1	2.8	280	42

improve the representation of air-sea fluxes (Gualdi et al. 2012; Dubois et al. 2012; Artale et al. 2010; Somot et al. 2008). In another study, Sanna et al. (2013) have shown that SSTs simulated through a high-resolution eddy-permitting ocean model have strong and beneficial effects on precipitation and cyclogenesis simulation.

The SSTs in regional atmosphere-only runs are prescribed and derived from reanalysis data such as the European Center for Medium-Range Weather Forecasts (ECMWF) Reanalysis Interim (ERA-Interim), which also include satellite observations. The quality of SSTs in this reanalysis is in good agreement with the observations (Simmons et al. 2006). However, due to the small size and short lifetimes of medicanes, the quality of the reanalysis data is compromised by the coarse time and space resolution. Most reanalysis datasets are available in 6-h intervals, whereas medicanes occur on short timescales (ranging from 12 to 90-h). Fine-scale feedback associated with air-sea interactions can influence the temporal and spatial structure of medicanes. A fully coupled regional model with adequate resolution could be useful for future projections and historical evaluation of these extreme events.

In the present study, a regional atmosphere-only and coupled model are examined for their robustness and stability in simulating the formation and life cycle of medicanes using different setups (horizontal grid spacings of 0.44, 0.22, and 0.08°and an ocean grid spacing of 1/12°). By applying spectral nudging to the atmospheric model, the same medicane events are also simulated in both coupled and atmosphere-only setups. The primary goal of this study is to investigate the impact of the air-sea interactions in the coupled model on the intensity of medicanes, as compared to the atmosphere-only model and adequate atmospheric grid resolution essential to resolve medicane features.

4.2 Experimental setup

In this study, the regional climate model COSMO-CLM v4.8 (CCLM), based on non-hydrostatic equations (Rockel et al. 2008), is used for the atmosphere-only simulations, and a recently developed regional ocean–atmosphere coupled model – consisting of an atmosphere component, CCLM, and an ocean component, NEMO-MED12 v3.2 – is used for the coupled simulations. The NEMO-MED12 is the regional part of the global ocean model NEMO v3.2 (Madec and NEMO Team 2008), specially tuned for the Mediterranean Sea (for more details see, e.g., Lebeaupin et al. 2011). Along with a full three-dimensional (3-D) configuration, the NEMO system also includes a one-dimensional (1-D) configuration that simulates a stand-alone water column. The 1-D NEMO can be applied to the ocean alone or to the ocean–ice system (Akhtar 2013). Vertical exchange processes across the air-sea boundary and vertical mixing throughout the water column affect the local conditions more rapidly and effectively than horizontal advection and mixing processes on short timescales (up to 1 year) (Niiler and Kraus 1977). Therefore, the horizontal gradients are assumed to be zero between water columns in 1-D models. The 1-D models can perform multiple model simulations in a relatively short time with simplified dynamics. In contrast, 3-D ocean models are computationally expensive and time-consuming, but include full 3-D dynamics. The 1-D models are very useful for short time simulations, especially in coupled ocean–atmosphere modeling, to investigate extreme events. The validation of a 1-D compared to a fully 3-D configuration has been conducted in a previous study (Akhtar 2013). The 1-D NEMO-MED12 is now coupled via the OASIS3 coupler (Valcke 2013) to CCLM. The 1-D NEMO-MED12 is employed with a basin-wide (covering the whole Mediterranean Sea and part of the Atlantic Ocean), single-column approach where each water column is isolated from the others. Each grid point in the 1-D NEMO-MED12 is treated as a single water column. The coupling process is executed every hour, where 1-D NEMO-MED12 passes SST to CCLM and, in exchange heat, momentum, and freshwater fluxes are obtained. A similar setup has been used by Van Pham et al. (2014) for the North and Baltic seas.

Different resolutions of CCLM – 0.44° (∼50 km; 118×83 grid points, and 32 σ levels), 0.22° (∼25 km; 206×120 grid points, and 32 σ levels), and 0.08° (∼9 km; 536×295 grid points, and 40 σ levels) that cover the Med-CORDEX domain (`www.medcordex.eu`) – are employed. For both the coupled and atmosphere-only simulations, the horizontal diffusion parameters in CCLM are tuned for better realization of medicanes. The factors to reduce the standard coefficient for numerical diffusion in case of humidity, cloud water, temperature and pressure smoothing are set to zero. The Runge–Kutta numerical scheme in CCLM is used for both the coupled and atmosphere-only simulations. The 1-D NEMO-MED12 has a resolution of 1/12° (∼6 to 8 km in latitude and ∼8.5 km in longitude, 567×264 grid points, and 50 vertical levels), which remains the same for all the coupled runs. The atmospheric model uses ERA-Interim reanalysis data from the ECMWF for both the coupled and atmosphere-only runs. However, in the coupled runs, SST over the Mediterranean Sea is calculated by 1-D NEMO-MED12 and elsewhere prescribed and derived from the reanalysis data. The monthly mean seasonal climatology from MEDATLAS–II

(Rixen 2012) is used to initialize 1-D NEMO-MED12.

The coupled and atmosphere-only models are used to simulate the historically listed medicane events from 1983 to 1999 (Table 4.1), at three different resolutions (0.44, 0.22, and 0.08°). The same set of simulations are also performed with the spectral nudging technique (Von Storch et al. 2000). In a study, Cavicchia and von Storch (2012) showed that the performance of CCLM to simulate the medicanes could be improved by applying the spectral nudging technique, particularly the spatial and temporal locations of the simulated medicanes. The spectral nudging was applied on the wind field components above 850 hPa in the interior domain with the aim to keep the large-scale circulation close to the reanalysis data (Cavicchia and von Storch 2012). The spectral nudging was applied at scales coarser than four ERA-Interim grid lengths. The wind field components at the lower levels are free to interact with local orography and other surface roughness features. The purpose of employing spectral nudging is to analyze its impact on the coupled simulations, as compared to the atmosphere-only simulations, and not to address the time and location of simulated medicanes. The main aim of this study is to examine the ability of the coupled model to simulate the medicanes compared to the atmosphere-only simulations with and without spectral nudging, and to validate it with observations.

Except the differences in atmospheric grid resolutions (0.44, 0.22, and 0.08°), all other configurations of CCLM remain the same in all the atmosphere-only and coupled without spectral nudging simulations. The same holds for spectral nudging simulations. For the remainder of this discussion, we used the abbreviations "CPLXXYY" for the coupled, and "CCLMXXYY" for the atmosphere-only simulations, where "XX" refers to the resolution ("44" for 0.44°, "22" for 0.22°, and "08" for 0.08°), and "YY" refers to spectral nudging ("sn").

Based on the satellite (infrared Meteosat) imagery analysis, 12 cases are documented from 1983 to 2003 (Table 4.1). The selection criteria of these events were based on cloud structure, size, and lifetime of the cyclones (Tous and Romero 2013). Because of the limited availability of the MEDATLAS–II climatology (1945–2002), only the first 11 medicane events from 1980 to 1999 are included in this study. Since the last event occurred in 2003 (Table 4.1), MEDATLAS–II climatology is not available to initialize the ocean model. For each medicane event, both the coupled and atmosphere-only simulations with and without spectral nudging are conducted over a period of 1 month, starting approximately 3 weeks prior to formation of the medicane. The reason of starting simulations 3 weeks before the medicane formation is to have a couple of weeks ocean spin-up in the coupled simulations. To be consistent with the coupled simulations, we used the same period in the atmosphere-only simulations (with ERA-Interim SST forcing).

The following datasets are used for validation:

- For wind speed, the NOAA "SeaWinds" dataset, available from 9 July 1987 to the present, is used. The product contains global high-resolution ocean winds and wind stresses at 6-h intervals on a 0.25° grid (Zhang et al. 2006). SeaWinds are generated by blending observations from multiple satellites.

- For sea level pressure and temperature, NASA's MERRA reanalysis (Rienecker et al. 2011), presently available from 1 January 1979 to 30 September 2013, is used. The state-of-the-art

MERRA reanalysis products are available globally for 6-h intervals at 0.5° resolution, and 42 vertical levels.

4.3 Results and discussion

In this section, we discuss the ability of the coupled and atmosphere-only model to simulate the medicanes at different resolutions with and without applying the spectral nudging technique. The meteorological variables, sea level pressure, temperature at mid-troposphere (in our case, 700 hPa level), and 10-m wind speeds, are analyzed. To simulate a medicane, one needs to find intense sea level pressure minima, a warm core at mid-troposphere, and strong cyclonic winds (Tous et al. 2013). The medicane tracks are constructed by following the sea level pressure minima in hourly model outputs in a grid box with less than 40% of land fraction. The same method is used to construct the medicanes track in the MERRA reanalysis data. Due to the coarse temporal resolution of the MERRA reanalysis data (6-h), it is not possible to track the full trajectories of medicanes. Therefore, only approximated tracks are shown here for MERRA reanalysis. Although the spatial resolution of the MERRA reanalysis data is coarse (0.5°), medicane features such as mean sea level pressure and warm-core structure are reasonably well represented due to the assimilation of observations such as satellite data. For the medicane's starting and ending times, we took the information available from satellite images on the website http://meteorologia.uib.eu/medicanes/.

We selected 4 different cases from 11 simulated medicane events for detailed validation and discussion. Our choices are motivated by the locations and sizes of these particular medicane events. We chose two cases (ME08 and ME09) from the western region of the Mediterranean Sea, and two (ME06 and ME10) from the central region. Two cases, ME06 from the central region and ME08 from the west, had maximum lifetimes, and two cases, ME10 from the central region and ME09 from the west, had intermediate lifetimes (Table 4.1). Due to unavailability of the NOAA dataset before 9 July 1987, only cases that occurred after 1988 were selected.

4.3.1 Case ME08

The ME08 case was recorded to have a lifetime of 90-h, making it one of the longest listed medicane events (Table 4.1). The medicane started to develop north of Algeria and reached maximum strength while it was moving between the Balearic Islands and Sardinia. Strong winds and severe damage were reported in the Aeolian Islands (north of Sicily). The medicane crossed Calabria and dissipated after making landfall in the coastal regions of Greece. The snapshots of coupled simulations at the three resolutions mentioned above, on 6 October at 03:00 UTC (30 min before the development of ME08), show a large-scale baroclinic disturbance that evolved over the western part of the Mediterranean Sea (Fig. 4.1). This intrusion of cold air into the upper and mid-troposphere can favor the development of medicanes. The synoptic-scale analysis shows that medicanes are not fully isolated structures of atmospheric circulation (Emanuel 2005; Homar

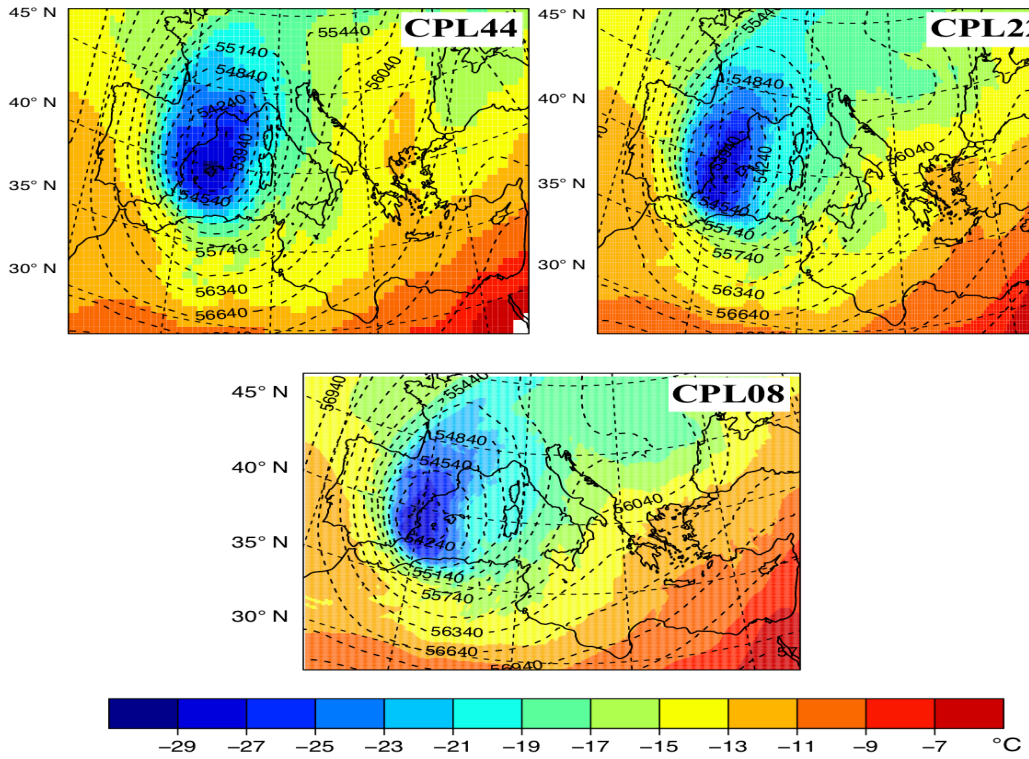

Figure 4.1: ME08; geopotential height ($m^2\,s^{-2}$; dotted contours lines at 300 $m^2\,s^{-2}$ intervals) and temperature (°C; colored contours at 2 °C intervals) at 500 hPa in the coupled (0.44, 0.22, and 0.08°) simulations on 6 October 1996 at 03:00 UTC

et al. 2003; Pytharoulis et al. 2000). Two dynamical processes are involved in the development of medicanes: the first phase is dominated by the baroclinic development, and the second is driven by convective tropical-like activity and air-sea interactions. The large-scale disturbance is well represented in CPL44, CPL22, and CLP08 simulations, and similar results are also observed in CCLM44, CCLM22, and CCLM08 (not shown here). According to the satellite observations, on 6 October at 03:30 UTC, the disturbance turned into a medicane that reached its mature phase at 18:00 UTC (Table 4.1). Figure 4.2 shows the mean sea level pressure and temperature in the mid-troposphere (700 hPa pressure level) on 7 October, at 18:00 UTC, along with the medicane track (black dots). In this case the medicane eye developed twice (7 October at 06:30 UTC and 8 October at 12:00 UTC). In CPL44 and CCLM44 simulations, the typical medicane signals (such as intense mean sea level pressure, warm core and cyclonic winds) are not found.

However, the medicane track is reasonably well represented in CCLM22 and CPL22, and even finer and more intense in CPL08 and CCLM08 (Fig. 4.2). The length of the simulated medicane track in CPL22 is shorter (74-h) compared to CCLM22 (90-h). The lowest minimum sea level pressure values, lifetimes, and start and end dates of all the simulated medicanes are shown in Table 4.2.

The track and warm-core structure of the medicane are better resolved and represented in 0.08° simulations, and are in good agreement with the MERRA reanalysis data (Fig. 4.2). This is due to the meso-scale characteristic of medicanes, which are not fully resolved at low resolutions

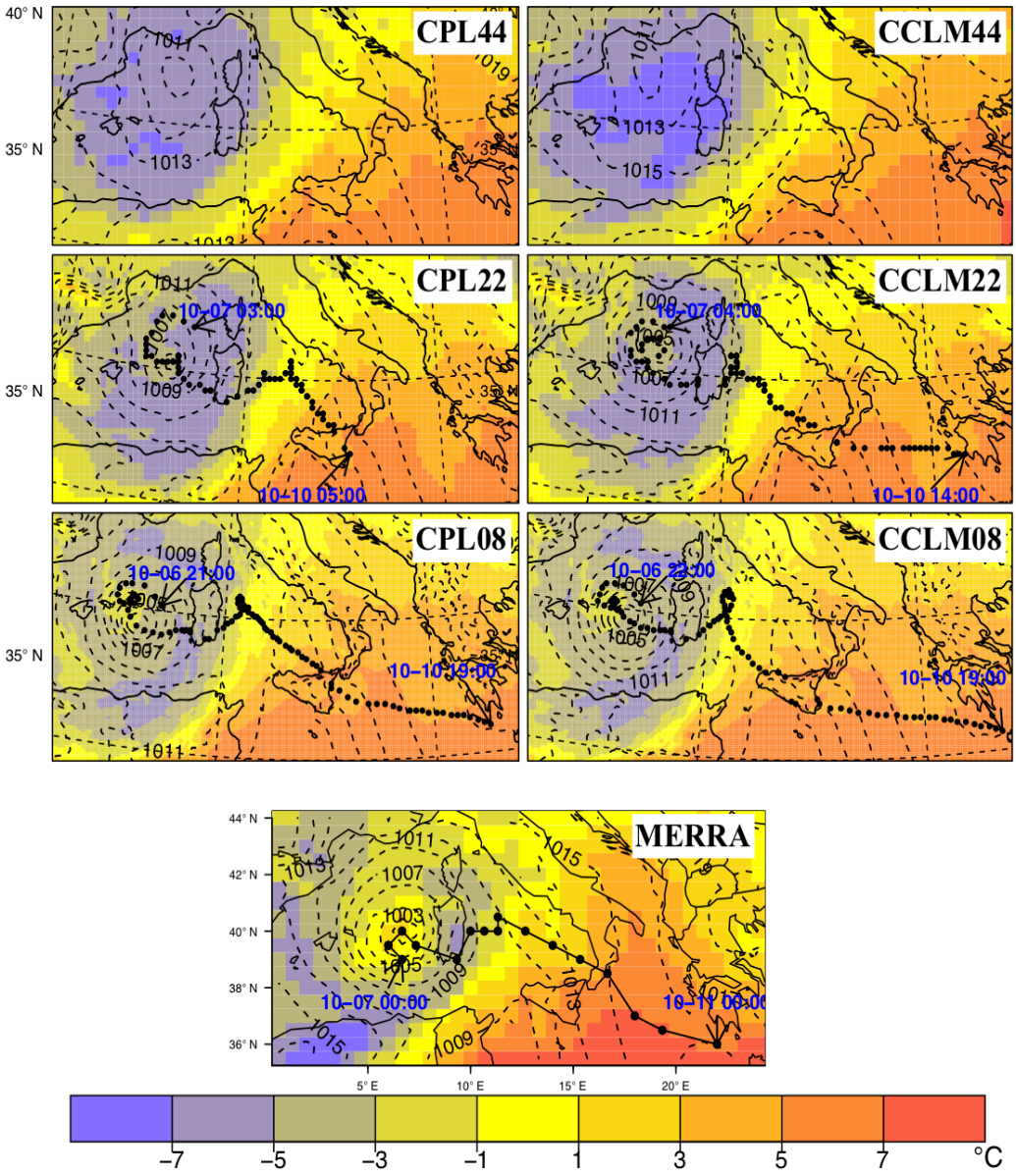

Figure 4.2: ME08; mean sea level pressure (hPa; dotted contours lines at 2 hPa intervals) and temperature (°C; colored contours at 2 °C intervals) at 700 hPa in the coupled and atmosphere-only (0.44, 0.22, and 0.08°) simulations and the MERRA reanalysis data on 7 October 1996 at 18:00 UTC. Black dots represent track of the medicane

(0.44 and 0.22°). The sea level pressure minimum appeared 1-h earlier in CPL08 compared to the CCLM08 simulations, and the warm core is more prominent in the CPL08 simulations. The medicane track length in CPL08 is 94-h, 92-h in CCLM08 and 72-h in MERRA reanalysis (Table 4.2). The medicane track in CPL08 is improved compared to CCLM08, and according to the MERRA reanalysis, with a more accurate position near the Sicily channel.

Figure 4.3 shows the wind speed patterns in all the simulations (0.44, 0.22, and 0.08°) of the ME08 event and the NOAA dataset on 7 October at 18:00 UTC. The high wind speeds associated with the medicane are not observed in the CPL44 and CCLM44 simulations. Compared to this, the wind speeds in the CPL22 and CCLM22 simulations are slightly improved, but still do not

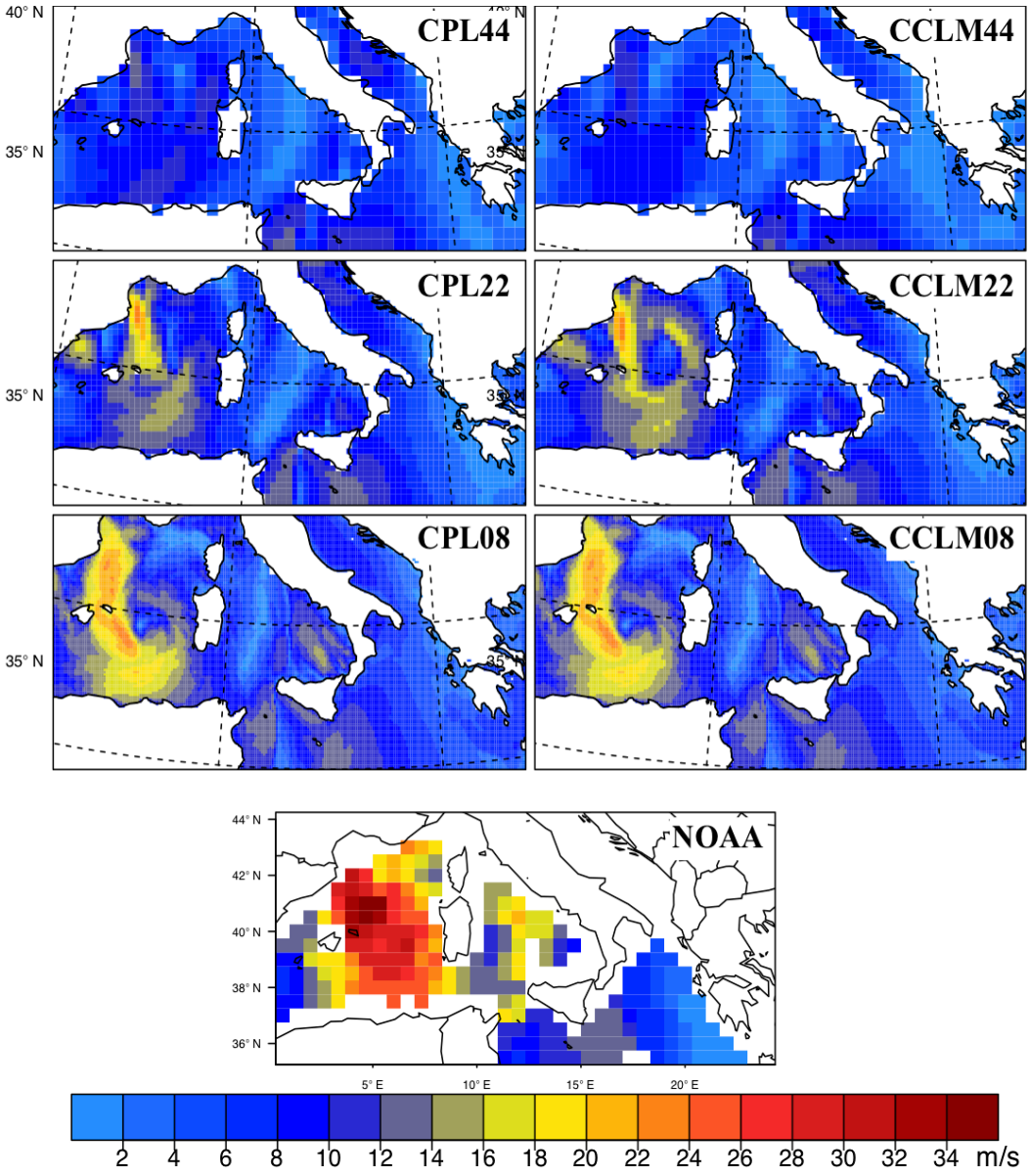

Figure 4.3: ME08; 10-m wind speed ($m\,s^{-1}$) in the coupled and atmosphere-only (0.44, 0.22, and 0.08°) simulations and the NOAA "Blended Sea Winds" on 7 October 1996 at 18:00 UTC

match the high values of the NOAA dataset. There is further improvement at 0.08° resolution; however, the maximum wind speed still does not match the maximum of 34 $m\,s^{-1}$ seen in the NOAA dataset. The wind speed patterns in the coupled simulations (CPL08) are more intense compared to the atmosphere-only (CCLM08) simulations, and the structures are more delicate. According to Cavicchia and von Storch (2012), the high wind speeds recorded in the NOAA dataset may be due to mistral winds, which are not well resolved in simulations.

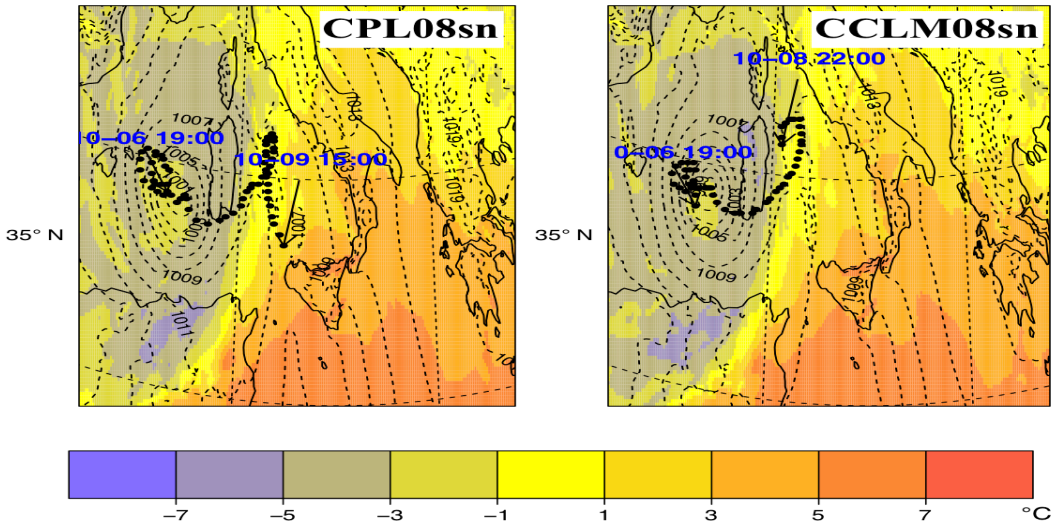

Figure 4.4: ME08; mean sea level pressure (hPa; dotted contours lines at 2 hPa intervals) and temperature (°C; colored contours at 2 °C intervals) at 700 hPa in the coupled and atmosphere-only (0.08°) with spectral nudging simulations, on 7 October 1996 at 18:00 UTC. Black dots represent track of the medicane

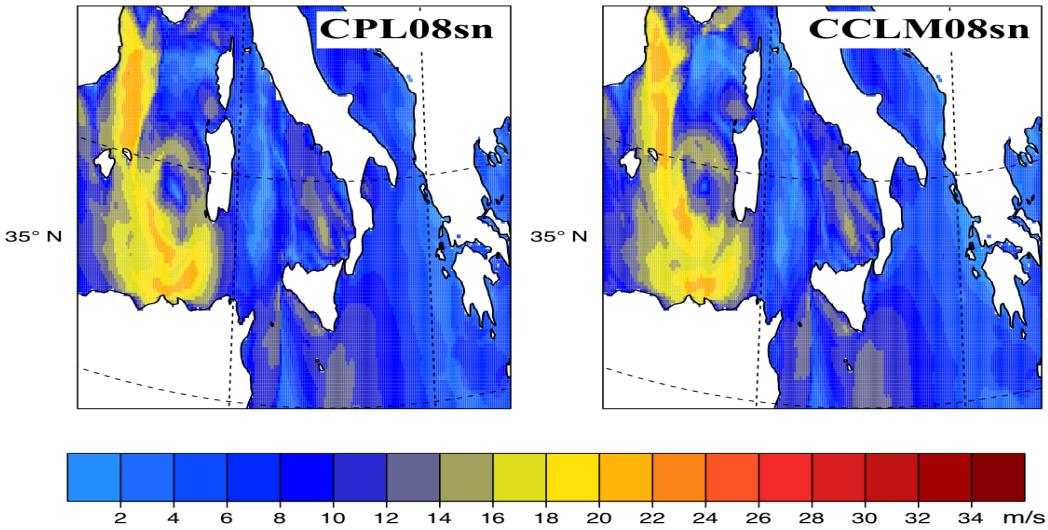

Figure 4.5: ME08; 10-m wind speed ($m\,s^{-1}$) in the coupled and atmosphere-only (0.08°) with spectral nudging simulations, on 7 October 1996 at 18:00 UTC

Most of the medicane features are well resolved at the higher-resolution of 0.08° (Fig. 4.2). The correct times and locations of simulated medicane formations are not in good agreement with the satellite images and MERRA reanalysis data. This may be due to the small size of medicanes, boundary layer parameterizations, the role of moist microphysics, and deep convection (Tous et al. 2013). Furthermore, the simulations starting 3 weeks before the medicane development and due to no data assimilation procedure, it is thus not possible to follow the real atmospheric conditions, as seen by the medicane tracks in CPL08 and CCLM08, which are significantly different from the MERRA reanalysis data. However, applying spectral nudging to CCLM increases the spatiotemporal characteristic of the medicanes. Thus, the same event is simulated

Table 4.2: Code, start and end time, lifetime (h; in round brackets) and lowest minimum sea level pressure (hPa; in square brackets) of medicane track in CPL22, CCLM22, CPL08 and CCLM08, and the MERRA reanalysis

Code	CPL22	CCLM22	CPL08	CCLM08	MERRA
ME01	26 Sep 1983, 19:00–28 Sep 1983, 14:00 **(43 h) [1005.6]**	26 Sep 1983, 19:00–28 Sep 1983, 15:00 **(44 h) [1006.0]**	28 Sep 1983, 02:00–28 Sep 1983, 08:00 **(06 h) [1011.2]**	28 Sep 1983, 01:00–28 Sep 1983,09:00 **(08 h) [1010.4]**	26 Sep 1983, 06:00–28 Sep 1983, 23:00 **(66 h) [1006.9]**
ME02	5 Apr 1984, 19:00–7 Apr 1984, 08:00 **(37 h) [993.6]**	5 Apr 1984, 20:00–7 Apr 1984, 09:00 **(37 h) [994.5]**	5 Apr 1984, 23:00–7 Apr 1984, 14:00 **(39 h) [994.4]**	5 Apr 1984, 00:00–7 Apr 1984, 16:00 **(39 h) [994.7]**	6 Apr 1984, 18:00–8 Apr 1984, 00:00 **(30 h) [1000.7.7]**
ME03	29 Dec 1984, 09:00–31 Dec 1984, 18:00 **(57 h) [1004.4]**	29 Dec 1984, 08:00-31 Dec 1984, 22:00- **(62 h) [999.7]**	29 Dec 1984, 03:00–31 Dec 1984, 23:00 **(68 h) [994.2]**	29 Dec 1984, 04:00–31 Dec 1984, 23:00 **(67 h) [997.9]**	29 Dec 1984, 06:00–1 Jan 1985, 00:00 **(66 h) [997.3]**
ME04	13 Dec 1985, 16:00–14 Dec 1985, 22:00 **(28 h) [1008.3]**	13 Dec 1985, 13:00–15 Dec 1985, 02:00 **(37 h) [1008.3]**	13 Dec 1985, 14:00–15 Dec 1985, 05:00 **(37 h) [1004.8]**	13 Dec 1985, 14:00–15 Dec 1985, 03:00 **(35 h) [1004.9]**	13 Dec 1985, 12:00–16 Dec 1985, 00:00 **(60 h) [1010.6]**
ME05	6 Dec 1991, 20:00–8 Dec 1991, 11:00 **(39 h) [985.1]**	6 Dec 1991, 20:00–8 Dec 1991, 09:00 **(37 h) [988.4]**	6 Dec 1991, 16:00–8 Dec 1991, 17:00 **(49 h) [982.6]**	6 Dec 1991, 18:00–8 Dec 1991, 15:00 **(45 h) [984.2]**	7 Dec 1991, 00:00–8 Dec 1991, 06:00 **(30 h) [987.4]**
ME06	14 Jan 1995, 01:00–15 Jan 1995, 15:00 **(38 h) [995.5]**	14 Jan 1995, 01:00–15 Jan 1995, 14:00- **(37 h) [995.2]**	15 Jan 1995, 00:00–16 Jan 1995, 18:00 **(42 h) [991.7]**	15 Jan 1995, 00:00–16 Jan 1995, 10:00 **(34 h) [991.1]**	15 Jan 1995, 00:00–17 Jan 1995, 12:00- **(48 h) [993.1]**
ME07	11 Sep 1996, 23:00–13 Sep 1996, 04:00 **(29 h) [990.3]**	11 Sep 1996, 22:00–12 Sep 1996, 07:00 **(09 h) [991.1]**	11 Sep 1996, 18:00–12 Sep 1996, 17:00 **(24 h) [992.0]**	12 Sep 1996, 04:00-12 Sep 1996, 17:00- **(13 h) [992.6]**	12 Sep 1996, 12:00–12 Sep 1996, 18:00 **(06 h) [998.1]**
ME08	7 Oct 1996, 03:00–10 Oct 1996, 05:00 **(74 h) [999.8]**	7 Oct 1996, 04:00–10 Oct 1996, 14:00 **(90 h) [995.6]**	6 Oct 1996, 21:00–10 Oct 1996, 19:00 **(94 h) [995.6]**	6 Oct 1996, 22:00–10 Oct 1996, 18:00 **(92 h) [994.1]**	7 Oct 1996, 00:00–11 Oct 1996, 00:00 **(72 h) [996.0]**
ME09	08 Dec 1996, 18:00–11 Dec 1996, 02:00 **(56 h) [984.0]**	8 Dec 1996, 18:00–10 Dec 1996, 10:00 **(40 h) [984.0]**	8 Dec 1996, 23:00–11 Dec 1996, 05:00 **(54 h) [988.8]**	9 Dec 1996, 01:00–11 Dec 1996, 03:00 **(50 h) [988.8]**	9 Dec 1996, 12:00–12 Dec 1996, 00:00 **(60 h) [1002.2]**
ME10	26 Jan 1998, 01:00–26 Jan 1998, 20:00 **(07 h) [1000.6]**	26 Jan 1998, 01:00–27 Jan 1998, 07:00 **(30 h) [1001.5]**	26 Jan 1998, 04:00–27 Jan 1998, 08:00 **(27 h) [997.8]**	26 Jan 1998, 03:00–27 Jan 1998, 08:00 **(28 h) [998.9]**	26 Jan 1998, 06:00–27 Jan 1998, 18:00 **(36 h) [1001.5]**
ME11	17 Mar 1999, 19:00–18 Mar 1999, 08:00 **(13 h) [995.01]**	17 Mar 1999, 19:00–18 Mar 1999, 08:00 **(13 h) [995.01]**	17 Mar 1999, 20:00–18 Mar 1999, 08:00 **(12 h) [994.55]**	17 Mar 1999, 20:00–18 Mar 1999, 02:00 **(06 h) [994.4]**	18 Mar 1999, 00:00–19 Mar 1999, 00:00 **(24 h) [992.8]**

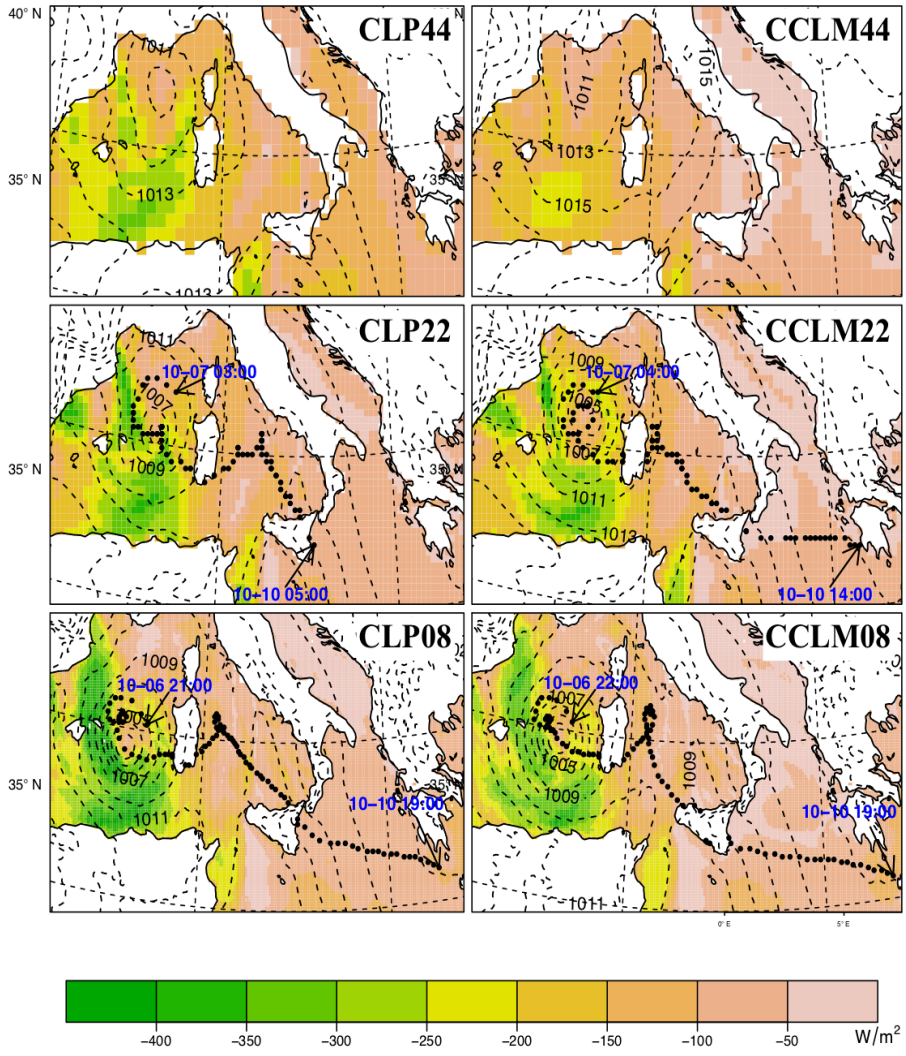

Figure 4.6: ME08; mean sea level pressure (hPa ; dotted contours lines at 2 hPa intervals) and latent heat flux ($W\,m^{-2}$; colored contours at $50\,W\,m^{-2}$ intervals) in the coupled and atmosphere-only (0.44, 0.22, and 0.08°) simulations on 7 October 1996 at 18:00 UTC. Black dots represent track of the medicane

again, this time with the spectral nudging technique applied to CCLM.

Figure 4.4 shows the results of the CPL08sn and CCLM08sn simulations on 7 October at 18:00 UTC, along with the medicane track (black dots). The lowest minimum sea level pressure value during a fully developed medicane period is 995.94 hPa in CLP08sn, and 995.34 hPa in CCLM08sn. The lowest sea level pressure values with and without spectral nudging simulations (Table 4.2) are not very different. The first sea level pressure minimum appeared 3–4-h earlier in simulations with spectral nudging compared to those without. Initially, the location of the medicane in spectral nudging simulations is shifted more to the south, which compares better with the satellite observations and MERRA reanalysis data. Although the timing and location of the medicane is improved by applying spectral nudging as expected (Cavicchia and von Storch 2012), compared to the satellite observations, the length of the track is reduced in this particular case. The length of the medicane track in CPL08sn (68-h) is longer than in CCLM08sn (51-h).

In most cases, the length of a medicane's track in spectral nudging simulations is approxi-

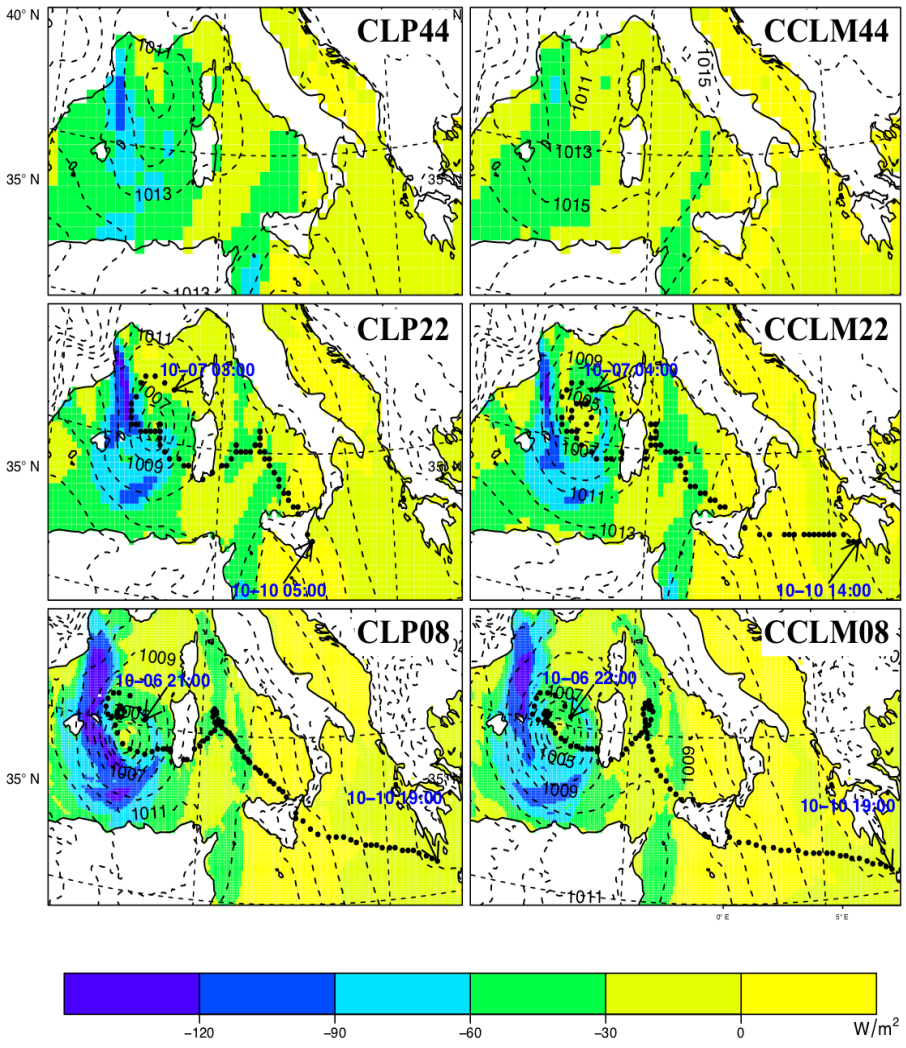

Figure 4.7: ME08; mean sea level pressure (hPa ; dotted contours lines at 2 hPa intervals) and sensible heat flux ($W\,m^{-2}$; colored contours at $30\,W\,m^{-2}$ intervals) in the coupled and atmosphere-only (0.44, 0.22, and 0.08°) simulations on 7 October 1996 at 18:00 UTC. Black dots represent track of the medicane

mately the same as in cases without spectral nudging (Table 4.2). Figure 4.5 shows the wind speed patterns in CPL08sn and CCLM08sn simulations on 7 October at 18:00 UTC. The wind speed did not show any improvement in simulations with spectral nudging compared to simulations without spectral nudging (see Fig. 4.3).

The surface heat fluxes (latent and sensible) play an important role in the formation and evolution of medicanes (Tous et al. 2013). Figure 4.6 and 4.7 show the mean sea level pressure, latent and sensible heat fluxes, respectively, on 7 October 1996 at 18:00 UTC along with the medicane track (black dots). The results show that the intensity of the latent and sensible heat fluxes increased with increasing atmospheric grid resolution. The CPL08 simulations showed higher absolute values of latent and sensible heat fluxes together with a more intense medicane than the atmosphere-only simulation. Thus, the medicane formation appears directly linked to surface heat fluxes.

Similar to the simulations without spectral nudging, the latent and sensible heat fluxes are

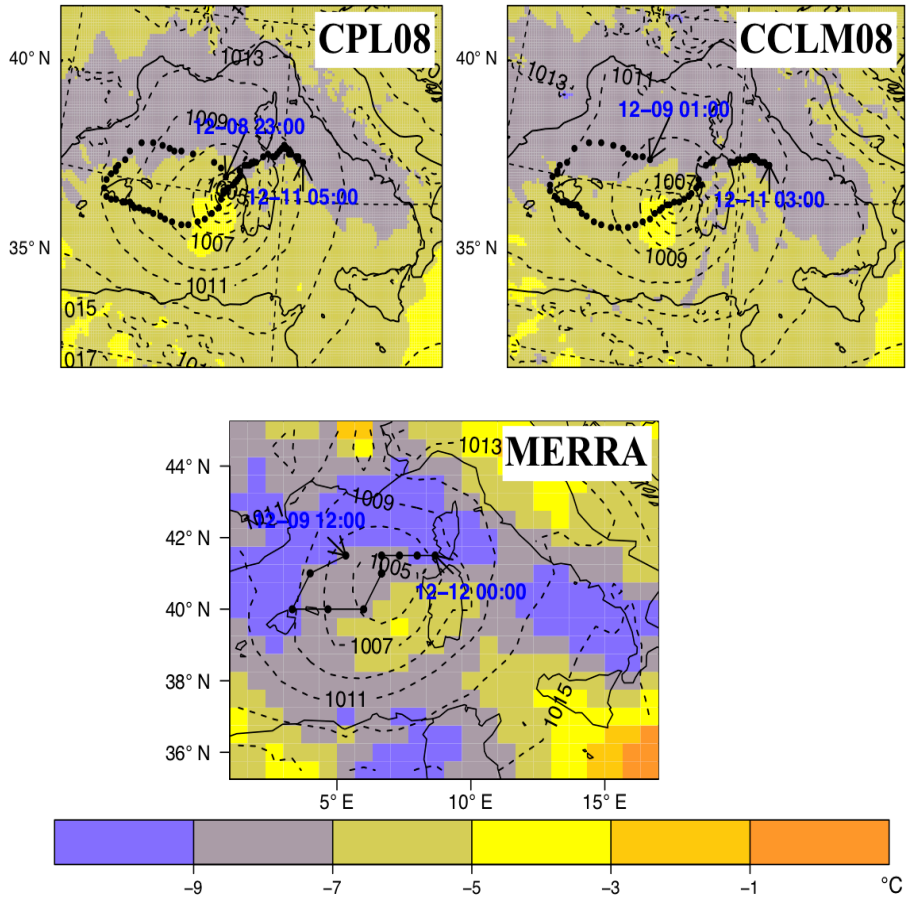

Figure 4.8: ME09; mean sea level pressure (hPa; dotted contours lines at 2 hPa intervals) and temperature (°C; colored contours at 2 °C intervals) at 700 hPa in the coupled and atmosphere-only (0.08°) simulations and the MERRA reanalysis data on 10 December 1996 at 18:00 UTC. Black dots represent track of the medicane

higher in the coupled spectral nudging simulations (not shown). The spectral nudging simulations did not show any significant differences in the latent and sensible heat fluxes compared to the simulations without spectral nudging, conforming its low effect.

Higher values of latent and sensible heat fluxes are seen when coupling with the high-resolution of the 1-D NEMO-MED12 ocean model, as well as the increasing of the atmospheric model resolution. On one hand, the ocean model allows the simulation of ocean meso-scale feature. Stanev et al. (2001) showed that the increasing the ocean model resolution modifies the SST according to the direct simulation of ocean meso-scale activities. In that case, it leads to an increase of 20 % in the ocean heat loss. On the other hand, increasing the atmosphere resolution allows the simulations of new atmospheric fine-scale processes. For example, rain bands over the Gulf of Lions were better simulated at 6.7 km than at 20 km in Weather Research and Forecasting (WRF) model (Lebeaupin et al. 2012). Most importantly, wind gusts are better simulated with higher resolution atmospheric models. These changes in the winds can have quantitative effects on the turbulent fluxes (latent and sensible) at the air-sea interface.

The first 11 medicane events listed in Table 4.1 are also simulated by applying the spectral nudging technique to CCLM in both the coupled and atmosphere-only setups. In most cases,

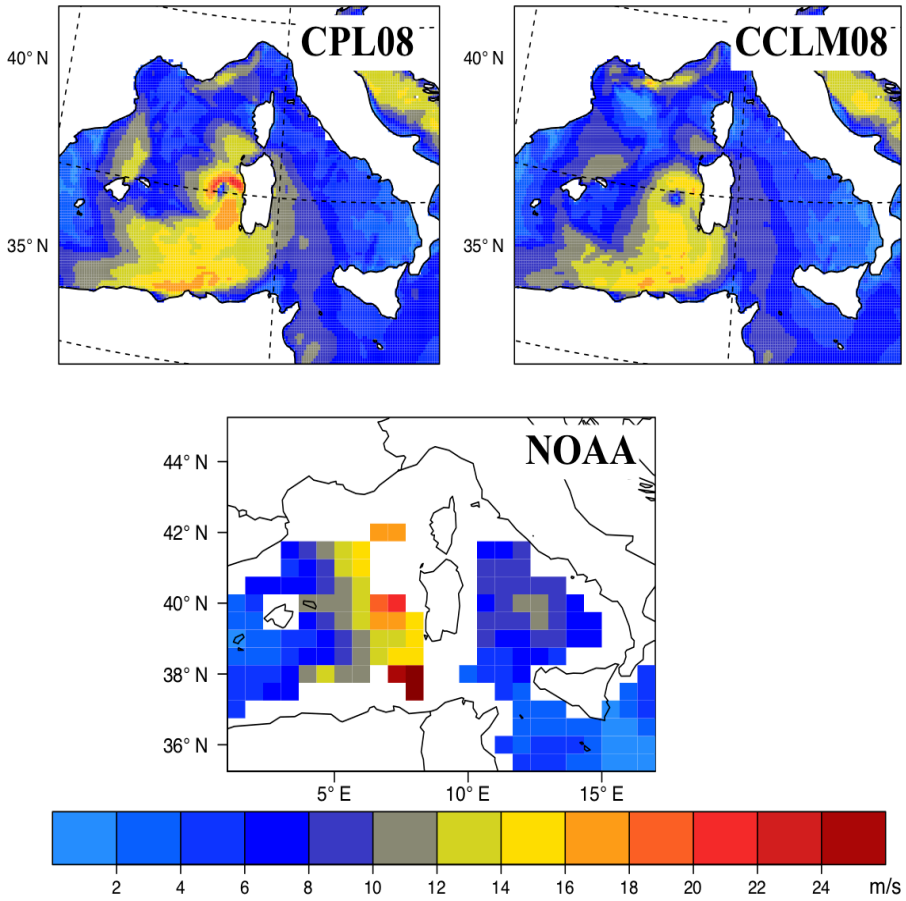

Figure 4.9: ME09; 10-m wind speed ($m\,s^{-1}$) in the coupled and atmosphere-only (0.08°) simulations and the NOAA "Blended Sea Winds" on 10 December 1996 at 18:00 UTC

simulations with spectral nudging improved the precision in the time and location of simulated medicanes. A similar conclusion was reached by Cavicchia and von Storch (2012) for atmosphere-only, CCLM simulations. The results show that applying spectral nudging did not significantly improve the wind speed estimates in both the coupled and atmosphere-only simulations. In all spectral nudging simulations, the coupled model performance is improved to the same extent as the atmosphere-only model, showing more intense and finer structure of medicanes in coupled simulations. As mentioned before in this study, our focus is not to address the precision in times and locations of simulated medicanes. We are more interested in examining the ability and added value of the coupled model to simulate medicanes. In subsequent examples, only the results of simulations without spectral nudging are described.

4.3.2 Case ME09

The ME09 case was a medicane event that was observed in the western part of the Mediterranean Sea. According to the satellite observations, the medicane started to develop on 8 December 1996 at 12:00 UTC and lasted for 48-h (Table 4.1). The medicane started to develop northwest of Sardinia, and moved towards the Balearic Islands. After reaching the Balearic Islands, it started

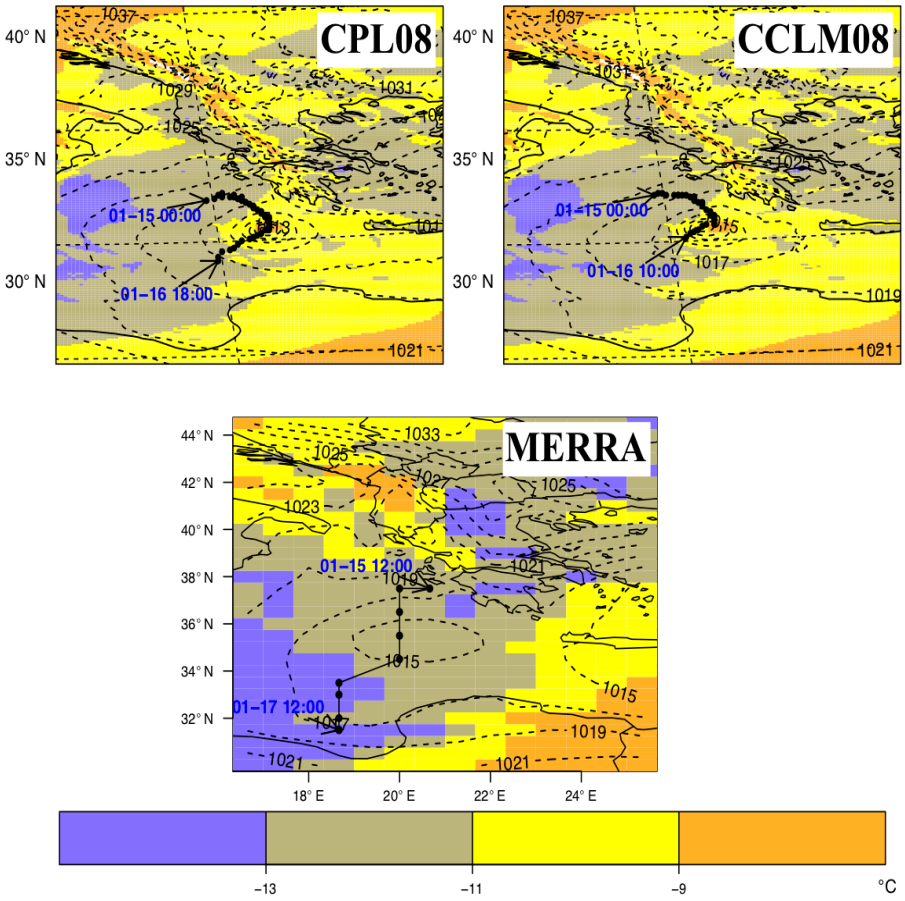

Figure 4.10: ME06; mean sea level pressure (hPa; dotted contours lines at 2 hPa intervals) and temperature (°C: colored contours at 2 °C intervals) at 700 hPa in the coupled and atmosphere-only (0.08°) simulations and the MERRA reanalysis data on 16 January 1995 at 12:00 UTC. Black dots represent track of the medicane

to move again towards Sardinia and dissipated after crossing it. Figure 4.8 shows the mean sea level pressure and temperature at 700 hPa in CPL08, CCLM08, and the MERRA reanalysis data on 12 December at 18:00 UTC, along with the medicane track (black dots). The length of the medicane track in CPL08 is 54-h, 50-h in CCLM08, and 60-h in the MERRA reanalysis data. Although the lowest minimum sea level pressure values are the same in both CCLM08 and CPL08, the length of the medicane track is longer in the latter (Table 4.2). Figure 4.9 shows the wind speed patterns in CPL08, CCLM08, and the NOAA dataset on 12 December at 18:00 UTC. The wind speed patterns in CPL08 are more intense and in good agreement with the NOAA dataset. Compared to the atmosphere-only simulations, the medicane tracks, warm-core structures, and wind speeds are improved in the coupled simulations.

4.3.3 Case ME06

The ME06 event is a well-known medicane that developed in the central Mediterranean Sea with striking similarities to a tropical cyclone. The satellite observations show that the medicane started to develop on 14 January 1995 at 12:00 UTC and ended on 18 January at 20:00 UTC. The

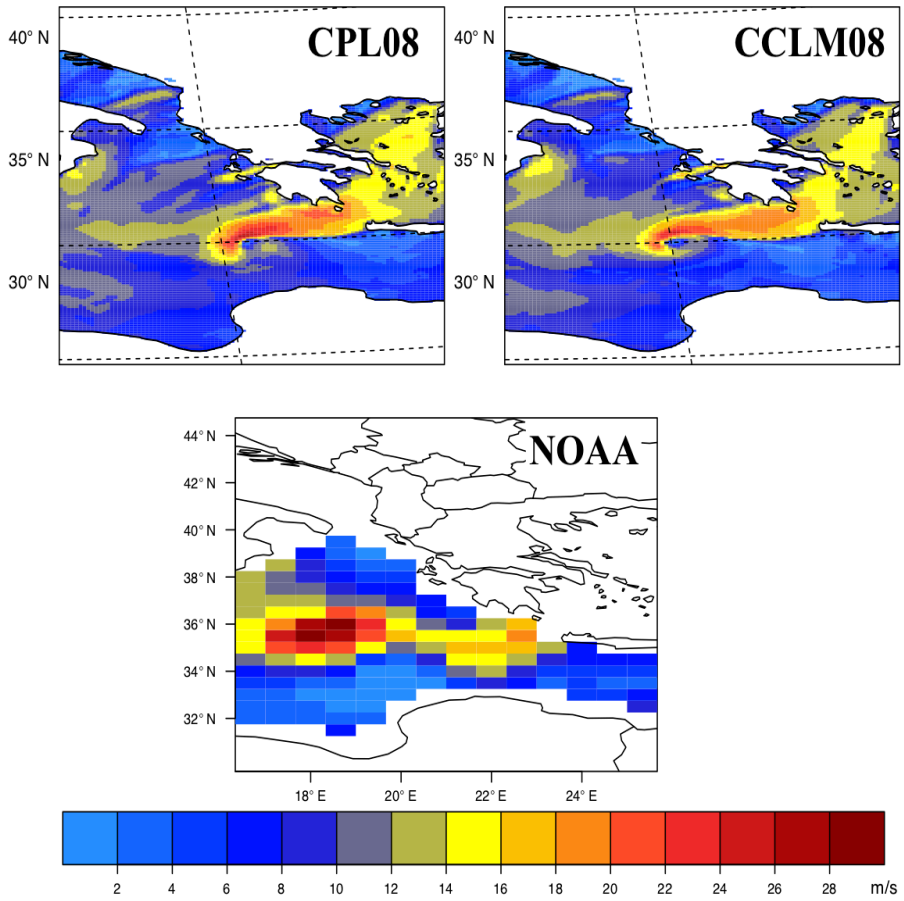

Figure 4.11: ME06; 10-m wind speed ($m\,s^{-1}$) in the coupled and atmosphere-only (0.08°) simulations and the NOAA "Blended Sea Winds" on 16 January 1995, at 12:00 UTC

eye of the medicane was clearly visible the majority of the time (15 January at 07:00 UTC to 18 January at 06:30 UTC). It was one of the longest medicane events to ever occur in the central Mediterranean Sea (Table 4.1). According to the satellite observations, a meso-scale low-pressure system moved from the central Mediterranean Sea and reached the coast of Greece in the late night of 14 January. It then started to move towards the coast of Libya. Strong winds, heavy rainfall, and positive temperature anomalies were reported during that time by ships cruising nearby (Cavicchia and von Storch 2012). The storm dissipated after making landfall in the Gulf of Sirte on 18 January. Figure 4.10 shows the comparison of mean sea level and temperature at 700 hPa on 16 January at 12:00 UTC in CPL08, CCLM08, and the MERRA reanalysis data along with the medicane track (black dots). The track does not appear in CPL08, CCLM08, and the MERRA reanalysis data during the first part of the medicane, when it was moving from south to north. This is due to the sea level pressure being less deep and steep in CLP08, CCLM08, and the MERRA reanalysis data. The length of the medicane track in CPL08 is 42-h, 34-h in CCLM08, and 48-h in the MERRA reanalysis. The lowest minimum sea level pressure values and warm-core structures are similar in both the CPL08 and CCLM08 simulations (Table 4.2). However, the track length in CPL08 is longer in comparison to the CCLM08 simulations. The medicane tracks in CPL08 and CCLM08 are shifted toward the east compared to the MERRA reanalysis

data. Compared to the atmosphere-only simulations, the medicane track and warm-core structure in the coupled simulations (CPL08) are in good agreement with the MERRA reanalysis data. Figure 4.11 shows the wind speed comparison in CPL08, CCLM08, and the NOAA dataset on 16 January 1995 at 12:00 UTC. The wind speed in CPL08 is more intense and in good agreement with the NOAA dataset, but the position of the maximum wind speed is shifted to the east in the simulations.

4.3.4 Case ME10

The ME10 medicane event occurred in the central part of the Mediterranean Sea. The satellite observations show a mature phase of the medicane on 26 January 1998 at 12:00 UTC (Table 4.1). The medicane started to develop in the southeast of the Sicily channel and dissipated after making landfall in the northeastern coast of Libya. The observed lifetime of this medicane was 30-h (Table 4.1). Figure 4.12 shows the comparison of the mean sea level and temperature at 700 hPa on 27 January at 00:00 UTC in CPL08, CCLM08, and the MERRA reanalysis data, along with the medicane track (black dots). The length of the simulated medicane track in CPL08 is 27-h, 28-h in CCLM08, and 36-h in the MERRA reanalysis data. The first sea level pressure minimum appeared 1-h earlier in the CCLM08 simulations compared to the CPL08 simulations. The mean sea level pressure is slightly deeper in CPL08 compared to CCLM08 (Table 4.2), and the warm-core values are approximately the same in both simulations. However, the MERRA reanalysis data show more intense values of mean sea level pressure (Table 4.2) and warm core. The medicane tracks in CLP08 and CCLM08 are shifted towards the south compared to the MERRA reanalysis data. Figure 4.13 shows the wind speed comparison of CPL08, CCLM08, and the NOAA dataset on 27 January at 00:00 UTC. The wind speed patterns in CPL08 are stronger and finer compared to the CCLM08 simulations, and in good agreement with the NOAA dataset.

4.3.5 Cases ME01–ME05, ME07, and ME11

In the remaining ME02–ME05 and ME07 cases, finer structure are only observed in high-resolution (0.08°) simulations. Table 4.2 shows the lengths of medicane tracks and lowest minimum sea level pressure values of all simulated medicanes. The ME01 case was not well simulated at high-resolution (0.08°); the track length is very short in both the CPL08 (6-h) and CCLM08 simulations (8-h) compared to the MERRA reanalysis (66-h) data (Table 4.2). For the ME11 case, the medicane tracks in both the 0.22° (CPL22; 13-h and CCLM22; 13-h) and 0.08° (CPL08; 12-h and CCLM08; 6-h) simulations are very short compared to the MERRA reanalysis data (24-h). Tous et al. (2013) investigated the impact of surface heat fluxes on the intensity and trajectories of the 12 medicanes listed in Table 4.1. They found that surface heat fluxes do not play significant roles in the intensity and trajectories of these two medicanes (ME01 and ME11). This may be the reason that these two medicanes are not well simulated.

Overall results show that there is no significant difference in the lengths of the medicane

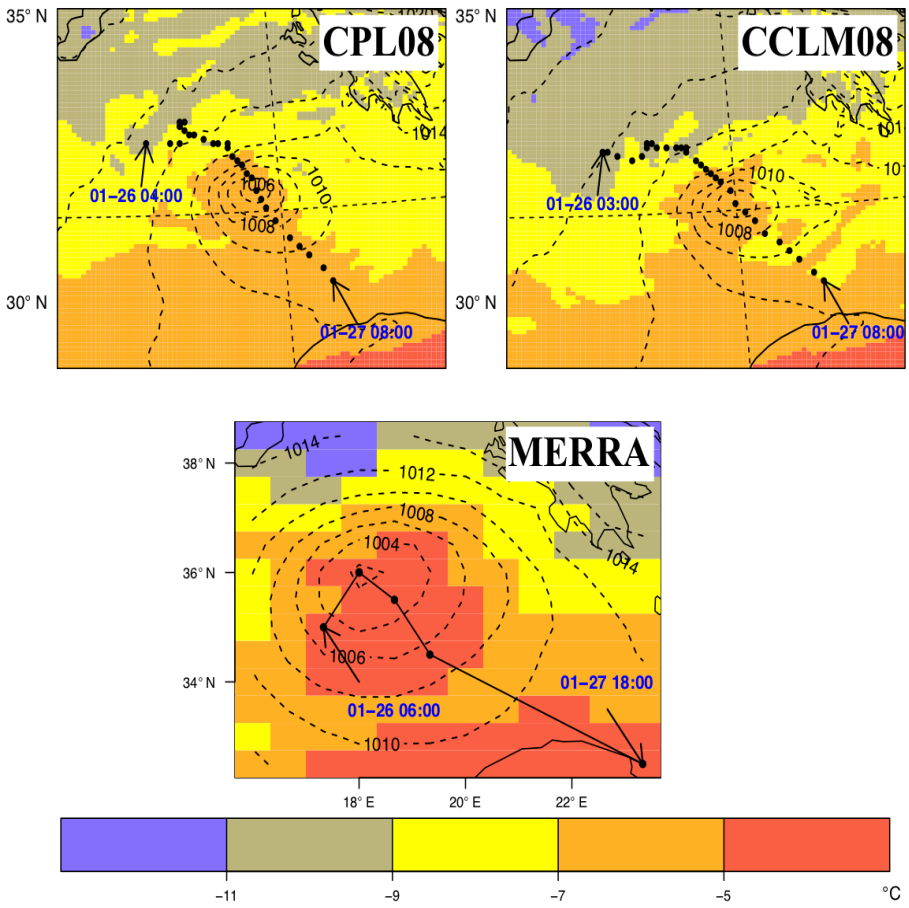

Figure 4.12: ME10; mean sea level pressure (hPa; dotted contours lines at 2 hPa intervals) and temperature (°C: colored contours at 2 °C intervals) at 700 hPa in the coupled and atmosphere-only (0.08°) simulations and the MERRA reanalysis data on 27 January 1998 at 00:00 UTC. Black dots represent track of the medicane

tracks between the CPL22 and CCLM22 simulations. The mean sea level pressure difference between CPL22 and CCLM22 ranges from 0 to 4.7 hPa. However, the lengths of the medicane track in CPL08 are longer than CCLM08, except ME02, where both have the same track length, and ME10 where CPL08 shows a shorter (1-h) track length compared to CCLM08. The difference between the lowest minimum sea level pressure values in most of the 0.08° simulations ranges from 0 to 1.6 hPa, except ME03, where the difference is slightly higher (3.7 hPa). The results show that warm-core structures are also more intense in the CPL08 simulations compared to CCLM08.

The wind speed is strongly underestimated in all cases of the 0.22° simulations. However, the wind speed is significantly improved in the 0.08° simulations. Compared to CCLM08, the wind speed in CPL08 is more intense and in good agreement with the NOAA dataset. The results show that 0.08° is an appropriate atmospheric grid resolution to resolve most of the meso-scale characteristics associated with medicanes in coupled and atmosphere-only simulations. The coupled simulations at 0.08° also improved the results, particularly the medicane's track lengths, warm-core and wind speed structures compared to atmosphere-only simulations.

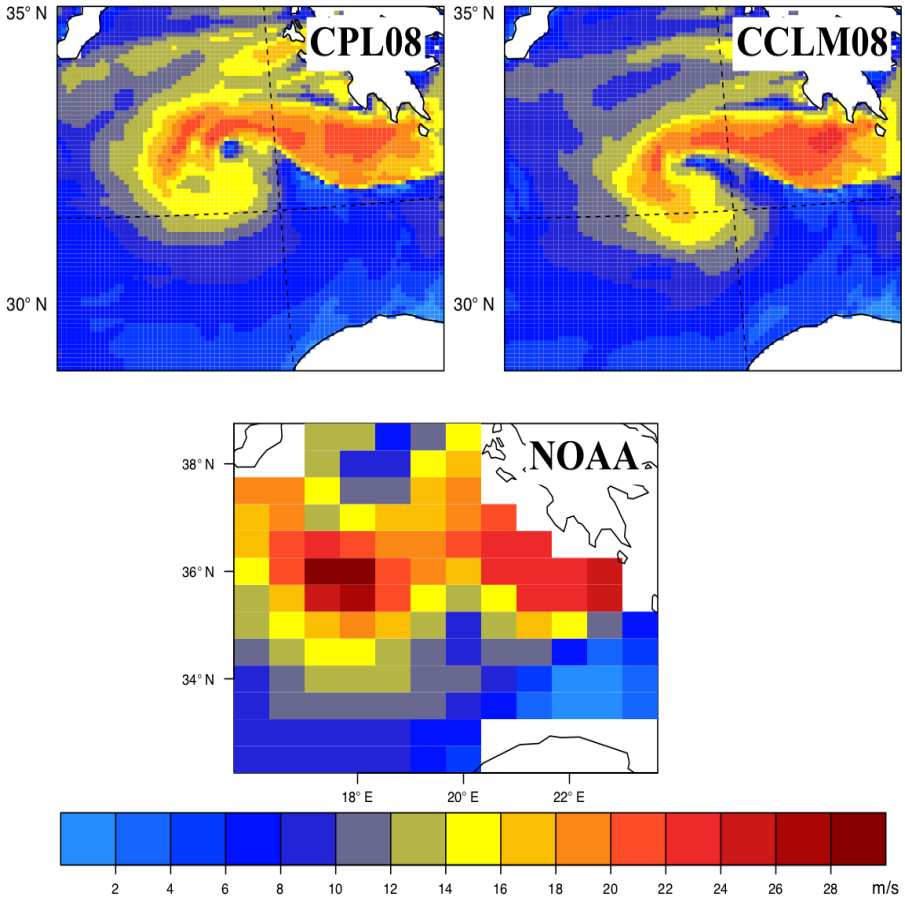

Figure 4.13: ME10; 10-m wind speed ($m\,s^{-1}$) in the coupled and atmosphere-only (0.08°) simulations and the NOAA "Blended Sea Winds" on 27 January 1998 at 00:00 UTC

4.4 Conclusions

In this study we examined the ability of the coupled atmosphere–ocean model COSMO-CLM/1-D NEMO-MED12 with atmospheric grid spacings of 0.44, 0.22, and 0.08° (about 50, 25, and 9 km, respectively) and an ocean grid spacing of 1/12° to simulate medicanes. The results show that the model's performance depends strongly on the atmospheric grid resolution. The large-scale disturbance is well simulated in all three resolutions. Medicane signals are not observed in the 0.44° simulations. In the 0.22° simulations, the mean sea level pressure and warm core are captured, and are more intense and finer in the 0.08° simulations. The wind speed is strongly underestimated in the 0.22° simulations compared to the NOAA dataset. Most of the medicane features are well resolved at high-resolution (0.08°) in both coupled and atmosphere-only simulations.

Compared to the atmosphere-only simulations, the coupled model did not show any significant improvement at 0.44 and 0.22° resolutions. In the 0.22° simulations, the coupled and the atmosphere-only simulations did not show any significant difference in the medicane track length. The wind speed and warm-core structures in the 0.22° (both coupled and atmosphere-only) simulations are not well represented. However, the coupled simulations improved significantly

compared to atmosphere-only simulations at higher atmospheric grid resolution (0.08°). The characteristic features of medicanes, such as warm cores and high wind speeds, are more intense in coupled simulations compared to atmosphere-only simulations. In most cases, medicane tracks in the coupled simulations are longer compared to the atmosphere-only simulations, and therefore in good agreement with observations. These results suggest that a 0.08° grid resolution produces accurate detailed results in medicane simulations, particularly with the coupled model. An atmospheric grid resolution higher than 0.22° is vital to simulate the medicanes more realistically in both coupled and atmosphere-only models.

The coupled and atmosphere-only simulations with the spectral nudging technique increased the accuracy of times and locations of generated medicanes. However, the simulations with spectral nudging did not result in any significant improvement in the mean sea level pressure and wind speed estimates. In the spectral nudging simulations, the medicane tracks and wind speeds in the coupled simulations are better represented compared to the atmosphere-only simulations, similar to simulations performed without spectral nudging.

The intensity of the latent and sensible heat fluxes increased with increasing atmospheric grid resolution. The absolute values of latent and sensible heat fluxes are higher in the coupled simulations than the atmosphere-only simulations. Thus, the results suggest that intensity of medicanes is strongly linked with surface heat fluxes and fine-scale features at the air-sea interface. The simulations with spectral nudging did not show any significant differences in the latent and sensible heat fluxes compared to the simulations without spectral nudging.

The present study shows that the coupled model is an effective tool for simulating extreme events such as medicanes. The presented coupled model can be a useful tool for studying tropical-like storms, particularly the ocean feedback effects. The impact of coupling on the vertical structures of medicanes and other important parameters such as precipitation and air-sea fluxes should be analyzed in detail. A full three-dimensional ocean model can be used for long-term climate simulations and future projections of these extreme events.

Acknowledgements

The authors acknowledge funding from the Hessian Initiative for the Development of Scientific and Economic Excellence (LOEWE) through the Biodiversity and Climate Research Centre (BiK–F), Frankfurt am Main. The authors thank the Center for Scientific Computing (CSC) of the Goethe University Frankfurt am Main for providing computational facilities, especially LOEWE-CSC. We acknowledge Cindy Lebeaupin Brossier, Jonathan Beuvier, Thomas Arzouse, Samuel Somot and Philippe Drobinski for their help for the NEMO-MED12 model and the atmospheric coupling and Eric Maisonnave for his support.We also acknowledge the French GIS and GMMC which have supported the NEMO-MED12 model development. B. Ahrens acknowledges the support from the German Federal Ministry of Education and Research (BMBF) under grant MiKliP: DECREG/01LP1118B. The authors also acknowledge the HyMeX and Med-CORDEX communities.

CHAPTER 5

European marginal seas in a regional atmosphere–ocean coupled model and their impact on Vb-cyclones and associated precipitation[1]

Abstract

Vb-cyclones are unique extratropical cyclones that propagate from the Western Mediterranean Sea and travel across the Eastern Alps into the Baltic region. Extreme precipitation over Central Europe associated with these cyclones is a potential trigger for significant flooding events. Improving our understanding and the predictability of Vb-cyclones would lower risks from adverse impacts. This study analyzes the robustness of an atmosphere-ocean regional coupled model, including models for the Mediterranean Sea (MED) and North- and Baltic Seas (NORDIC), in reproducing observed Vb-cyclones characteristics and the impact of air-sea coupling on cyclone trajectories and precipitation intensity. We use the regional climate model (RCM) COSMO-CLM in uncoupled and coupled configurations with the regional ocean model MED and NORDIC for $1979-2014$. SST is evaluated to demonstrate the stability and reliability of the coupled configurations. Compared to observations, SSTs simulated using coupled configurations show biases ($\sim 1^{\circ}$C) over the coupling regions especially during winter and summer. In general, all model configurations are able to replicate Vb-cyclones, their trajectories, and associated precipitation fields. The atmosphere-ocean coupling has an overall positive, although strongly case-by-case varying, impact on the trajectories and intensity of Vb-cyclones due to the variation in moisture source for each event. Furthermore, the average structure of the precipitation field is best represented in the coupled configurations MED+NORDIC and NORDIC. The results suggest that regional coupled systems are a useful tool for studying the impact of highly resolved SSTs on European extreme events and regional climate, a crucial prerequisite for understanding future climate conditions.

[1] **Submitted to Clim Dyn:** Akhtar N, Krug A, Brauch J, Arsouze T, Dieterich C, Ahrens B. European Marginal Seas in a regional atmosphere-ocean coupled model and their impact on Vb-cyclones and associated precipitation

5.1 Introduction

The Mediterranean region is one of the world's primary cyclogenetic regions (Pettersen 1956; Hoskins and Hodges 2002; Wernli and Schwierz 2006). Complex air-sea interactions and orographic features play a predominant role in determining Mediterranean climate. For example, high evaporation over the Mediterranean Sea favors frequent cyclonic activities in the region (Alpert et al. 1995). One specific type of characteristic cyclone that develops over the Western Mediterranean Sea, typically over the Gulf of Genoa, and travels across the Eastern European Alps toward the Baltic region is the Vb-cyclone (Van Bebber 1891; Messmer et al. 2015). Persistent strong cut-off lows drive synoptic scale atmospheric circulation, including the Vb-pathway, and are responsible for extreme weather conditions (Stucki et al. 2013; Ulbrich et al. 2003a,b). A typical Vb-type weather condition occurs when a high-pressure system is located over the Baltic region and, at the same time, an intense low-pressure system moves from the Western Mediterranean Sea toward Central or Eastern Europe. During such events, significant moisture is transported toward the northern side of the Alps and into Central Europe due to the counterclockwise rotation of the cyclone. Such a condition can last for several days and often yields large-scale intense precipitation events and floods in Central Europe (Mudelsee et al. 2004; Nied et al. 2014). Hofstätter et al. (2017) reported that during summer almost every second Vb-cyclone is related to heavy precipitation over the Czech Republic and Austria. The authors also found that the precipitation intensity associated with Vb-cyclones is high in summer due to high air temperatures. In addition, Nissen et al. (2014) showed that flooding associated with Vb-cyclones is mainly a summer phenomenon. Examples of extreme Vb flooding events include those in Switzerland in September 1993 (Stucki et al. 2013), the Czech Republic and Austria in July 1997 (Ulbrich et al. 2003b; Cyberski et al. 2006; Godina et al. 2006; Ho-Hagemann et al. 2015), Central Europe in August 2002 (Ulbrich et al. 2003a; Grazzini and van der Grijn 2003), the Alpine region in August 2005 (Beniston 2013), and Central Europe in May–June 2013 (Grams 2014; Kelemen et al. 2016) and May 2014 (Stadtherr et al. 2016). Such extreme events often led to substantial economic and personal losses (Graefe and Hegg 2004; Mudelsee et al. 2004; MeteoSchweiz 2006; Mitzschke 2013; Held et al. 2013).

The Mediterranean region is often referred as a climate change "hotspot" for global warming (Giorgi 2006). Strong warming of the Mediterranean Sea surface temperature (SST) was observed already by the end of the 20th century (Rixen 2012). By the end of the 21st century, more than 2 K additional warming is projected compared to 1980–1999 (IPCC 2007). These thermodynamic changes may significantly change the air-sea interaction, which can influence the occurrence and intensity of Mediterranean cyclones. Although mean precipitation is expected to decrease in the long-term (Christensen and Christensen 2007), an increase in evaporation and moisture transport can potentially impact short-term extreme precipitation events over Central Europe (e.g., Gimeno et al. 2010; Volosciuk et al. 2016; Messmer et al. 2017). A decrease in frequency and an increase in intensity of Vb-cyclones is projected under future climate change conditions (Muskulus and Jacob 2005; Nissen et al. 2013).

The dynamics of synoptic-scale atmospheric circulation and contribution of moisture flux from different sources influence the precipitation amount associated with Vb-cyclones (Messmer et al. 2015). The precipitation is potentially most intense if the cut-off low is located over the northern or eastern parts of the Alps (Awan and Formayer 2016). Gimeno et al. (2010) and Volosciuk et al. (2016) found that intense precipitation events over Central Europe are directly linked to the thermodynamic conditions in the Mediterranean area. However, most Vb studies have focused on individual cases, and thus general conclusions have to be drawn with care. For example, the August 2002 event is one of the most frequently analyzed cases (Ulbrich et al. 2003a; Grazzini and van der Grijn 2003; Stohl and James 2004; Kaspar and Müller 2008). In addition to evaporation over the Mediterranean Sea, inland evaporation was a major source of moisture for the August 2002 Vb-event (Ulbrich et al. 2003a; Sodemann et al. 2009). Sodemann et al. (2009) further proposed that the Atlantic and long-range advection should not be ignored. The latter is supported by Winschall et al. (2012), who investigated various extreme precipitation events over Central Europe and recognized that the North Atlantic, in addition to the Mediterranean Sea and inland evaporation, is an important moisture source. Similar conclusions were also drawn by James et al. (2004) and Stohl and James (2004) using a backward tracking method and particle dispersion model, respectively, in analyzing the August 2002 case. In contrast, Gangoiti et al. (2011) concluded that the Mediterranean Sea was the main moisture source for the August 2002 Vb-event. In a recent model-based study, Messmer et al. (2017) found a non-linear relationship between Mediterranean SST and precipitation intensity. An increase of 5 K in Mediterranean SST increases the precipitation amount by 24%, whereas a 5 K reduction induces a decrease of only 9% in precipitation intensity over Central Europe during Vb-events. However, no significant differences in the precipitation intensity are found between $+1$ and $+3$ K.

Most Vb-cyclone studies investigated reanalysis datasets or uncoupled regional or global atmospheric model simulations, which exhibit considerable uncertainty ($-7\pm21\,\mathrm{W\,m^{-2}}$) in the Mediterranean Sea surface heat fluxes (Sanchez–Gomez et al. 2011). These uncertainties can strongly affect the intensity and tracks of Mediterranean cyclones. Currently, state-of-the-art regional climate models (RCMs) achieve horizontal resolution finer than 50 km with a more realistic representation of local features (Herrmann and Somot 2008). However, RCMs often use coarse-resolution SST from coupled global model simulations or reanalysis (e.g., ERA-Interim and NCEP/NCAR) datasets as lower boundary conditions (Christensen and Christensen 2007). Indeed, these datasets do not well represent the European marginal seas (Mediterranean, North- and Baltic Seas). Nonetheless, SST variations in these marginal seas are essential to regional climate at different temporal and spatial scales (Somot et al. 2008; Li 2006; Akhtar et al. 2018).

The recent availability of atmosphere-ocean regional climate models (AORCMs) represents an opportunity to study the impact of increased resolution and air-sea coupling on extreme events, such as Vb-cyclones. Studies show that air-sea coupling over the Mediterranean Sea effects simulated temperature and precipitation both over the coupling domain and over land (e.g., Somot et al. 2008; Van Pham et al. 2014). Further, SSTs simulated with high-resolution (less than 10 km) ocean models can have a strong and beneficial effect on cyclogenesis and precipitation (Sanna

et al. 2013). Akhtar et al. (2018) showed that a high-resolution AORCM improves trajectories and the intensity of simulated Mediterranean hurricanes (medicanes) compared to RCM due to better resolved mesoscale processes and turbulent fluxes. An improved representation of simulated fluxes, including momentum fluxes, using an AORCM instead of an RCM was also shown in Akhtar et al. (2018). There is general agreement that high-resolution AORCMs are a prerequisite for resolving small-scale features of the Mediterranean (e.g., Somot et al. 2008; Herrmann et al. 2011; Ruti et al. 2016) and North- and Baltic Seas (e.g., Van Pham et al. 2014; Ho-Hagemann et al. 2015).

The value of using AORCMs was highlighted by Ho-Hagemann et al. (2015), who used an AORCM with a coupled North- and Baltic Seas model to investigate the July 1997 Oder flooding event, which was associated with a sequence of two ("Xolska" and "Zoe") Vb-cyclones. For the second Vb phase, they identified large-scale convergence of moisture from the Mediterranean Sea together with moisture coming from the North Atlantic Ocean via the North Sea and inland evaporation as responsible for heavy rainfall and floods in Central Europe. Their analysis explicitly showed the added value of coupled North- and Baltic Seas models for simulating the event. The impact of air-sea interactions and feedbacks over European marginal seas, Mediterranean Sea, and North- and Baltic Seas on the characteristics of Vb-cyclones have not yet been investigated using an AORCM. The present work evaluates SST simulated using a new developed AORCM and addresses the impact of atmosphere-ocean coupling (1) over the Mediterranean Sea, (2) over the North- and Baltic Seas, and (3) over both marginal seas in a combined system on trajectories and precipitation characteristics of selected Vb-cyclones in the ERA-Interim period. This paper is structured as follows. Section 5.2 describes the details of the models, experimental set-up, datasets, and analysis methods. The results and discussion are provided in Section 5.3. Finally, the main conclusions and future research prospective are presented in Section 5.4.

5.2 Modeling system and experiment setups

In this study, we used the COSMO-CLM (CCLM) RCM in combination with regional ocean models NEMO-MED12 for the Mediterranean Sea and NEMO-NORDIC for the North- and Baltic Seas to generate three AORCM for analyses.

5.2.1 CCLM

The atmospheric model CCLM v5.7 is a non-hydrostatic RCM based on primitive equations (Rockel et al. 2008). The model configuration follows the EURO-CORDEX extent (Fig. 1.1; Giorgi et al. 2009; Van Pham et al. 2014) with an atmospheric grid resolution of 0.22° (∼25 km; 232×226 grid points and 40 σ levels). In our configuration, CCLM uses a numerical time step of 150 s with a third order Runge-Kutta numerical integration scheme and Tegen et al. (1997) aerosol optical depth data. Furthermore, CCLM uses a one-dimensional prognostic turbulent kinetic energy scheme for vertical turbulent diffusion parameterization and a delta–two–stream

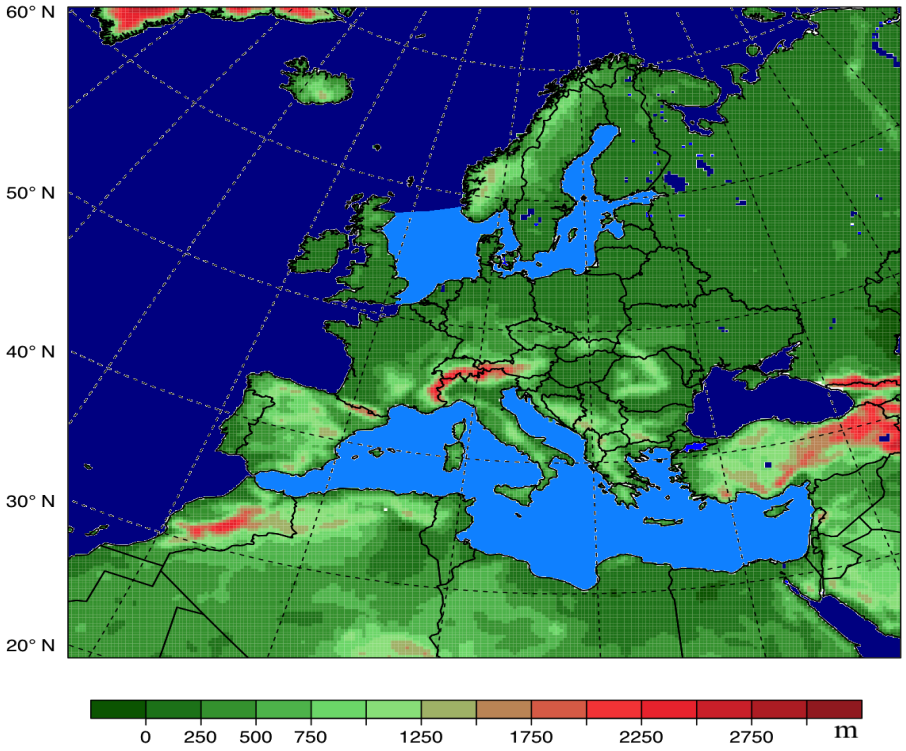

Figure 5.1: Atmospheric model domain, sky blue color indicates the coupling regions for the Mediterranean Sea and North- and Baltic Seas

radiation scheme (Ritter and Geleyn 1992). To better represent sea ice in the North- and Baltic Seas, a sub-grid scale sea ice mask was implemented in the CCLM coupled configuration over that region to account for partially sea ice covered grid boxes. In the coupled setup, the CCLM model receives the sea ice mask from NEMO-NORDIC and calculates the weighted average of the albedo in a grid cell based on the fraction of ice and open water (for more details see Van Pham et al. 2014). The initial and lateral boundary conditions for CCLM were taken from the ECMWF's ERA-Interim reanalysis provided every 6-h with 0.75° grid resolution for 1979–2014 (Dee et al. 2011). However, in the coupled configurations, the SSTs and ice fraction (only for the North- and Baltic Seas) in the coupling regions (sky blue areas in 5.1) are calculated using the following regional ocean models.

5.2.2 NEMO-MED12

NEMO-MED12 is a regional implementation of the ocean general circulation model NEMO v3.6 (Madec and NEMO Team 2008) for the Mediterranean Sea (Beuvier et al. 2012; Lebeaupin et al. 2011, 2012; Akhtar et al. 2018). The NEMO-MED12 grid covers the whole Mediterranean Sea plus a small part of the Atlantic Ocean west of Gibraltar as a buffer zone for open boundary conditions (Beuvier et al. 2012); however, the coupling is only performed over the Mediterranean Sea (see Fig. 5.1). It has the standard irregular ORCA grid with 1/12° resolution (∼6.5–8.0 km in latitude and ∼5.5–7.5 km in longitude; 567×264 grid points). In the vertical, 75 unevenly z-

levels are used with a layer thickness of 1 m at the surface increasing to 135 m at the bottom. It is an eddy-resolving regional ocean model, as the Rossby radius for deformation over the Mediterranean Sea is on the order of 15 km (Lebeaupin et al. 2011). The numerical time step of the model is 720 s in our configuration. The initial conditions for three-dimensional potential temperature and salinity are provided by the MEDATLAS–II (Rixen 2012) monthly mean seasonal climatology (1945–2002) in the Mediterranean Sea. A 30–year coupled spin-up simulation driven by randomly resampled ERA-Interim data (1979–1990) balanced the initial state. Water exchange with the Atlantic Ocean is relaxed to the Levitus et al. (2005) climatology prescribed in the buffer zone. The Black Sea and runoff water input were prescribed from the climatological average of interannual data from Ludwig et al. (2009). For more details, we refer the reader to Beuvier et al. (2012), Lebeaupin et al. (2011), and Akhtar et al. (2018).

5.2.3 NEMO-NORDIC

NEMO-NORDIC is a regional implementation of the NEMO v3.3 for the North- and Baltic Seas (see e.g., Dieterich et al. 2013; Van Pham et al. 2014). The NEMO-NORDIC grid covers the whole Baltic and North Sea with two open boundaries in the Atlantic Ocean. The northern zonal boundary is the cross-section between Hebrides and Norway and the southern meridional boundary lies in the English Channel (Fig. 5.1). It has a resolution of 2 nautical minutes ($\sim$3.7 km; 619$\times$523 grid points) and 56 stretched vertical levels with a thickness of 3 m at the surface and 22 m at the bottom of the Norwegian Sea. Such a high horizontal resolution allows the mesoscale variability to be marginally resolved in the North- and Baltic Seas (Meier et al. 2003), as the average Rossby radius of deformation over the Baltic Sea is on the order of 7 km (Osiński et al. 2010). NEMO-NORDIC uses the NEMO sea ice model LIM3, which includes the dynamics and thermodynamic processes of sea ice (Vancoppenolle et al. 2009). NEMO-NORDIC employs a numerical time step of 180 s and free surface scheme to include tidal forcing in the dynamics. The tidal potential is prescribed at the open boundaries in the North Sea from the global tidal model of Egbert and Erofeeva (2002) and Egbert et al. (2010). The initial conditions for three-dimensional potential temperature and salinity are provided by Janssen et al. (1999) and the lateral boundary conditions in the North Sea are prescribed from ORAS4 reanalysis data (Balmaseda et al. 2013). Freshwater inflow of the rivers is provided from daily time series of the E-HYPE model output (Lindström et al. 2010).

5.2.4 Coupler and coupling fields

The coupling of the atmospheric (CCLM) and ocean models (NEMO-MED12 and NEMO-NORDIC) is achieved using the OASIS3-MCT coupler (Craig et al. 2017). The OASIS3-MCT coupler synchronizes the models and also interpolates the coupling fields from one model grid to another. In the coupled setup, the ocean model sends SST to CCLM through OASIS3-MCT and in turn receives solar energy, non-solar heat, momentum, and freshwater fluxes. In addition, NEMO-NORDIC sends the sea ice fraction to CCLM and receives sea level pressure. The

coupling fields are exchanged every 3-h. A more detailed description of the coupling strategy and its implementation can be found in Will et al. (2017).

5.2.5 Experiment and analyses methods

Hereafter, "CCLM" refers to uncoupled simulations, "MED" refers to CCLM coupled with NEMO-MED12, "NORDIC" refers to CCLM coupled with NEMO-NORDIC, and "MED+NORDIC" refers to CCLM simultaneously coupled with the two regional ocean models NEMO-MED12 and NEMO-NORDIC. Four simulations (CCLM, MED, NORDIC, and MED+NORDIC) were performed for 1979–2014.

First, the newly developed AORCM with one or two coupled European marginal seas was evaluated comparing mean simulated seasonal and annual SST over the coupling region with observations. Next, eight Vb-type events were selected from 1979–2014 (Table 5.1). These Vb-events triggered extreme precipitation over the northern slopes of the Alps and in Central Europe (see, e.g., Hofstätter and Chimani 2012; Ho-Hagemann et al. 2015; Messmer et al. 2017). The first two Vb-events (i.e., July 1981 and August 1985) were relatively weak events in terms of precipitation intensity (Messmer et al. 2017). The later events were associated with extreme floods, as described in section 5.1.

The cyclone trajectories in the reanalysis data and model simulations were detected with an objective method following Hofstätter and Chimani (2012) and Hofstätter et al. (2016). As this tracking method works only for regular grids, CCLM rotated horizontal wind and geopotential height fields were derotated and interpolated on a regular grid. A discrete cosine filter (Denis et al. 2002) was applied to avoid spurious structures and false detections of cyclone centers due to local minima, especially at the edge of low-pressure systems. The low-pass filter removed structures smaller than 400 km, decreased smoothly up to 1000 km, and passed all large scales (Hofstätter and Chimani 2012). The cyclone centers were localized at each time step as closed local minima for a geopotential height of 700 hPa. To determine the corresponding cyclone center at the following time step t_{n+1}, a first guess was estimated. For the first guess, the predicted cyclone propagation vector after (Hofstätter et al. 2016), equation (2), was applied. The horizontal wind at 700 hPa and 500 hPa was used for the first guess estimation. The detected cyclone center at t_{n+1} nearest to the position of the first guess was then chosen as the following track position. Based on this tracking method, it was not possible to detect continuous cyclone tracks for some events. In such cases, the corresponding following track some time steps later was considered.

To verify simulated cyclone precipitation against observations, an object-based measure of the Structure, Amplitude, and Location (SAL) of the precipitation field in a pre-specified domain was calculated according to Wernli et al. (2008). A 30×30 model grid box centered around the EOBS' precipitation maxima and threshold factor of 1/15 to identify objects were used to calculate SAL. An object defines a grid point of a local precipitation maximum above threshold values, which includes neighboring grid points as long as the grid point values are larger than the threshold values (Wernli et al. 2008). The amplitude component A of SAL describes the normalized domain averaged field difference of the simulated and observed precipitation.

Table 5.1: Selected Vb-cyclone events, the second and third columns show the length of cyclone tracks in days presented in Fig. 5.4 and period with most extreme precipitation, respectively

July 1981	18.07. (18 UTC)–23.07.1981 (00 UTC)	18.07–20.07.1981
August 1985	06.08. (12 UTC)–10.08.1985 (06 UTC)	06.08–08.08.1985
September 1993	23.09. (12 UTC)–25.09.1993 (06 UTC)	22.09–24.09.1993
July 1997	17.07. (06 UTC)–22.07.1997 (00 UTC)	18.07–20.07.1997
August 2002	09.08. (06 UTC)–19.08.2002 (00 UTC)	11.08–13.08.2002
August 2005	20.08. (00 UTC)–24.08.2005 (18 UTC)	20.08–22.08.2005
May/June 2013	28.05. (18 UTC)–02.06.2013 (06 UTC)	31.05–02.06.2013
May 2014	13.05. (18 UTC)–20.05.2014 (00 UTC)	14.05–16.05.2014

Its values range from -2 to $+2$, with 0 indicating a perfect forecast and $-1/+1$ indicating underestimation/overestimation of spatially averaged precipitation by a factor of 3. The structure component S describes the volume of the normalized precipitation object, using its size and shape. It ranges from -2 to $+2$ with 0 indicating area similarity of simulated and observed precipitation object. The third component, location L, computes the normalized distance between the center of mass of the simulated precipitation object and observed one. Additionally, mean differences in daily precipitation values of simulations and observations were used as simple statistical measures.

The following reference datasets were also incorporated into the analyses:

- NOAA Daily Optimum Interpolation SST (OISST), available from September 1981 to present on a 0.25° global grid every 6-h. It is based on observations from satellites, ships, and buoys (Reynolds et al. 2007).
- ENSEMBLES observations (EOBS) v15.0 precipitation dataset, available from 1950 to present. Daily accumulated EOBS precipitation values are used on the available 0.22° rotated grid. It is based on station observations mainly over European land (Haylock et al. 2008).
- ECMWF's ERA-Interim reanalysis precipitation, geopotential height, and horizontal wind datasets, available from 1979 to present on a 0.75° global grid (Dee et al. 2011).
- NASA's MERRA-2 reanalysis geopotential height and horizontal wind datasets, available from 1980 to present on a 0.5°×0.625° grid (Gelaro et al. 2017).

5.3 Results and discussion

In this section, we analyze the ability of the uncoupled and coupled models in reproducing observed Vb-cyclone characteristics. Because results from the newly developed regional atmospheric model coupled with two marginal seas are presented for the first time, we first

briefly evaluate the simulated SSTs for 1982–2014, which are distinct in coupled and uncoupled simulations.

5.3.1 SST

Simulated SST time series averaged over each of the coupling regions were compared against observed OISST. Figure 5.2 shows that simulated SSTs in MED+NORDIC display very small differences compared to MED or NORDIC. The differences between CCLM and observed OISST are small, as the ERA-Interim forcing's SSTs are based on observational data. MERRA-2 SSTs similarly assimilate observational data.

Mediterranean SSTs were warmer in the coupled simulations (both in MED and MED+NORIC) for 1979–1995 than OISST and colder after 2005. This underestimation of the warming trend might be linked to the aerosol climatology used in the simulations, which suppresses a positive trend in solar radiation absorption in the sea. In contrast, the North- and Baltic SSTs in the coupled simulations are generally slightly colder than OISST. All simulations reproduced SST interannual variability quite well in comparison to MERRA-2 and OISST. The abrupt cooling (blue asterisk) and warming (red asterisk; see e.g., Brankart and Pinardi 2001), are well reproduced in the Mediterranean Sea as well as in the North- and Baltic Seas. Notably, warming trends are larger in the North- and Baltic Seas (NORDIC: 2.1 °C, ERA-Interim: 2.3 °C) than the Mediterranean Sea (MED: 0.4 °C, ERA-Interim: 0.85 °C) for 1979–2014 in the simulations.

Figure 5.3 shows the mean seasonal differences between the coupled simulation MED+NORDIC and observations for 1982–2014 (as OSISST is available from September 1981). The SST differences between the coupled simulations and OISST are most pronounced during summer (0.8 °C) and winter (-1.1 °C) over the Mediterranean Sea. Therefore, the coupled model simulated a larger annual temperature amplitude. Locally, these differences are up to ± 2.5 °C in the Levantine basin and central Mediterranean Sea. In some parts of the Northwest Mediterranean Sea (e.g., Golf of Lions), the SST in the coupled simulations is lower than observed. These differences are very small in the Gulf of Genoa during summer where Vb-cyclones form. In the North- and Baltic Seas, the mean SSTs in the coupled simulations are colder in all seasons, with the most pronounced difference during summer (-1.2 °C) and differences are largest along coastlines. This can partly be explained with different spatial resolutions of the coupled sea model ($\sim$3.7 km) and OISST ($\sim$28 km) dataset.

5.3.2 Vb-cyclones

In this section, we focus on the reproducibility of Vb-cyclones, their trajectories, and associated heavy precipitation characteristics in the models with and without coupling of the marginal seas. The investigated cyclone events are listed in Table 5.1.

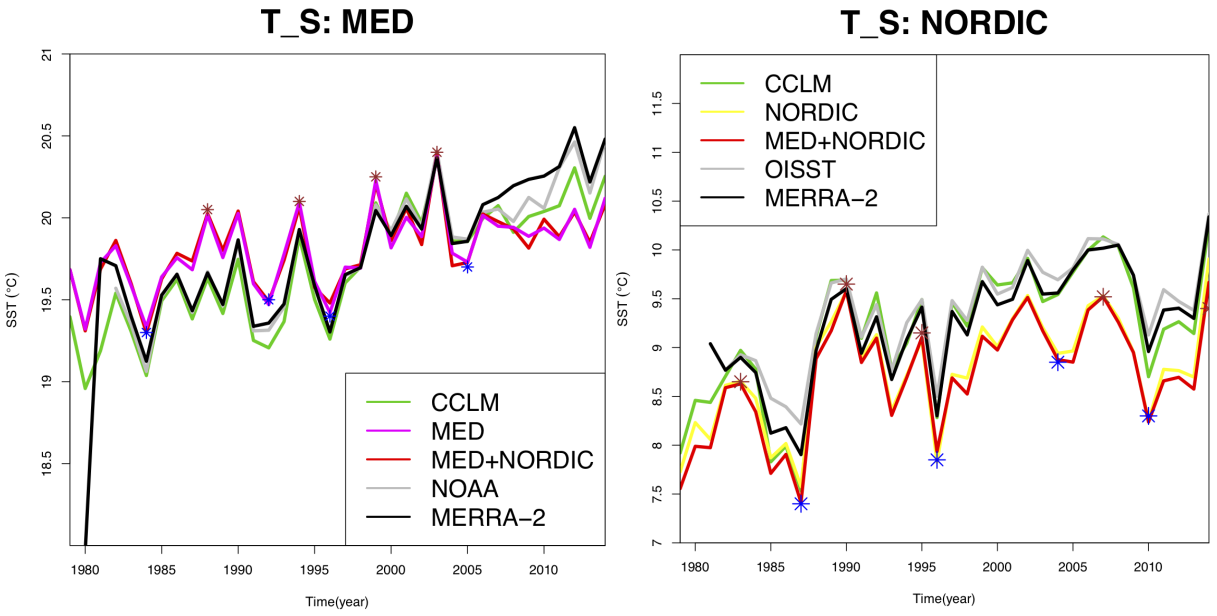

(a) (b)

Figure 5.2: Mean annual SST (°C) averaged over the (a) Mediterranean Sea and (b) North- and Baltic Seas for the period 1979–2014. The red and blue asterisks indicate abrupt warming and cooling periods, respectively

5.3.2.1 Cyclone Trajectories

Figure 5.4 shows the trajectories of the selected events. The dashed lines represent the trajectories obtained using reanalysis data for reference. The simulated trajectories agree well with the reanalysis data, which highlights the ability of the uncoupled and coupled models to simulate relevant physical processes of such rare and extreme events as Vb-cyclones. In particular, during deepening and mature phase of the cyclone, the model trajectories agreed well with the reanalysis trajectories. The July 1997 event (Zoe) was a special case with two cyclones contributing to extreme precipitation: one propagating from the Mediterranean Sea northeastward (1997/I), and a second one (1997/II) from the North Atlantic via the North Sea to Central Europe (Ho-Hagemann et al. 2015). The path of the first cyclone (1997/I) is not captured in ERA-Interim by our tracking algorithm, which considered only closed depressions.

The median of the geodesic distances and differences in core geopotential heights for the cyclone tracks were calculated for the three consecutive days of highest precipitation (as listed in Table 5.1). For each event, the median of the geodesic distances between the simulated or ERA-Interim trajectories and those from MERRA-2 are summarized in Fig. 5.5a. Note that the temporal resolution of the ERA-Interim and MERRA-2 tracks is 6-h, while model data output was available at 3-h. Therefore, only every second model track point was used to calculate the median Δx_{median} of the geodesic distance deviations Δx from the reference tracks in the MERRA-2 reanalysis data. The medians Δx_{median} for the ERA-Interim tracks are less than 100 km for all events. Overall, coupling improves the position of all simulated Vb-cyclones, excluding the 2013 event. However, the best suited coupling set up (NORDIC, MED, or MED+NORDIC) varies from event to event according to the reference trajectories. This was also the case for the core

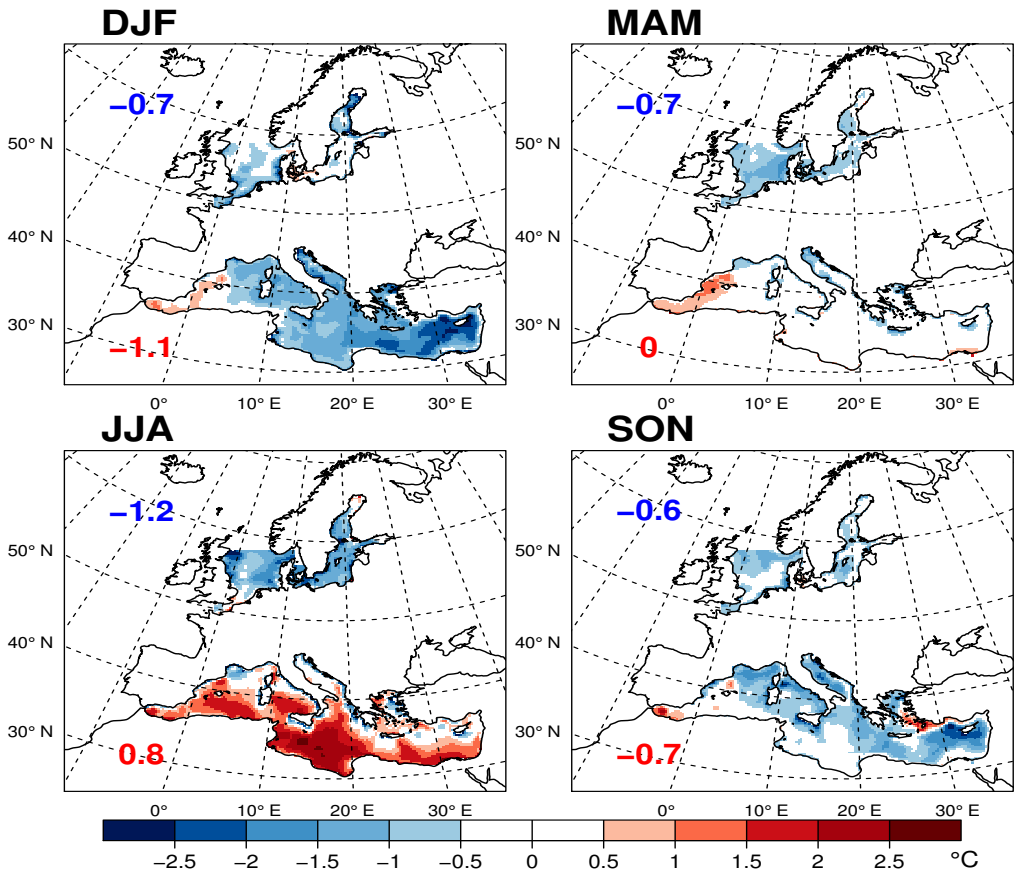

Figure 5.3: Mean seasonal differences in SST (°C) between MED+NORDIC and OISST for 1982–2014. The colored numbers indicate mean differences in the Mediterranean Sea (red) and in North- and Baltic Seas (blue)

geopotential heights, which is a measure of cyclone intensity and life cycle phase. Figure 5.5b shows, analogous to Fig. 5.4, the medians Δh_{median} of the core geopotential height differences to the reference tracks (MERRA-2). Only during the 1981, 1997/I, and 2002 events, does coupling not improve the simulated core geopotential heights. Note that the average core geopotential heights of all MERRA-2 track points were about 296 geopotential decameter (gpdam). Thus, all medians Δh_{median} are about 1% of the average MERRA-2 core geopotential height. The observation that no coupling configuration performed best for all events indicates that for some events the North- and Baltic Seas coupling has a measurable influence on Vb-cyclones and that this influence varies on a case-by-case basis.

5.3.2.2 Precipitation

To evaluate the performance of the uncoupled and coupled models in simulating precipitation intensities associated with Vb-cyclones, we selected the highest three consecutive precipitation days for each event (cf. Table 5.1). Figure 5.6 shows composite daily precipitation fields (averaged over three days for each event) of selected Vb-events for all model simulations, ERA-Interim reanalysis, and EOBS. In most simulated events, precipitation mainly fell over the northern side of Alps and extended toward East and Central Europe following the cyclone trajectories (Fig.

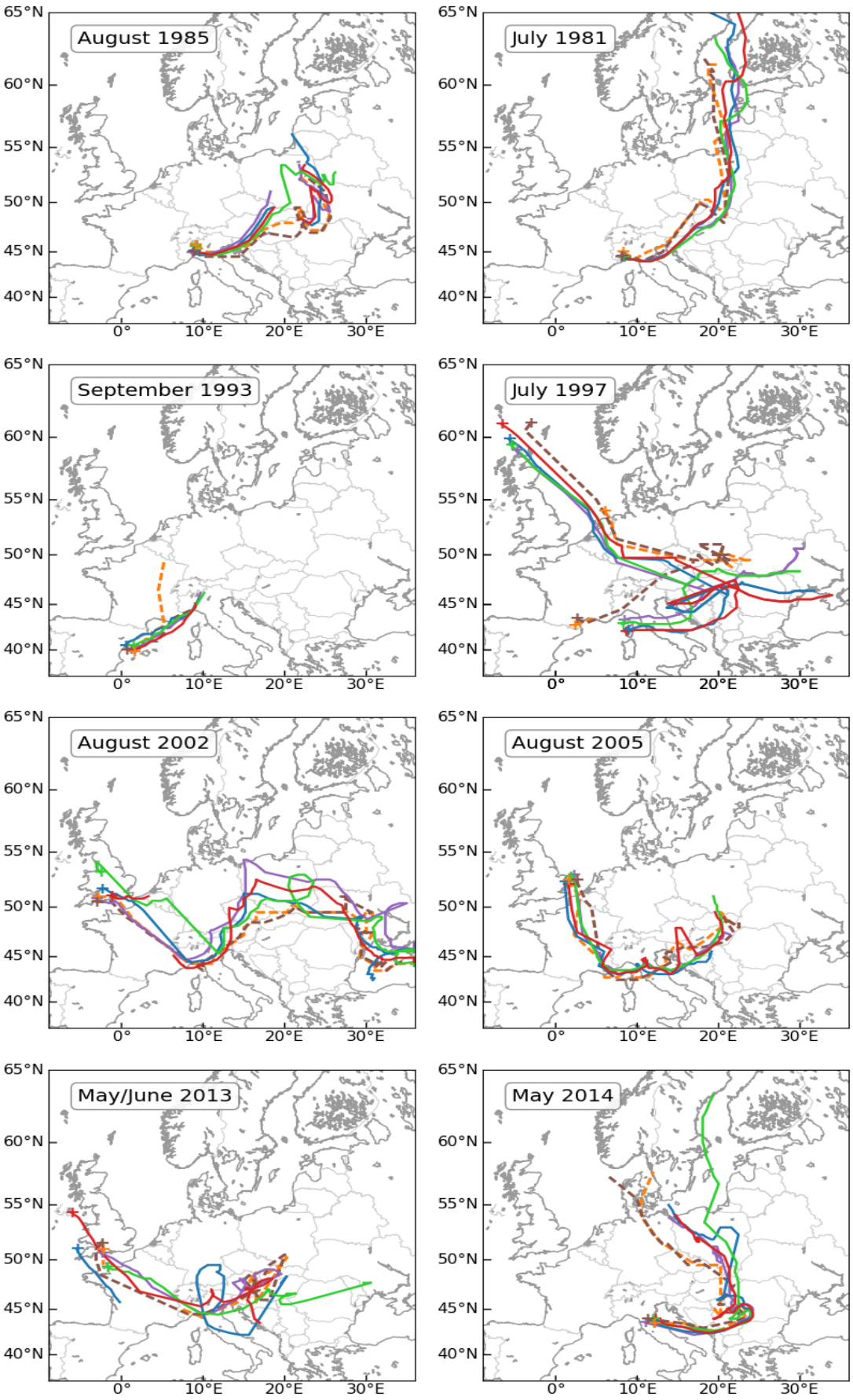

Figure 5.4: Tracks of the eight selected Vb-cyclones from the CCLM (purple), MED (blue), NORDIC (green), MED+NORDIC (red), ERA-Interim (orange, dashed), and MERRA-2 (brown, dashed)

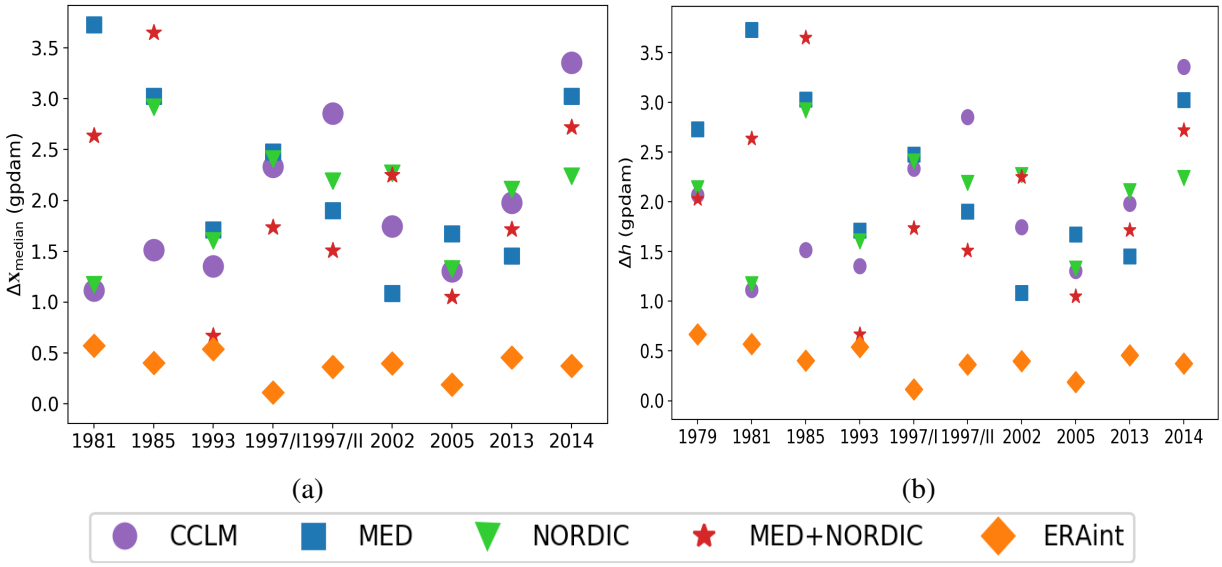

Figure 5.5: (a) Median values of geodesic cyclone path distances (Δx_{median}) and (b) core geopotential height differences (Δh_{median}) compared to MERRA-2 reanalysis data for each event (colored symbols). Only track points during the three consecutive extreme precipitation days (see Table 5.1) were chosen

5.4). During the decaying phase, the cyclone paths diverged, but most precipitation occurs during the intensification and mature phase; Messmer et al. (2017) also found the diversion of tracks during the decaying phase. Thus, the later stage track divergence does not have a large influence on the simulated precipitation fields. The locations of precipitation maxima are different among model simulations and in comparison to EOBS. However, the positions of the precipitation maxima (Fig. 5.5) agreed well with the corresponding cyclone trajectories (Fig. 5.4). This is in contrast to the findings of Messmer et al. (2017), who found no relevant influence of cyclone tracks on changed precipitation fields due to changes in SST and soil moisture.

In the 1981, 1993, and 2014 events, the location of the precipitation maxima were close among all coupling configurations, similar to the corresponding cyclone trajectories during the mature phase. In the July 1997 event, CCLM shifted the precipitation location eastward compared to the other simulations and observations, with NORDIC closest to observations. This result was also found by Ho-Hagemann et al. (2015), where the coupling of North- and Baltic Seas improved the precipitation simulation of the July 1997 event. The authors suggested this was due to a better representation of pressure patterns in their coupled simulation. In August 1985, the precipitation maximum in the ERA-Interim was located in the Alpine region, while in the EOBS it was at the border of the Czech Republic, Poland, and Slovakia. The NORDIC simulation shifted the cyclone track most northward compared to MERRA-2 and ERA-Interim reanalysis data for this event (see Fig. 5.5a); however, its precipitation maximum was located close to the observed EOBS data. This observation indicates that for this event, the physical processes involved were better captured in NORDIC than in the reanalysis data. The simulated precipitation and tracks for the August 2002 event also showed large differences between models. Compared to observations, the tracks and precipitation were better represented in MED. The May/June 2013 event was best represented in the uncoupled CCLM.

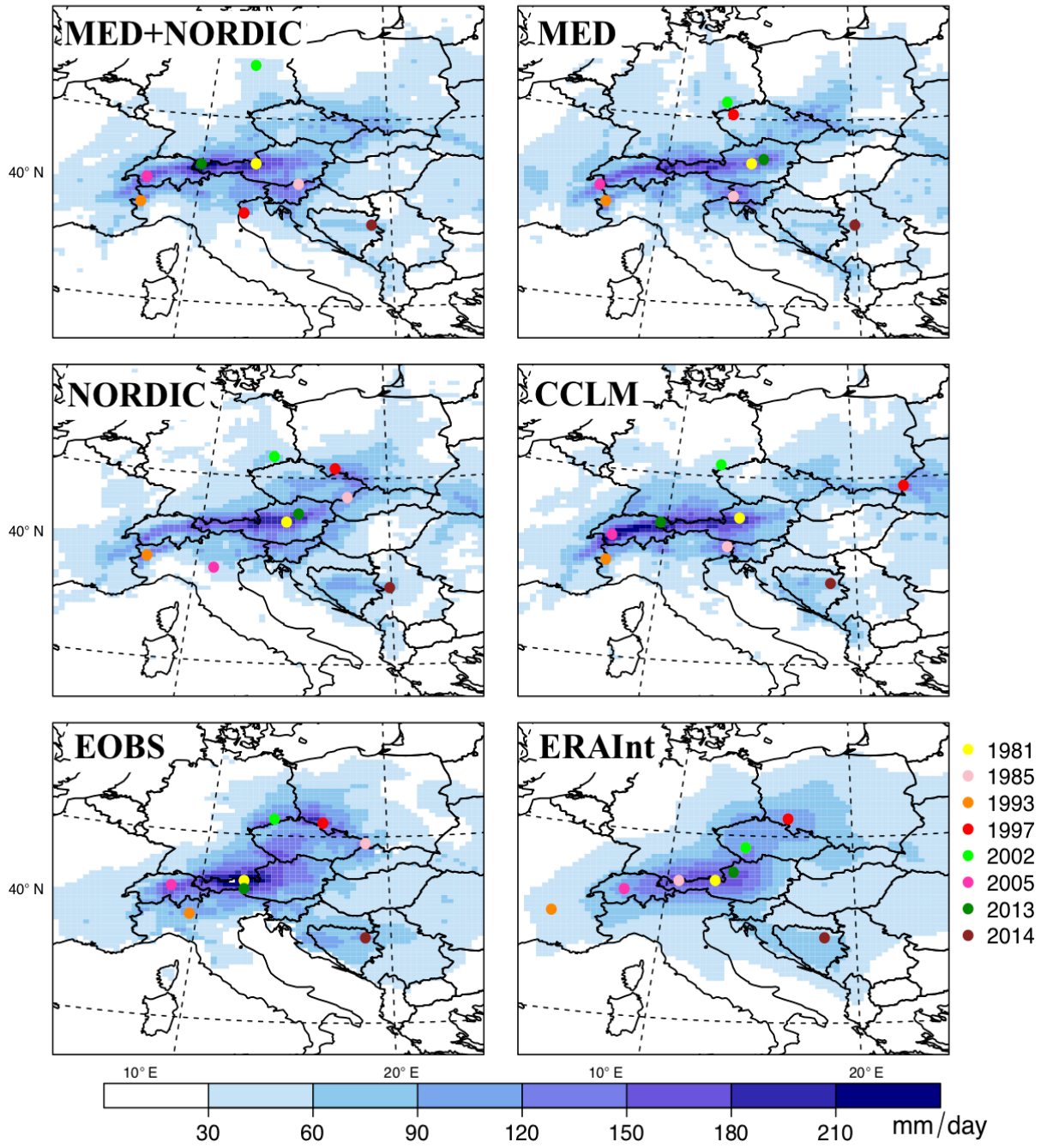

Figure 5.6: Composite precipitation (mm/day) averaged over each event from all simulations, ERA-Interim, and observation EOBS. Colored points indicate the precipitation maxima for each event

Figure 5.7 shows the difference in mean precipitation (in a domain of 30×30 grid boxes centered around the EOBS maximum) between simulations and EOBS. In most analyzed cases, the inter-model differences were small, except in July 1997, August 2002 and May/June 2013, where a model performed better or poor than another. Simulated precipitation is underestimated in most events, potentially due to coarse model grid-spacing (25 km in our case), which does not sufficiently resolve the orographic features and underestimates heavy convection in Vb precipitation events. The object-based quality measure SAL (Wernli et al. 2008) was used for more detailed analysis of daily amplitude, spatial shift, and structure of the precipitation fields.

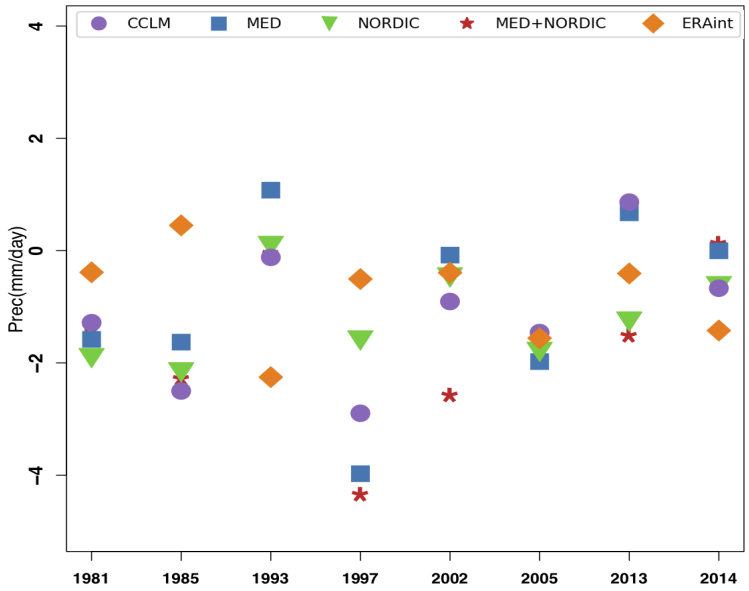

Figure 5.7: Mean precipitation difference over three days for each event compared to EOBS

Table 5.2: Average SAL values for selected cases with model simulations and ERA-Interim. A perfect coincidence with observation data is indicated by S, A, and L values of 0

	MED+NORDIC	MED	NORDIC	CCLM	ERAint
S	−0.101	−0.197	−0.083	−0.167	0.523
A	−0.030	0.002	−0.020	−0.003	0.006
L	0.237	0.240	0.232	0.227	0.165

Observed EOBS precipitation fields were used as a reference. Figure 5.8 shows the SAL diagram for the three consecutive days of highest precipitation (Table 5.1) of the Vb-events. In the top left quadrant of the panels, the amplitude is overestimated while the structure is underestimated, indicating too much precipitation with too small or/and peaked objects. In the bottom left quadrant, both amplitude and structure are underestimated, indicating too low precipitation and too small or/and peaked objects. In the top right quadrant, both amplitude and structure are overestimated while in bottom right quadrant, amplitude is underestimated with too large or/and flat objects. Most simulated SA values are in the left half of the diagram, indicating too small or/and peaked precipitation objects. In most cases, ERA-Interim's SA values are in the right half of the diagram, indicating too large or/and flat objects compared to EOBS. Location component L is best (close to zero) for NORDIC and showed the highest number of days when precipitation fell close to the observations (i.e., in the range of 0 to 0.1; see Fig. 5.8).

Table 5.2 summarizes the mean values of SAL components. Here, all models simulate too small or/and peaked objects and have similar mean location errors. The largest inter-model scatter is simulated in the S component, which is best in MED+NORDIC and NORDIC. The ERA-Interim is poorest in the S component.

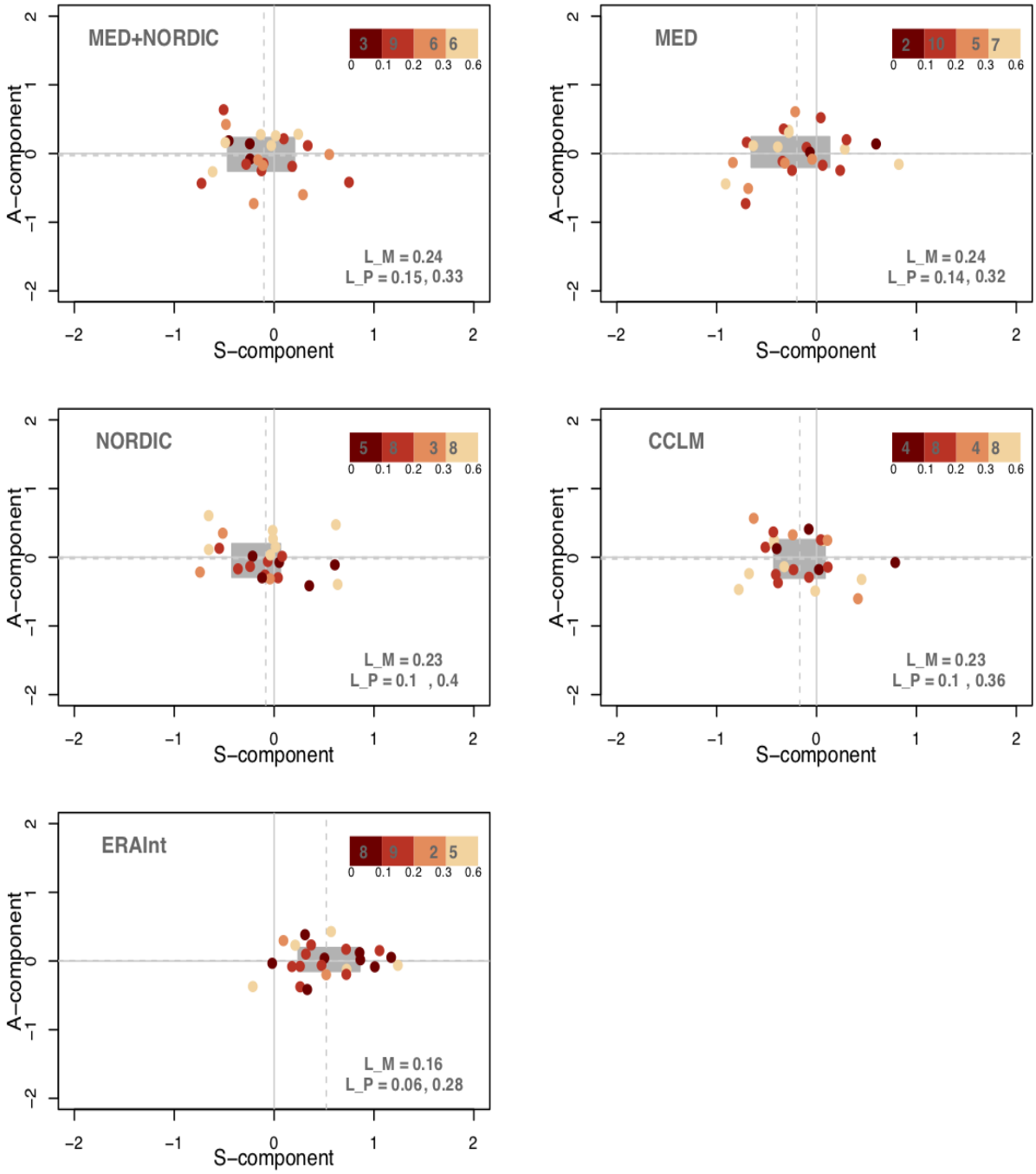

Figure 5.8: SAL diagram for daily precipitation (three days with highest precipitation days per event) forecast for uncoupled and coupled models and ERA-Interim for the simulated Vb-events. The location of each dot shows the daily values of the S (Structure) and A (Amplitude) components, whereas the dot colors indicate the values of L (Location). Dashed lines show the mean values for the S and A components, and gray boxes extend from the 20^{th} to 80^{th} percentile of S and A, respectively. L_M and L_P represent the mean and 20^{th} to 80^{th} percentile values of the L component, respectively

5.4 Conclusions

This study evaluated the robustness of a newly developed regional atmosphere-ocean model, which incorporated coupling of two European marginal seas, the Mediterranean and North- and Baltic Seas, to simulate Vb-cyclones, a weather phenomenon that often leads to intense precipitation over Central Europe. We investigated the effect of coupling, and the subsequent impact of more detailed simulations of air-sea interactions over the European marginal seas, on the trajectories and intensities of Vb-cyclones.

We first evaluated the simulated sea surface temperature (SST) from simulations over the coupling regions. The results showed that the mean seasonal and annual SSTs simulated in MED+NORDIC are similar to MED for the Mediterranean Sea and to NORDIC for the North- and Baltic Sea. The SST annual mean values and trends in the Mediterranean and North- and Baltic Seas fit quite well with observations. Compared to uncoupled simulations or observations, SSTs simulated using the coupled configurations show biases ($\sim$1 °C) over the coupling regions, especially during winter and summer. The coupled model configurations are stable and robust, and the model's SST uncertainties are promisingly small given the observational uncertainties in the marginal seas.

In general, all model configurations were able to reproduce the trajectories of Vb-cyclones and their main features, such as core geopotential heights. However, in most cases, the position, intensity, and life cycle of Vb-cyclones simulated in the coupled models were as close or even closer to cyclone characteristics derived from reanalysis datasets than those from the uncoupled model. In contrast to the findings of Messmer et al. (2017), the positions of the precipitation maxima agreed well with the corresponding cyclone trajectories. The evaluation of the simulated precipitation fields revealed that all models were able to capture intense precipitation patterns, but the patterns were peaked differently and shifted. More generally, the simulated precipitation underestimated EOBS precipitation data, possibly caused by the coarse model grid-spacing of 25 km, which does not sufficiently resolve orographic features and underestimates heavy convection in heavy Vb precipitation events.

Because ERA-Interim's OISST driven SSTs were applied in uncoupled sea areas, it is not surprising that no specific coupled configuration performed best in all cases. Additionally, coupling only the North- and Baltic Seas also showed an added value in simulating Vb-cyclones, especially in the July 1997 case (also shown in Ho-Hagemann et al. 2015). This advantage is linked to the contribution of different moisture sources for each individual case (cf. Gimeno et al. 2010; Volosciuk et al. 2016; Messmer et al. 2017).

The presented results indicate that a coupled system with two marginal seas is a useful tool for simulating regional climate over Europe and to study extreme events, such as Vb-cyclones. Furthermore, such a tool, with highly resolved SSTs and high-frequency air-sea coupling over two main European marginal seas, will be useful for studying future climate conditions. This coupled system with two marginal seas model is a step forward toward a high-resolution fully coupled regional climate system. Ongoing developments (e.g., closing the water cycle with a

river routing model) will advance the presented coupled model toward a convection-permitting regional climate system model.

Acknowledgements

The authors would like to thank the Center for Scientific Computing (CSC) of the Goethe University Frankfurt am Main and the Deutsches Klimarechenzentrum (DKRZ) for providing computational facilities. B. Ahrens acknowledges support by Senckenberg Biodiversity and Climate Research Centre (BiK–F), Frankfurt am Main. B. Ahrens and A. Krug acknowledge support by Deutsche Forschungsgemeinschaft (DFG, Research Unit For 2416: Space-Time Dynamics and Extreme Floods). B. Ahrens and N. Akhtar acknowledge support from the German Federal Ministry of Education and Research (BMBF) under grant MiKliP II (FKZ 01LP1518C). This work is part of the Med-CORDEX initiative (http://www.medcordex.eu) supported by the HyMeX (https://www.hymex.org/). Naveed Akhtar acknowledges Burkhardt Rockel (HZG) for his support and help. We acknowledge the EOBS dataset from the EU-FP6 project ENSEMBLES (http://ensembles-eu.metoffice.com) and the data providers in the ECAD project (www.ecad.eu).

CHAPTER 6

Conclusions

6.1 Summary

This thesis addresses the role of the Mediterranean Sea in the regional Mediterranean climate. It investigates the impact of fine-scale air-sea interactions and feedback mechanisms on sea surface heat fluxes, wind speed, and on potentially threatening Mediterranean cyclones (medicanes and Vb-cyclone). Additionally, it examinest the effect of horizontal atmospheric grid resolution on sea surface heat fluxes, wind speed, and medicanes. For this purpose, a new atmosphere-ocean regional climate model (AORCM) has been developed that includes a regional atmospheric climate model, COSMO-CLM (CCLM) and models for the Mediterranean Sea (MED) and/or the North- and Baltic Seas (NORDIC). Such a high-resolution coupled system allows for a better representation of the orography and detailed SST patterns.

Several experiments were performed using CCLM in uncoupled and coupled configuration in the context of this study. Both the coupled and uncoupled models were able to reproduce the main characteristics of the Mediterranean climate. Addressing the research questions highlighted in Chapter 1, the new developed AORCM leads to the following conclusions.

1. **Investigation of the sea surface heat fluxes and wind speed over the Mediterranean Sea:**
   In investigating the impact of horizontal atmospheric grid resolution (0.08°∼9 km vs. 0.44°∼50 km) and ocean coupling on sea surface heat fluxes and wind speed at sub-daily, seasonal, and annual timescales over the Mediterranean Sea, the following conclusions were drawn:

   - Fine-grid simulations gave a better representation of winds, particularly near the coastline and in the western Mediterranean Sea than coarse-grid simulations. Consequently, the fine atmospheric grid had a positive impact on turbulent fluxes.
   - In addition, ocean coupling improved the turbulent fluxes compared to the uncoupled model.
   - Radiative fluxes are slightly better represented in the coarse-grid simulations, due to the better representation of cloud cover. However, estimates of net heat flux (NH) are more realistic in the fine-grid coupled simulations.

- Furthermore, the coupled model simulates the sub-daily SST variations that are missing in ERA-Interim reanalysis. The results show that the sub-daily variations are of minor importance for the mean atmospheric state in the Mediterranean region.

2. **Investigation of medicanes**
   In investigating the impact of horizontal atmospheric grid resolution (0.44°∼50 km vs. 0.22°∼25 km, vs. 0.08°∼9 km) and ocean coupling on medicane tracks and intensity, the following conclusions were drawn:

   - Model performance depends strongly on the horizontal atmospheric grid resolution. Although the large-scale disturbance is reasonably well simulated at all three resolutions, medicane signals were not detected at the 0.44° resolution.
   - The mean sea level pressure and warm core structure were reasonably well captured in the 0.22° simulations, but wind speed was strongly underestimated. These features were more profound and refined in the 0.08° coupled and uncoupled simulations.
   - In comparison to the uncoupled simulations, the coupled simulations did not show any significate improvement at the 0.44° and 0.22° resolution.
   - At the 0.22° resolution, medicane tracks were almost identical in both the coupled and uncoupled simulations. However, at 0.08° resolution medicane track, warm core structure, and wind speed were largely improved in the coupled simulations compared to the uncoupled simulations.
   - In the majority of the cases, medicane tracks in the coupled simulations with 0.08° resolution were longer and closer to the observed ones. These results suggest that a 0.08° grid resolution produced more detailed features of medicanes, particularly with the coupled model.
   - The spectral nudging technique increased the accuracy in time and location of simulated medicanes. However, no improvement was observed in the mean sea level pressure and wind speed estimates.
   - Similar to the simulations performed without spectral nudging, in the nudged simulations, medicane tracks and wind speeds in the coupled simulations were better represented compared to the atmosphere-only simulations.
   - The intensities of the latent and sensible heat fluxes increased with ocean coupling and increasing atmospheric grid resolution. However, spectral nudging did not show any significant impact on the latent and sensible heat fluxes. Thus, the results suggest that the intensity of medicanes is strongly linked with surface heat fluxes and fine-scale features at the air-sea interface.

3. **Investigation of Vb-cyclones**
   In analyzing the impact of ocean coupling over the Mediterranean and North- and Baltic Seas on the trajectories and intensity of Vb-cyclones at a 0.22° (∼25 km) atmospheric grid

resolution and the performance of the AORCM which incorporates the coupling of two European marginal seas (MED+NORDIC), the following conclusions were drawn:

- The mean seasonal and annual SSTs simulated in MED+NORDIC were similar to MED for the Mediterranean Sea and to NORDIC for the North- and Baltic Sea.
- The annual mean values and trends of SST in the Mediterranean and the North- and Baltic Seas compared well with observations.
- Compared to uncoupled simulations or observations, SSTs simulated using the coupled configurations showed biases ($\sim$1 °C) over the coupling regions, especially during winter and summer.
- The coupled model configurations were stable and robust, and the model's SST uncertainties were promisingly small given the observational uncertainties in the marginal seas.
- In general, all model configurations were able to reproduce the trajectories of Vb-cyclones and their main features, such as core geopotential heights. However, in most cases, the position, intensity, and life cycle of Vb-cyclones simulated in the coupled models were as close as or even closer than cyclone characteristics derived from reanalysis datasets than those from the uncoupled model.
- The positions of the precipitation maxima agreed well with the corresponding cyclone trajectories.
- The evaluation of simulated precipitation fields revealed that all models were able to capture intense precipitation patterns, but the patterns peaked and shifted differently. In general, the simulated precipitation underestimated EOBS precipitation data, possibly caused by the coarse model grid-spacing of 25 km, which does not sufficiently resolve orographic features and underestimates heavy convection in heavy Vb precipitation events.
- Additionally, coupling only the North- and Baltic Seas also showed a benefit in simulating Vb-cyclones, especially in the July 1997 case (also shown in Ho-Hagemann et al. 2015). This advantage is linked to the contribution of different moisture sources for each individual case (cf. Gimeno et al. 2010; Volosciuk et al. 2016; Messmer et al. 2017).

Final remarks

The models analyzed here are able to reproduce the main characteristics of the physical processes involved in the Mediterranean Sea surface heat fluxes, wind speed, medicanes, and Vb-cyclones. It was found that the coupled model together with fine atmospheric grid resolution (< 10 km) improved the representation of sea surface heat fluxes, wind speed, and medicanes. Regarding the simulations of Vb-cyclones, ocean coupling had an overall positive, although with a strong

case-by-case variation, impact on the cyclone trajectories and intensity due to the variation in moisture source for each event. The ability of the AORCM to simulate its own highly resolved SST makes it more beneficial than the uncoupled atmospheric models. This study is a first step towards the use of new more complex modeling system. Further developments are required to overcome the current deficiencies in climate simulations.

6.2 Future prospects

The present AORCM with the two marginal seas (Mediterranian and North-Baltic-Seas) coupled to the atmosphere is a step forward toward a high-resolution fully coupled regional climate system, which can be used for further research in the area. In light of this thesis, some recommendations are presented below.

- Given the uncertainties in the radiation fluxes shown and the findings in the literature (Nabat et al. 2013), the prescription of aerosol optical depths should be investigated.
- Model inter-comparison within the Med-CORDEX and EURO-CORDEX projects could be useful for assessing the source of uncertainty in different model physics/parameterizations and to investigate the Vb-cyclones.
- Further, this study could be extended to investigate the impact of sub-daily variations in SST on extreme events such as heavy precipitation and medicanes,
- A numerical tool with highly resolved SSTs and high-frequency air-sea coupling over two main European marginal seas can be useful to study future climate conditions.
- Similar to the medicane, investigating the impact of different atmospheric grid resolutions could be investigated for Vb-cyclones.
- A river routing model with realistic river runoff has not been taken into account. However, they should be applied in future. Simulations including a river routing scheme can be useful to study the surface fluxes and the Mediterranean hydrological cycle.
- Presently the coupled model uses climatological values of sea surface height. Experiments with more realistic yearly values of sea surface height can be more useful to study the Mediterranean hydrological cycle.
- The presented coupled model can be used to study the role of air-sea interaction at the convective scale.

APPENDIX A

A.1 The COSMO-CLM 4.8 regional climate model coupled to regional ocean, land surface and global earth system models using OASIS3-MCT: description and performance

Will A, Akhtar N, Brauch J, Breil M, Davin E, Ho-Hagemann HTM, Maisonnave E, Thürkow M, and Weiher S (2017) The COSMO-CLM 4.8 regional climate model coupled to regional ocean, land surface and global earth system models using OASIS3-MCT: description and performance. Geosci Model Dev 10:1549–1586. doi:10.5194/gmd-10-1549-2017

A.2 Assessment of an ensemble of ocean-atmosphere coupled and uncoupled regional climate models to reproduce the climatology of Mediterranean cyclones

Flaounas E, Kelemen FD, Wernli H, Gaertner MA, Reale M, Sanchez-Gomez E, Lionello P, Calmanti S, Podrascanin Z, Somot S, Akhtar N, Romera R, Conte D (2018) Assessment of an ensemble of oceanatmosphere coupled and uncoupled regional climate models to reproduce the climatology of Mediterranean cyclones. Clim Dyn 51:1023–1040. doi:10.1007/s00382-016-3398-7

Bibliography

Akhtar N (2013) New approach with a basin-wide single column ocean model set-up to study the Mediterranean Sea dynamics. Master's thesis, Goethe University, Frankfurt am Main

Akhtar N, Brauch J, Dobler A, Bérenger K, Ahrens B (2014) Medicanes in an ocean-atmosphere coupled regional climate model. Nat Hazards Earth Syst Sci 14:2189–2201. doi:10.5194/nhess-14-2189-2014

Akhtar N, Brauch J, Ahrens B (2017) Climate Modeling over the Mediterranean Sea: Impact of Resolution and Ocean Coupling. Clim Dyn 51:933–948. doi:10.1007/s00382-017-3570-8

Alexander MA, Blade I, Newman M, Lanzante JR, Lau NC, Scott JD (2002) The atmospheric bridge: the influence of ENSO teleconnections on air-sea interaction over the global oceans. J Climate 15:2205–2231. doi:10.1175/1520-0442(2002)015<2205:Tabtio>2.0.Co;2

Alpert P, Neeman BU, Shay-El Y (1990) Climatological analysis of Mediterranean cyclones using ECMWF data. Tellus A 42:65–77. doi:10.1034/j.1600-0870.1990.00007.x

Alpert P, Stein U, Tsidulko M (1995) Role of sea fluxes and topography in eastern Mediterranean cyclogenesis. Global atmos and ocean syst 3:55–79

Alpert P, Baldi M, Ilani R, Krichak S, Price C, Rodo X, Saaroni H, Ziv B, Kishcha P, Barkan J, Mariotti A, Xoplaki E (2006) Relations between Climate Variability in the Mediterranean Region and the Tropics: ENSO, South Asian and African Monsoons, Hurricanes and Saharan Dust. Develop Earth Envir Sci 4:149–177. doi:10.1016/S1571-9197(06)80005-4

Artale V, Calmanti S, Rizzoli PM, Pisacane G, Rupolo V, Tsimplis M (2006) The Atlantic and Mediterranean Sea as connected systems. Dev Earth Environ Sci 4:283–323. doi:10.1016/S1571 -9197(06)80008-X

Artale V, Calmanti S, Carillo A, Dell'Aquila A, Herrmann M, Pisacane G, Ruti P, Sannino G, Struglia MV, Giorgi F, Bi X, Pal JS, Rauscher S, The PROTHEUS Group (2010) An atmosphere-ocean regional climate model for the Mediterranean area: assessment of a present climate simulation. Clim Dyn 35:721–740. doi:10.1007/s00382-009-0691-8

Awan NK, Formayer H (2016) Cut-off low systems and their relevance to large-scale extreme precipitation in the European Alps. Theor Appl Climatol 129:149–158. doi:10.1007/s00704-016-1767-0

Balmaseda MA, Mogensen K, Weaver AT (2013) Evaluation of the ECMWF ocean reanalysis system ORAS4. Q J R Meteorol Soc 139:1132–1161. doi:10.1002/qj.2063

Beniston M (2006) August 2005 intense rainfall event in Switzerland: Not necessarily an analog for strong convective events in a greenhouse climate. Geophys Res Lett 33:L05701. doi:10.1029/2005GL025573

Beuvier J, Béranger K, Lebeaupin–Brossier C, Somot S, Sevault F, Drillet Y, Bourdallé–Badie R, Ferry N, Lyard F (2012) Spreading of the Western Mediterranean Deep Water after winter 2005: time scales and deep cyclone transport. J Geophys Res 117:C07022. doi:10.1029/2011JC007679

Brankart JM, Pinardi N (2001) Abrupt cooling of the Mediterranean Levantine intermediate water at the beginning of the 1980s: observational evidence and model simulation. J Phys Oceanogr 31:2307–2320. doi:10.1175/1520-0485(2001)031<2307:ACOTML>2.0.CO;2

Bryden HL, Candela J, Kinder TH (1994) Exchange through the Strait of Gibraltar. Prog oceanogr 33:201–248. doi:10.1016/0079-6611(94)90028-0

Businger S, Reed R (1989) Cyclogenesis in cold air masses. Weather Forecast 4:133–156. doi:10.1175/1520-0434(1989)004<0133:CICAM>2.0.CO;2

Calmanti S, Artale V, Sutera A (2006) North Atlantic MOC variability and the Mediterranean Outflow: a box-model study. Tellus A Dyn Meteorol Oceanogr 58(3):416–423. doi:10.1111/j.1600-0870.2006.00176.x

Cavicchia L, Von Storch (2012) The simulation of medicanes in a high-resolution regional climate model. Clim Dyn 39:2273–2290. doi:10.1007/s00382-011-1220-0

Cavicchia L, Von Storch H, Gualdi S (2014a) A long-term climatology of medicanes. Clim Dyn 43:1183–1195. doi:10.1007/s00382-013-1893-7

Cavicchia L, Von Storch H, and Gualdi S (2014b) Mediterranean Tropical-Like Cyclones in Present and Future Climate. J Climate 27:7493–7501. doi:10.1175/JCLI-D-14-00339.1

Christensen JH, Christensen O (2007) A summary of the PRUDENCE model projections of changes in European climate by the end of this century. Global Planet Change 81(1):7–30. doi:10.1007/s10584-006-9210-77-30

Conte D, Miglietta MM, Levizzani V (2011) Analysis of instability indices during the development of a Mediterranean tropical-like cyclone using MSG-SEVIRI products and the LAPS model. Atmos Res 101:264–279. doi:10.1016/j.atmosres.2011.02.016

Craig A, Valcke S, Coquart L (2017) Development and performance of a new version of the OASIS coupler, OASIS3-MCT_3.0. Geosci Model Dev 10:3297–3308. doi:10.5194/gmd-10-3297-2017

Cyberski J, Grzes M, Gutry-Korycka M, Nachlik E, Kundzewicz ZW (2006) History of floods on the River Vistula. Hydrol Sci 51:799817. doi:10.1623/hysj.51.5.799

Dee DP, Uppala SM, Simmons AJ, Berrisford P, Poli P, Kobayashi S, Andrae U, Balmaseda, MA, Balsamo G, Bauer P, Bechtold P, Beljaars ACM, van de Berg L, Bidlot J, Bormann N, Delsol C, Dragani R, Fuentes M, Geer AJ, Haimberger L, Healy SB, Hersbach H, Hólm EV, Isaksen L, Kållberg P, Köhler M, Matricardi M, McNally AP, Monge-Sanz BM, Morcrette JJ, Park BK, Peubey C, de Rosnay P, Tavolato C, Thépaut JN, Vitart F (2011) The ERA-Interim reanalysis: configuration and performance of the data assimilation system. Q J R Meteorol Soc 137:553–597. doi:10.1002/qj.828

Dell'Aquila A, Calmanti S, Ruti P, Struglia MV, Pisacane G, Carillo A, Sannino G (2012) Effects of seasonal cycle fluctuations in an A1B scenario over the Euro-Mediterranean. Clim Res 52:135–157. doi:10.3354/cr01037

Denis B, Côté J, Laprise R (2002) Spectral Decomposition of Two-Dimensional Atmospheric Fields on Limited-Area Domains Using the Discrete Cosine Transform (DCT). Mon Wea Rev 130:1812–1829. doi:10.1175/1520-0493(2002)130<1812:SDOTDA>2.0.CO;2

Dieterich C, Schimanke S, Wang S, Väli G, Liu Y, Hordoir R, Axell L, Meier H (2013) Evaluation of the SMHI coupled atmosphere-ice-ocean model RCA4-NEMO. Tech Rep 47, Swedish Meteorological and Hydrological Institute (SMHI), Sweden

Drobinski P, Ducrocq V, Alpert P, Anagnostou E, Béranger K, Borga M, Braud I, Chanzy A, Davolio S, Delrieu G, Estournel C, Boubrahmi NF, Font J, Grubišić V, Gualdi S, Homar V, Ivančan-Picek B, Kottmeier C, Kotroni V, Lagouvardos K, Lionello P, Llasat MC, Ludwig W, Lutoff C, Mariotti C, Richard E, Romero R, Rotunno R, Roussot O, Ruin I, Somot S, Taupier-Letage I, Tintore J, Uijlenhoet R, Wernli H (2014) HyMeX: A 10-year multidisciplinary program on the Mediterranean water cycle. Bull Am Meteorol Soc 95:1063–1082. doi:10.1175/BAMS-D-12-00242.1

Dubois C, Somot S, Calmanti S, Carillo A, Déqué M, Dell'Aquila A, Elizalde A, Gualdi S, Jacob D, L'Hévéder B, Li L, Oddo P, Sannino G, Scoccimarro E, Sevault F (2012) Future projections of the surface heat and water budgets of the Mediterranean Sea in an ensemble of coupled atmosphere-ocean regional climate models. Clim Dyn 39:1859–1884. doi:10.1007/s00382-011-1261-4

Egbert GD, Erofeeva SY (2002) Efficient Inverse Modeling of Barotropic Ocean Tides. J Atmos Ocean Tech 19:183–204. doi:10.1175/1520-0426(2002)019<0183:EIMOBO>2.0.CO;2

Egbert GD, Erofeeva SY, Ray RD (2010) Assimilation of altimetry data for nonlinear shallow-water tides: Quarter-diurnal tides of the Northwest European Shelf. Continental Shelf Res 30(6):668–679. doi:10.1016/j.csr.2009.10.011

Elguindi N, Somot S, Déqué M, Ludwig W (2011) Climate change evolution of the hydrological balance of the Mediterranean, Black and Caspian Seas: impact of climate model resolution. Clim Dyn 24:205–228. doi:10.1007/s00382-009-0715-4

Emanuel K (1986) An air–sea interaction theory for tropical cyclones, Part I: Steady-state maintenance. J Atmos Sci 43:585–605. doi:1680-7359/adgeo/2005-2-217

Emanuel K, Rotunno R (1987) An air–sea interaction theory for tropical cyclones, Part II: Evolutionary study using a nonhydrostatic axisymmetric numerical model. J Atmos Sci 44:542–561. doi:10.1175/1520-0469(1987)044<0542:AAITFT>2.0.CO;2

Emanuel K (2005) Genesis and maintenance of "Mediterranean hurricanes". Adv Geosci 2:217–220. doi:10.5194/adgeo-2-217-2005

Ernst JA, Matson M (1983) A Mediterranean tropical storm. Weather 38:332–337. doi:10.1002/j.1477-8696.1983.tb04818.x

Fairall CW, Bradley EF, Godfrey JC, Wick GA, Edson JB, Young GS (1996) Cool–skin and warm-layer effects on sea surface temperature. J Geophys Res 101:1295–1308. doi:10.1029/95JC03190

Fernández J, Sáenz J, Zorita E (2003). Analysis of wintertime atmospheric moisture transport and its variability over southern Europe in the NCEP Reanalyses. Climate Res 23(3):195–215. doi:10.3354/cr023195

Fischer EM, Sedláçek J, Hawkins E, Knutti R (2014) Models agree on forced response pattern of precipitation and temperature extremes. Geophys Res Lett 41:8554–8562. doi:10.1002/2014GL062018

Fita L, Romero R, Luque A, Emanuel K, Ramis C (2007) Analysis of the environments of seven Mediterranean tropical-like storms using an axisymmetric, nonhydrostatic, cloud resolving model. Nat Hazards Earth Syst Sci 7:41–56. doi:10.5194/nhess-7-41-2007

Flaounas E, Di Luca A, Drobinski P, Mailler S, Arsouze T, Bastin S, Beranger K, Lebeaupin Brossier C (2016) Cyclone contribution to the Mediterranean Sea water budget. Clim Dyn 44:1–15. doi:10.1007/s00382-015-2622-1

Flaounas E, Kelemen FD, Wernli H, Gaertner MA, Reale M, Sanchez-Gomez E, Lionello P, Calmanti S, Podrascanin Z, Somot S, Akhtar N, Romera R, Conte D (2018) Assessment of an ensemble of ocean–atmosphere coupled and uncoupled regional climate models to reproduce the climatology of Mediterranean cyclones. Clim Dyn 51:1023–1040. doi:10.1007/s00382-016-3398-7

Gaertner MA, Jacob D, Gil V, Domínguez M, Padorno E, Sánchez E, Castro M (2007) Tropical cyclones over the Mediterranean Sea in climate change simulations. Geophys Res Lett 34:L14711. doi:10.1029/2007GL029977

Gaertner MA, González-Alemán JJ, Romera R, Domínguez M, Gil V, Sánchez E, Gallardo C, Miglietta MM, Walsh K, Sein D, Somot S, Dell'Aquila A, Teichmann C, Ahrens B, Buonomo E, Colette A, Bastin S, van Meijgaard E, Nikulin G (2018) Simulation of medicanes over the Mediterranean Sea in a regional climate model ensemble: impact of ocean–atmosphere coupling and increased resolution. Clim Dyn 51:1041–1057. doi:10.1007/s00382-016-3456-1

Gangoiti G, Sáez de Cámara E, Alonso L, Navazo M, Gómez MC, Iza J, García JA, Ilardia JL, Millán MM (2011) Origin of the water vapor responsible for the European extreme rainfalls of August 2002: High resolution simulations and tracking of air masses. J Geophys Res 116:D21102. doi:10.1029/2010JD015530

Gao X, Pal JS, Giorgi F (2006) Projected changes in mean and extreme precipitation over the Mediterranean region from a high resolution double nested RCM simulation. Geophys Res Lett 33:L03706. doi:10.1029/2005GL024954

Gelaro R, McCarty W, Suárez MJ, Todling R, Molod A, Takacs L, Randles CA, Darmenov A, Bosilovich MG, Reichle R, Wargan K, Coy L, Cullather R, Draper C, Akella S, Buchard V, Conaty A, da Silva AM, Gu W, Kim G, Koster R, Lucchesi R, Merkova D, Nielsen JE, Partyka G, Pawson S, Putman W, Rienecker M, Schubert SD, Sienkiewicz M, Zhao B (2017) The Modern-Era Retrospective Analysis for Research and Applications, Version 2 (MERRA–2). J Climate 30:5419–5454. doi:10.1175/JCLI-D-16-0758.1

Gimeno L, Drumond A, Nieto R, Trigo RM, Stohl A (2010) On the origin of continental precipitation. Geophys Res Lett 37:L13804. doi:10.1029/2010GL043712

Giorgi F (2006) Climate change hot-spots. Geophys Res Lett 33:L08707. doi:10.1029/2006GL025734

Giorgi F, Jones C, Asrar GR (2009) Addressing climate information needs at the regional level: the CORDEX framework. Bull World Meteorol Organ 58:175–183

Graefe H, Hegg (2004) Ereignisanalyse Hochwasser August 2002 in den Osterzgebirgsüssen. Tech rep Säachsisches Landesamt für Umwelt und Geologie 176

Grams CM, Binder H, Pfahl S, Piaget N, Wernli H (2014) Atmospheric processes triggering the central European floods in June 2013. Nat Hazards Earth Syst Sci 14:1691–1702. doi:10.5194/nhess-14-1691-2014

Grazzini F, Van der Grijn G (2003) Central European floods during summer 2002. ECMWF Newslett 96:18–28

Godina R, Lalk P, Lorenz P, Müller G, Weilguni V (2006) Hochwasser 2005. Ereignisdokumentation: Teilbericht des Hydrographischen Dienstes, Federal Ministry for Agriculture, Forestry, Environment, and Water Management. Sekt VII Vienna 30

Gualdi S, Somot S, Li L, Artale V, Adani M, Bellucci A, Braun A, Calmanti S, Carillo A, Dell'Aquila A, Déqué M, Dubois C, Elizalde A, Harzallah A, Jacob D, L'Hévéder B, May W, Oddo P, Ruti P, Sanna A, Sannino G, Scoccimarro E, Sevault F, Navarra A (2012) The CIRCE simulations: a new set of regional climate change projections performed with a realistic representation of the Mediterranean Sea. Bull Am Meteorol Soc 94:65–81. doi:10.1175/BAMS-D-11-00136.1

Haylock MR, Hofstra H, Klein Tank AMG, Klok EJ, Jones PD, New M (2008) A European daily high resolution gridded dataset of surface temperature and precipitation. J Geophys Res 113:D20119. doi:10.1029/2008JD10201

Held H, Gerstengarbe F-W, Pardowitz, T, Pinto JG, Ulbrich U, Born K, Donat MG, Karremann MK, Leckebusch GC, Ludwig P, Nissen KM, Österle H, Prahl BF, Werner PC, Befort DJ, Burghoff O (2013) Projections of global warming-induced impacts on winter storm losses in the German private household sector. Climatic Change 121:195–207. doi:10.1007/s10584-013-0872-7

Herrmann M, Somot S (2008) Relevance of ERA40 dynamical downscaling for modeling deep convection in the North-Western Mediterranean Sea. Geophys Res Lett 35:L04607. doi:10.1029/2007GL032442

Herrmann M, Somot S, Calmanti S, Dubois C, Sevault F (2011) Representation of daily wind speed spatial and temporal variability and intense wind events over the Mediterranean Sea using dynamical 594 downscaling: impact of the regional climate model configuration. Nat Hazards Earth Syst Sci 11:1983–2001. doi:10.5194/nhess-11-1983-2011

Hofstätter M, Chimani B (2012) Van Bebber's cyclone tracks at 700 hPa in the Eastern Alps for 1961–2002 and their comparison to circulation type classifications. Meteorol Z 21:459–473. doi:10.1127/0941-2948/2012/0473

Hofstätter M, Chimani B, Lexer A, Blöschl G (2016) A new classification scheme of European cyclone tracks with relevance to precipitation. Water Resour Res 52:7086–7104. doi:10.1002/2016WR019146

Hofstätter M, Lexer A, Homann M, Blöschl G (2017) Large-scale heavy precipitation over central Europe and the role of atmospheric cyclone track types. Int J Climatol 38:497–517. doi:10.1002/joc.5386

Ho-Hagemann H, Stefan H, Rockel B (2015) On the role of soil in the generation of heavy rainfall during the Oder flood event in July 1997. Tellus A Dyn Meteorol and Oceanogr (67):28661. doi:10.3402/tellusa.v67.28661

Homar V, Romero R, Stensrud D, Ramis C, Alonso S (2003) Numerical diagnosis of a small, quasi-tropical cyclone over the Western Mediterranean: dynamical vs. boundary factors. Q J R Meteorol Soc 129:1469–1490. doi:10.1256/qj.01.91

Hoskins B, Hodges K (2002) New perspectives on the Northern Hemisphere winter storm tracks. J Atmos Sci 59:1041–1061. doi:10.1175/1520-0469(2002)059<1041:NPOTNH>2.0.CO;2

Hurrell JW (1995) Decadal Trends in the North Atlantic Oscillation: Regional Temperatures and Precipitation. Science 269:676–679. doi:10.1126/science.269.5224.676

IPCC (2007) Climate change 2007: The physical science basis-IPCC working group 1 contribution to AR4 Intergovernmental Panel on Climate Change, Cambridge University Press, Cambridge

James P, Stohl A, Spichtinger N, Eckhardt S, Forster C (2004) Climatological aspects of the extreme European rainfall of August 2002 and a trajectory method for estimating the associated evaporative source regions. Nat Hazards Earth Syst Sci 4:733–746. doi:10.5194/nhess-4-733-2004

Jansá A (1986) Genoa cyclones and other Western Mediterranean cyclones. WMO/TD No 128 App 8:59–70

Jansá A, Genovés A, Picornell M, Campins J, Riosalido OCR (2001) Western Mediterranean cyclones and heavy rain. Part 2: statistical approach. Meteorol Appl 8:43–56. doi:10.1017/S1350482701001049

Janssen F, Schrum C, Backhaus JO (1999) A Climatological Data Set of Temperature and Salinity for the Baltic Sea and the North Sea. Hydrographische Zeitschrift 51. doi:10.1007/BF02933676

Josey SA (2003) Changes in the heat and freshwater forcing of the eastern Mediterranean and their influence on deep water formation. J Geophys Res 108:1–18. doi:10.1029/2003JC001778

Josey SA, Somot S, Tsimplis M (2011) Impacts of atmospheric modes of variability on Mediterranean Sea surface heat exchange. J Geophys Res 116(C2):C02032. doi:10.1029/2010JC006685

Kaspar M, Müller M (2008) Selection of historic heavy large-scale rainfall events in the Czech Republic. Nat Hazards Earth Syst Sci 8:1359–1367. doi:10.5194/nhess-8-1359-2008

Kawai Y, Wada A (2007) Diurnal sea surface temperature variation and its impact on the atmosphere and ocean: A review. J Oceanogr 63:721–744. doi:10.1007/s10872-007-0063-0

Kelemen F, Ludwig P, Reyers M, Ulbrich S, Pinto J (2016) Evaluation of moisture sources for the Central European summer flood of May/June 2013 based on regional climate model simulations. Tellus A Dyn Meteorol and Oceanogr 68:1. doi:10.3402/tellusa.v68.29288

Köppen W, Geiger R (1936) Das geographische system der klimate. Handbuch der klimatologie. Bd 1, Teil C. Verlag Gebrüder Bornträger, Berlin

Kothe S, Panitz HJ, Ahrens B (2014) Analysis of the radiation budget in regional climate simulations with COSMO-CLM for Africa. Meteorol Z 23(2):123–141. doi:10.1127/0941-2948/2014/0527

Lebeaupin Brossier C, Drobinski P (2009) Numerical high–resolution air-sea coupling over the Gulf of Lions during two tramontane/mistral events. J Geophys Res 114:D10110. doi:10.1029/2008JD011601

Lebeaupin Brossier C, Béranger K, Deltel C, Drobinski P (2011) The Mediterranean response to different space-time resolution atmospheric forcings using perpetual mode sensitivity simulations. Ocean Modelling 36:1–25. doi:10.1016/j.ocemod.2010.10.008

Lebeaupin Brossier C, Béranger K, Drobinski P (2012) Sensitivity of the northwestern Mediterranean Sea coastal and thermohaline circulations simulated by the $1/12°$–resolution ocean model NEMOMED12 to the spatial and temporal resolution of atmospheric forcing. Ocean Modelling 43–44:94–107. doi:10.1016/j.ocemod.2011.12.007

Lebeaupin Brossier C, Bastin S, Béranger K, Drobinski P (2014) Regional mesoscale air-sea coupling impacts and extreme meteorological events role on the Mediterranean Sea water budget. Clim Dyn 44:1029–1051. doi:10.1007/s00382-014-2252-z

Levitus S, Antonov J, Boyer T (2005) Warming of the world ocean, 1955-2003. Geophys Res Lett 32:L02604. doi:10.1029/2004GL021592

Li L (2006) Atmospheric GCM response to an idealized anomaly of the Mediterranean Sea surface temperature. Clim Dyn 27:543–552. doi:10.1007/s00382-006-0152-6

Lindström G, Pers CP, Rosberg R, Strömqvist J, Arheimer B (2010) Development and test of the HYPE (Hydrological Predictions for the Environment) model–A water quality model for different spatial scales. Hydrol Res 41:295–319. doi:10.2166/nh.2010.007

Lionello P, Malanotte-Rizzoli, Boscolo R, Alpert P, Artale V, Li L, Luterbacher J, May W, Trigo R, Tsimplis M, Ulbrich U, Xoplaki E (2006a) The Mediterranean climate: an overview of the main characteristics and issues. Develop Earth Envir Sci 4:1–26. doi:10.1016/S1571-9197(06)80003-0

Lionello P, Bhend J, Buzzi A, Della-Marta PM, Krichak SO, Jansá A, Maheras P, Sanna A, Trigo IF, Trigo R (2006b) Cyclones in the Mediterranean region: climatology and effects on the environment. Develop Earth Envir Sci 4:325–372. doi:10.1016/S1571-9197(06)80009-1

Louka P, Galanis G, Siebert N, Kariniotakis G, Katsafados P, Pytharoulis I, Kallos G (2008) Improvements in wind speed forecasts for wind power prediction purposes using kalman filtering. J wind Engin Indus Aerody 96(12):2348–2362. doi:10.1016/j.jweia.2008.03.013

Ludwig W, Dumont E, Meybeck M, Heussner S (2009), River discharges of water and nutrients to the Mediterranean and Black Sea: Major drivers for ecosystem changes during past and future decades. Prog oceanogr 80:199–217. doi:10.1016/j.pocean.2009.02.001

Luque A, Fita L, Romero R, Alonso S (2007) Tropical-like Mediterranean storms: an analysis from satellite. EUMETSAT 07 proceedings

Madec G, the NEMO Team (2008) NEMO Ocean Engine, Note Pôle Modél. 27, Inst Pierre-Simon Laplace, Paris

Mariotti A, Struglia MV, Zeng N, Lau K-M (2002) The Hydrological Cycle in the Mediterranean Region and Implications for the Water Budget of the Mediterranean Sea. J Climate, 13(13):1674–1690. doi:10.1175/1520-0442(2002)015<1674:THCITM>2.0.CO;2

Marshall J, Schott F (1999) Open-ocean convection: observations, theory and models. Rev Geophys 37:1–64. doi:10.1029/98RG02739

McDonald AM, Candela J, Bryden HL (1994) An estimate of the net heat transport flux trough the strait of Gibraltar. Seasonal and interannual variability of the Western Mediterranean Sea. AGU 46:12–32. doi:10.1029/CE046p0013

McKnight TL, Hess D (2000) Climate Zones and Types: The Köppen System. Physical Geography: A Landscape Appreciation. Upper Saddle River, Prentice Hall. ISBN: 0-13-020263-0

Meier H, Kauker F (2003) Modeling decadal variability of the Baltic Sea: Role of freshwater inflow and large-scale atmospheric circulation for salinity. J Geophys Res 108(C11):3368. doi:10.1029/2003JC001797

Messmer M, Gómez-Navarro JJ, Raible CC (2017) Sensitivity experiments on the response of Vb cyclones to sea surface temperature and soil moisture changes. Earth Syst Dyn 8:477–493. doi:10.5194/esd-8-477-2017

Messmer M, Gómez-Navarro JJ, Raible CC (2015) Climatology of Vb cyclones, physical mechanisms and their impact on extreme precipitation over Central Europe. Earth Syst Dyn 6:541–553. doi:10.5194/esd-6-541-2015

MeteoSchweiz (2006) Starkniederschlagsereignis August 2005 Arbeitsberichte der Schweiz 211:63

Miglietta MM, Moscatello A, Conte D, Mannarini G, Lacorata G, Rotunno R (2011) Numerical analysis of a Mediterranean "hurricane" over south-eastern Italy: sensitivity experiments to sea surface temperature. Atmos Res 101:412–426. doi:10.1016/j.atmosres.2011.04.006

Miglietta MM, Laviola S, Malvaldi A, Conte D, Levizzani V, Price C (2013) Analysis of tropical-like cyclones over the Mediterranean Sea through a combined modeling and satellite approach. Geophys Res Lett 40:2400–2405. doi:10.1002/grl.50432

Millán MM, Estrela MJ, Sanz MJ, Mantilla E, Martín M, Pastor F, Salvador R, Vallejo R, Alonso L, Gangoiti G, Ilardia JL, Navazo M, Albizuri A, Artíñano B, Ciccioli P, Kallos G, Carvalho RA, Andrés D, Hoff A, Werhahn J, Seufert G, Versino B (2005) Climatic Feedbacks and Desertification: The Mediterranean Model. J Climate 18(5):684–701. doi:10.1175/JCLI-3283.1

Mitzschke H (2013) Gewässerkundlicher Monatsbericht mit vorläufiger Auswertung des Hochwassers. Tech rep Sächsisches Landesamt für Umwelt, Landwirtschaft und Geologie 69

Moscatello A, Miglietta MM, Rotunno R (2008) Observational analysis of a Mediterranean "hurricane" over south-eastern Italy. Mon Weather Rev 136:4373–4397. doi:10.1002/wea.231

Mudelsee M, Borngen M, Tetzlaff G, Grunewald U (2004) Extreme floods in Central Europe over the past 500 years: Role of cyclone pathway Zugstrasse Vb. J Geophys Res 109:D23101. doi:10.1029/2004JD005034

Muskulus M, Jacob D (2005) Tracking cyclones in regional model data: the future of Mediterranean storms. Adv Geosci 2:13–19. doi:10.5194/adgeo-2-13-2005

Nabat P, Somot S, Mallet M, Chiapello I, Morcrette J, Solmon F, Szopa S, Dulac F, Collins W, Ghan S, Horowitz LW, Lamarque JF, Lee YH, Naik Y, Nagashima T, Shindell D, Skeie R (2013) A 4-D climatology (1979–2009) of the monthly tropospheric aerosol optical depth distribution over the Mediterranean region from a comparative evaluation and blending of remote sensing and model products. Atmos Meas Tech 6:1287–1314. doi:10.5194/amt-6-1287-2013

Nied M, Pardowitz T, Nissen K, Uwe U, Hundecha Y, Merz B (2014) On the relationship between hydro-meteorological patterns and flood types. J Hydrol 519:3249–3262. doi:10.1016/j.jhydrol.2014.09.089

Niiler PP, Kraus EB (1977) One-dimensional models of the upper ocean. Modelling and Prediction of the Upper Layers of the Oceans 143–172

Nissen KM, Leckebusch GC, Pinto JG, Ulbrich U (2013) Mediterranean cyclones and windstorms in a changing climate. Reg. Environ Change, 14:1873–1890. doi:10.1007/s10113-012-0400-8

Nissen KM, Ulbrich U, Leckebusch GC (2014) Vb cyclones and associated rainfall extremes over Central Europe under present day and climate change conditions, Meteorol Z 22:649–660. doi:10.1127/0941-2948/2013/0514

Obermann A, Bastin S, Belamari S, Conte D, Gaertner MA, Li L, Ahrens B (2018) Mistral and Tramontane wind speed and wind direction patterns in regional climate simulations. Clim Dyn 51:693–703. doi:10.1007/s00382-017-3635-8

Osiński R, Rak D, Walczowski W, Piechura J (2010) Baroclinic Rossby radius of deformation in the southern Baltic Sea. Oceanologia 52(3):417–429. doi:10.5697/oc.52-3.417

Palmen E (1948) On the formation and structure of tropical hurricanes. Geophysica 3:26–48

Panthou G, Vrac M, Drobinski P, Bastin S, Li L (2018) Impact of model resolution and Mediterranean Sea coupling on hydrometeorological extremes in RCMs in the frame of HyMeX and MED-CORDEX. Clim Dyn 51:915–932. doi:10.1007/s00382-016-3374-2

Papadopoulos VP, Josey SA, Bartzokas A, Somot S, Ruiz S, Drakopoulou P (2012a) Large–scale atmospheric circulation favoring deep- and intermediate-water formation in the Mediterranean Sea. J Climate 25:6079–6091. doi:10.1175/Jcli-D-11-00657.1

Peel MC, Finlayson BL, McMahon TA (2007) Updated world map of the Köppen-Geiger climate classification. Hydrol Earth Syst Sci 11(5):1633–1644. doi:10.5194/hess-11-1633-2007

Perry K (2001) Sea winds on QuikSCAT level 3 daily, gridded ocean wind vectors (JPL sea winds Project) guide document

Pettersen S (1956) Weather Analysis and Forecasting. Mac Graw Hills Book Company

Price C, Stone L, Rajagopalan B, Alpert P (1998) A possible link between El Niño and precipitation in Israel. Geophys Res Lett 25:3963-3966. doi:10.1029/1998GL900098

Pytharoulis I, Craig G, Ballard S (2000) The hurricane-like Mediterranean cyclone of January 1995. Meteorol Appl 7:261–279. doi:10.1017/S1350482700001511

Rasmussen E, Zick C (1987) A subsynoptic vortex over the Mediterranean with some resemblance to polar lows. Tellus A Dyn Meteorol and Oceanogr 39:408–425. doi:10.3402/tellusa.v39i4.11770

Reale O, Feudale L, Turato B (2001) Evaporative moisture sources during a sequence of floods in the Mediterranean region. Geophys Res Lett 28(10):2085–2088. doi:10.1029/2000GL012379

Reynolds WR, Smith TM, Liu C, Chelton DB, Casey KS, Schlax MG (2007) Daily high-resolution-blended analyses for sea surface temperature. J Climate 20:5473–5496. doi:10.1175/2007JCLI1824.1

Rienecker MM, Suarez JM, Gelaro R, Todling R, Bacmeister J, Liu E, Bosilovich MG, Schubert SD, Takacs L, Kim GK, Bloom S, Chen J, Collins D, Conaty A, Silva A, Gu W, Joiner J, Koster RD, Lucchesi R, Molod A, Owens T, Pawson S, Pegion P, Redder CR, Reichle R, Robertson FR, Ruddick AG, Sienkiewicz M, Woollen J (2011) MERRA-NASA's Modern-Era Retrospective Analysis for Research and Applications. J Climate 24:3624–3648. doi:10.1175/JCLI-D-11-00015.1

Ritter B, Geleyn J-F (1992) A comprehensive radiation scheme for numerical weather prediction models with potential applications in climate simulations. Mon Weather Rev 120(2):303–325. doi:10.1175/1520-0493(1992)120<0303:ACRSFN>2.0.CO;2

Rixen M (2012) MEDAR/MEDATLAS-II, GAME/CNRM. doi:10.6096/hymex.medar/medatlas-ii.20120112

Rockel B, Geyer B (2008) The performance of the regional climate model CLM in different climate regions, based on the example of precipitation. Meteorol Z 17:487–498. doi:10.1127/0941-2948/2008/0297

Rockel B, Will A, Hense A (2008) The regional climate model COSMO-CLM (CCLM). Meteorol Z 17:347–348. doi:10.1127/0941-2948/2008/0309

Rodriguez-Fonseca B, De Castro M (2002) On the connection between winter anomalous precipitation in the Iberian Peninsula and North West Africa and the summer subtropical Atlantic sea surface temperature. Geophys Res Lett 29:1863. doi:10.1029/2001GL014421

Rodwell MJ, Hoskins BJ (1996) Monsoons and the dynamics of deserts. Q J R Meteorol Soc 122:1385–1404. doi:10.1002/qj.49712253408

Roether WB, Manca B, Klein B, Bregant, Georgopulos D, Beitzel V, Kovacevic V, Lucchetta A (1995) Recent changes in eastern Mediterranean deep water. Science 271:333–335. doi:10.1126/science.271.5247.333

Romero R (2008) A method for quantifying the impacts and interactions of potential vorticity anomalies in extratropical cyclones. Q J R Meteorol Soc 134:385–402. doi:10.1002/qj.219

Romero R, Emanuel K (2013) Medicane risk in a changing climate. J Geophys Res Atmos 118:5992–6001. doi:10.1002/jgrd.50475

Ruiz S, Gomis D, Sotillo MG, Josey SA (2008) Characterization of surface heat fluxes in the Mediterranean Sea from a 44–year high–resolution atmospheric dataset. Global Planet Change 63:258–274. doi:10.1016/j.gloplacha.2007.12.002

Ruti PM, Marullo S, D'Ortenzio F, Tremant M (2008) Comparison of analyzed and measured wind speeds in the perspective of oceanic simulations over the Mediterranean basin: analyses, QuikSCAT and buoy data. J Mar Syst 70:33–48. doi:10.1016/j.jmarsys.2007.02.026

Ruti PM, Somot S, Giorgi F, Dubois C, Flaounas E, Obermann A, Dell'Aquila A, Pisacane G, Harzallah A, Lombardi E, Ahrens B, Akhtar N, Alias A, Arsouze T, Aznar R, Bastin S, Bartholy J, Béranger K, Beuvier J, Bouffies-Cloché S, Brauch J, Cabos W, Calmanti S, Calvet J-C, Carillo A, Conte D, Coppola E, Djurdjevic V, Drobinski P, Elizalde-Arellano A, Gaertner M, Galàn P, Gallardo C, Gualdi S, Goncalves M, Jorba O, Jordà G, L'Heveder B, Lebeaupin-Brossier C, Li L, Liguori G, Lionello P, Maciàs-Moy D, Nabat P, Önol B, Rajkovic B, Ramage K, Sevault F, Sannino G, Struglia MV, Sanna A, Torma C, Vervatis V (2016) MED-CORDEX initiative for Mediterranean Climate studies. Bull Am Meteorol Soc 97:1187–1208. doi:10.1175/BAMS-D-14-00176.1

Sanchez-Gomez E, Somot S, Josey SA, Dubois C, Elguindi N, Déqué M (2011) Evaluation of Mediterranean Sea water and heat budgets simulated by an ensemble of high resolution regional climate models. Clim Dyn 37:2067–2086. doi:10.1007/s00382-011-1012-6

Sanna A, Lionello P, Gualdi S (2013) Coupled atmosphere ocean climate model simulations in the Mediterranean region: effect of a high–resolution marine model on cyclones and precipitation. Nat Hazards Earth Syst Sci 13:1567–1577. doi:10.5194/nhess-13-1567-2013

Schicker I, Radanovics S, Seibert P (2010) Origin and transport of Mediterranean moisture and air. Atmos Chem Phys 10(11):5089–5105. doi:10.5194/acp-10-5089-2010

Schrodin E, Heise E (2002). A new multi-layer soil model. COSMO Newsletter 2:149-151

Sevault F, Somot S, Alias A, Dubois C, Lebeaupin-Brossier C, Nabat P, Adloff F, Déqué M, Decharme B (2014) A fully coupled Mediterranean regional climate system model: design and evaluation of the ocean component for the 1980–2012 period. Tellus A Dyn Meteorol and Oceanogr 66:1. doi:10.3402/tellusa.v66.23967

Simmons A, Uppala S, Dee D, Kobayashi S (2006) New ECMWF reanalysis products from 1989 onwards. ECMWF Newsletter 110:26–35. doi:10.21957/pocnex23c6

Sodemann H, Wernli H, Schwierz C (2009) Sources of water vapour contributing to the Elbe flood in August 2002–A tagging study in a mesoscale model. Q J R Meteorol Soc 135:205–223. doi:10.1002/qj.374

Somot S, Sevault F, Déqué, M, Crépon M (2008) 21th century climate change scenario for the Mediterranean using a coupled atmosphere–ocean regional climate model. Global Planet Change 63:112–126. doi:10.1016/j.gloplacha.2007.10.003

Stadtherr L, Coumou D, Petoukhov V, Petri S, Rahmstorf S (2016) Record Balkan floods of 2014 linked to planetary wave resonance. Sci Adv 2(4):1501428. doi:10.1126/sciadv.1501428

Stanev EV, Staneva JV (2001) The sensitivity of the heat exchange at sea surface to meso and sub-basin scale eddies Model study for the Black Sea. Dyn Atmos Oceans 33:163–189. doi:10.1016/S0377-0265(00)00063-4

Steppeler J, Doms G, Schättler U, Bitzer H, Gassmann A, Damrath U, Gregoric G (2003) Meso-gamma scale forecasts using the nonhydrostatic model LM. Meteor Atmos Phys 82:75–96. doi:10.1007/s00703-001-0592-9

Stohl A, James P (2004) A Lagrangian analysis of the atmospheric branch of the global water cycle, Part I: Method description, validation, and demonstration for the August 2002 flooding in Central Europe. J Hydrometeorol 5:656–678. doi:10.1175/1525-7541(2004)005<0656:ALAOTA>2.0.CO;2

Stucki P, Martius O, Brönnimann S, Franke J (2013) The extreme flood event of Lago Maggiore in September 1993. Weather extremes during the past 140 years. Geographica Bernensia G89:53–58. doi:10.4480/GB2013.G89.06

Sumner G, Homar V, Ramis C (2001) Precipitation seasonality in eastern and southern coastal spain. Int J Climatol 21:219–247. doi:10.1002/joc.600

Tegen I, Hoorig P, Chin M, Fung I, Jacob D, Penner J (1997) Contribution of different aerosol species to the global aerosol extinction optical thickness: Estimates from model results. J Geophys Res 102(D20):23895–23915. doi:10.1029/97JD01864

Theocharis A, Nittis K, Kontoyiannis H, Papageorgiou E, Balopoulos E (1999) Climatic changes in the Agean Sea influence the eastern Mediterranean thermohaline circulation (1986–1997). Geophys Res Lett 26:1617–1620. doi:10.1029/1999GL900320

Trigo IF, Trevor TD, Bigg GR (2000) Decline in the Mediterranean rainfall caused by weakening of Mediterranean cyclones. Geophys Res Lett 27:2913–1916. doi:10.1029/2000GL011526

Trigo IF, Bigg GR, Davies TD (2002) Climatology of cyclogenesis mechanisms in the Mediterranean. Mon Wea Rev 130(3):549-569. doi:10.1175/1520-0493(2002)130<0549:COCMIT>2.0.CO;2

Trigo RM, Trigo IF, Da Camara C, Osborn TJ (2004) Climate impact on the European winter blocking episodes from the NCEP/NCAR reanalyses. Clim Dyn 23:17–28. doi:10.1007/s00382-004-0410-4

Trigo RM, Xoplaki E, Zorita E, Luterbacher J, Krichak S, Alpert P, Jacobeit J, Sáenz J, Fernández J, González-Rouco F, Garcia-Herrera R, Rodo X, Brunetti M, Nanni T, Maugeri M, Türkes M, Gimeno L, Ribera P, Brunet M, Trigo F, Crepon M, Mariotti A (2006) Relations between variability in the Mediterranean region and mid-latitude variability. Develop Earth Envir Sci 4:179–226. doi:10.1016/S1571-9197(06)80006-6

Tsimplis MN, Bryden HL (2000) Estimation of the transport through the strait of Gibraltar. Oceanogr Res 47:2219–2242. doi:10.1016/S0967-0637(00)00024-8

Tomassini L, Elizalde A (2012) Does the Mediterranean Sea Influence the European Summer Climate? The Anomalous Summer 2003 as a Test Bed. J Climate 25:7028–7045. doi:10.1175/JCLI-D-11-00330.1

Tous M, Romero R (2013) Meteorological environments associated with medicane development. Int J Climatol 33:1–14. doi:10.1002/joc.3428

Tous M, Romero R, Ramis C (2013) Surface heat fluxes influence on medicane trajectories and intensification. Atmos Res 123:400–411. doi:10.1016/j.atmosres.2012.05.022

Trenberth K (2005) Uncertainty in hurricanes and global warming. Science 308:1753–1754. doi:10.1126/science.1112551

Ulbrich U, Brücher T, Fink AH, Leckebusch GC, Krüger A, Pinto JG (2003a) The central European floods of August 2002: Part 1–Rainfall periods and flood development. Weather 58:371–377. doi:10.1256/wea.61.03A

Ulbrich U, Brücher T, Fink AH, Leckebusch GC, Krüger A, Pinto JG (2003b) The central European floods of August 2002: Part 2–Synoptic causes and considerations with respect to climatic change. Weather 58:434–442. doi:10.1256/wea.61.03B

Valcke S (2013) The OASIS3 coupler: A European climate modelling community software. Geosci Model Dev 6:373–388. doi:10.5194/gmd-6-373-2013

Van Bebber (1891) Die Zugstrassn der barometrischen Minima nach den Bahnenkarten der Deutschen Seewarte für den Zeitraum 1875–1890. Meteorol Z 8:361–366

Van Pham T, Brauch J, Dieterich C, Frueh B, Ahrens B (2014) New coupled atmosphere-ocean-ice system COSMO-CLM/NEMO: On the air temperature sensitivity on the North and Baltic Seas. Oceanologia 56:167–189. doi:10.5697/oc.56-2.167

Vancoppenolle M, Fichefet T, Goosse H, Bouillon S, Madec G, Maqueda M (2009) Simulating the mass balance and salinity of arctic and Antarctic sea ice. Ocean Modelling 27:33–53. doi:10.1016/j.ocemod.2008.10.005

Volosciuk C, Maraun D, Semenov VA, Tilinina N, Gulev SK, Latif M (2016) Rising Mediterranean Sea Surface Temperatures Amplify Extreme Summer Precipitation in Central Europe. Sci Rep 6:32450. doi:10.1038/srep32450

von Storch H, Langenberg H, Feser F (2000) A spectral nudging technique for dynamical down-scaling purposes. Mon Weather Rev 128:3664–3673. doi:10.1175/1520-0493(2000)128<3664:ASNTFD>2.0.CO;2

Walsh K, Giorgi F, Coppola E (2014) Mediterranean warmcore cyclones in a warmer world. Clim Dyn 42:1053–1066. doi:10.1007/s00382-013-1723-y

Wernli H, Schwierz C (2006) Surface cyclones in the ERA–40 dataset (1958–2001), Part I: Novel identification method and global climatology. J Atmos Sci 2486–2507. doi:10.1175/JAS3766.1

Wernli H, Paulat M, Hagen M, Frei C (2008) SAL–A Novel Quality Measure for the Verification of Quantitative Precipitation Forecasts. Mon Wea Rev 136:4470-4487. doi:10.1175/2008MWR2415.1

Will A, Akhtar N, Brauch J, Breil M, Davin E, Ho-Hagemann H, Maisonnave E, Thürkow M, Weiher S (2017) The COSMO-CLM 4.8 regional climate model coupled to regional

ocean, land surface and global earth system models using OASIS3-MCT: description and performance. Geosci Model Dev 10:1549–1586. doi:10.5194/gmd-10-1549-2017

Winschall A, Pfahl S, Sodemann H, Wernli H (2012) Impact of North Atlantic evaporation hot spots on southern Alpine heavy precipitation events. Q J R Meteorol Soc 138:1245–1258. doi:10.1002/qj.987

Xoplaki E, Gonzalez-Rouco JF, Luterbacher J, Wanner H (2003) Mediterranean summer air temperature variability and its connection to the large-scale atmospheric circulation and SSTs. Clim Dyn 20:723–739. doi:10.1007/s00382-003-0304-x

Xoplaki E, González-Rouco JF, Luterbacher J, Wanner H (2004) Wet season Mediterranean precipitation variability: influence of large-scale dynamics and trends. Clim Dyn 23:63–78. doi:10.1007/s00382-004-0422-0

Yu L, Jin X, Weller RA (2008) Multidecade Global Flux Datasets from the Objectively Analyzed Air-sea Fluxes (OAFlux) Project: Latent and sensible heat fluxes, ocean evaporation, and related surface meteorological variables. Woods Hole Oceanogr Inst, OAFlux Project Technical Report OA-2008-01, Woods Hole

Zappa G, Hawcroft MK, Shaffrey L, Black E, Brayshaw DJ (2015) Extratropical cyclones and the projected decline of winter Mediterranean precipitation in the CMIP5 models. Clim Dyn 45:1727–1738. doi:10.1007/s00382-014-2426-8

Zhang HM, Bates JJ, Reynolds RW (2006) Assessment of composite global sampling: Sea surface wind speed. Geophys Res Lett 33:L17714. doi:10.1029/2006GL027086

Zhang C, Dong M, Gualdi S, Hendon HH, Maloney ED, Marshall A, Sperber KR, Wang W (2006) Simulations of the Madden-Julian Oscillation by Four Pairs of Coupled and Uncoupled Global Models. Clim Dyn 27:573–592. doi:10.1007/s00382-006-0148-2

Supplement: Zusammenfassung

Dieser Abschnitt enthalt eine deutschsprachige Zusammenfassung der vorliegenden Arbeit. Hierzu werden die wesentlichen Ergebnisse und Aussagen der Kapitel 1 bis 5 wiedergegeben.

S.1 Hintergrund, Motivation und Ziele

Rückkopplungen zwischen dem Mittelmeer und der Atmosphäre auf verschiedenen zeitlichen und räumlichen Skalen spielen eine wichtige Rolle im regionalen Klimasystem des Mittelmeerraums und darüber hinaus. Das Mittelmeer ist eine Feuchtequelle aufgrund von übermäßiger Verdunstung. Im langfristigen Durchschnitt induziert das Mittelmeer eine Erwärmung der unteren Atmosphäre infolge des Wärmeverlustes an der Grenzfläche zwischen Luft und Meer. Die komplexen Luft-Wasser-Wechselwirkungen und Rückkopplungen im Mittelmeerbecken regulieren stark die Flüsse an der Meeresoberfläche und begünstigen mehrere zyklogenetische Aktivitäten unter bestimmten meteorologischen Bedingungen. Beispiele sind die Medicanes (Mediterrane Hurrikane) und Vb-Zyklonen. Medicanes sind mesoskalige, marine Mittelmeer-Zyklonen mit warmen Kern, die einige Ähnlichkeiten mit tropischen Zyklonen aufweisen. Vb-Zyklonen sind extratropisch und wandern vom westlichen Mittelmeer aus über die osteuropäischen Alpen in die mitteleuropäische Region. Extrem starke Winde und Starkniederschläge stehen im Zusammenhang mit diesen Zyklonen und führen zu schweren Zerstörungen und Überschwemmungen. Zyklone im Mittelmeer sind Extremfälle von Atmosphäre-Ozean-Interaktionen. Eine bessere Darstellung der Wechselwirkungen und Rückkopplungen kann die Abschätzungen der Wärmeströme an der Meeresoberfläche verbessern und die Darstellung und Vorhersagbarkeit von Extremereignissen weiter verbessern. Obwohl bekannt ist, dass Zyklonen im Mittelmeerraum von Zeit zu Zeit auftreten, haben ihre Häufigkeit und Intensität in den letzten Jahrzehnten zugenommen. Die räumliche und zeitliche Verteilung dieser Extremereignisse ist unregelmäßig. Änderungen in der Intensität und Häufigkeit von Wirbelstürmen werden auch im zukünftigen Klima projiziert, indem insbesondere die Mittelmeerregion nach jetzigem Erkenntnisstand ein Hotspot in Bezug auf steigende Temperaturen sein wird.

Die derzeitigen Bemühungen zur Bewertung der Flüsse zwischen Atmosphäre und Mittelmeer fußen auf Beobachtungs- oder Reanalyse daten mit einer groben räumlichen Auflösung (83–125 km) oder konventionellen, grobaufgelösten ($\sim$150 km) globalen Atmosphären-Ozean-Zirkulationsmodellen (AOGCMs). Trotz der Tatsache, dass die AOGCM die Atmosphäre-Ozean-Wechselwirkungen berücksichtigen, ist der Mittelmeerraum weder in den globalen Atmosphärenmodellen noch in globalen Meeresmodellen allgemein gut dargestellt. Im Allgemeinen können AOGCM mit grober Auflösung die lokalen und mesoskaligen Prozesse, die den Mittelmeerraum charakterisieren, nicht ausreichend auflösen. Auf der anderen Seite sind hochauflösende

AOGCMs noch zu rechenaufwändig. Die Entwicklung von hochauflösenden regionalen Klimamodellen (RCMs) hat unser Verständnis der Prozesse, die das Mittelmeerklima charakterisieren, vorangetrieben. Es bestehen jedoch nach wie vor große Unsicherheiten hinsichtlich der Berechnung von Flüssen zwischen Atmosphäre und Meer, welche sich wiederum auf die Simulation des mediterranen Klimas auswirken. Diese Unsicherheiten können verschiedene Faktoren zugeschrieben werden, wie z. B. Datenqualität, zeitliche und räumliche Auflösung und falsche Darstellung physikalischer Prozesse.

Bei der Betrachtung der komplexen Wechselwirkungen zwischen verschiedenen Komponenten des Erdsystems ist die Kopplung numerischer Modelle ein üblicher Ansatz (z.B Will et al. 2017). Um die wechselseitigen Wechselwirkungen an der Schnittstelle zwischen Atmosphäre und Ozean in der Mittelmeerregion aufzulösen, ist ein hochauflösendes regional gekoppeltes Atmosphären-Ozean-Modell (AORCM) erforderlich (Somot et al. 2008). Der Einfluss der Atmosphäre-Ozean-Kopplung auf die oberflächennahen Flüsse wurde in früheren Studien untersucht. Es wurde festgestellt, dass bidirektionale, hochfrequente Wechselwirkungen und eine höhere räumliche Auflösung der SST die Darstellung von Wärmeströmen, hydrologischen Parametern und Winden im Mittelmeerraum verbessern (Lebeaupin and Drobinski 2009; Dubois et al. 2012; Lebeaupin et al. 2014; Sevault et al. 2014). Darüber hinaus können SSTs, die mit hochauflösenden Ozeanmodellen simuliert wurden, einen starken und positiven Effekt auf Zyklogenese und Niederschlagssimulationen haben (Sanna et al. 2013). In einer anderen Studie haben Sevault et al. (2014) gezeigt, dass die Ozeankopplung das NH verbessert, aber große Fehler in einzelnen Komponenten (besonders in LH und LW) auftraten. Dubois et al. (2012) verwendeten ein Ensemble von fünf AORCMs und zeigten, dass sich der Durchschnitt der NH-Komponenten im Mittelmeerbecken zwischen den Ensemblemitgliedern signifikant unterschied. Diese Studien zeigen, dass, obwohl die AORCM die Darstellung von oberflächennahen Flüssen über dem Mittelmeer verbessert haben, große Unsicherheiten bestehen bleiben. Solche Unsicherheiten in den Wärmeströmen können die Simulationen von Mittelmeer-Zyklonen (Medicanes und Vb-Zyklone) stark beeinflussen.

Die meisten Studien zu Medicanes (siehe z.B Romero and Emanuel 2013; Cavicchia et al. 2014b; Walsh et al. 1996) und Vb-Zyklonen (siehe z.B Hofstätter and Chimani 2012; Nissen et al. 2014; Grams 2014; Kelemen et al. 2016; Messmer et al. 2017) verwenden RCM-Simulationen oder Reanalysedaten. Daher fehlen in diesen Datensätzen feinskalige Rückkopplungen, die mit den Atmosphäre-Ozean-Wechselwirkungen zusammenhängen, denn diese beeinflussen stark die zeitliche und räumliche Struktur der Wirbelstürme im Mittelmeerraum. Flaounas et al. (2018) fanden heraus, dass die Kopplung zwischen Atmosphäre und Ozean nur einen schwachen Einfluss auf die Klimatologie und Intensität der mediterranen Zyklone hat, einschließlich der Medicanes (für weitere Details siehe Anhang A). Für Vb-Zyklonen wurde der Einfluss von Atmosphäre-Meer-Wechselwirkungen und diesbezügliche Rückkopplungen auf Vb-Charakteristika noch nicht mit einem AORCM untersucht. Der Nutzen von der Verwendung von gekoppelten AORCMs für die Simulation von Vb-Zyklonen wurde von Ho-Hagemann et al. (2015) hervorgehoben, welche ein RCM mit einem gekoppelten Nord- und Ostseemodell nutzten, um das Hochwasserereignis

im Oktober 1997 zu untersuchen. Sie kamen zu dem Schluss, dass 3 Prozesse maßgeblich für die starken Regenfälle und Überschwemmungen in Mitteleuropa waren: a) eine großräumige Konvergenz von Luftfeuchte aus dem Mittelmeer und b) Feuchteadvektion aus dem Nordatlantik über die Nordsee und c) Verdunstung über dem Inland. Ihre Analyse ergab, dass die Verwendung eines gekoppelten Nord- und Ostseemodells für die Simulation des Ereignisses von Vorteil ist.

Um einige dieser Inkonsistenzen zu überwinden, wurde Es wurde ein neues hochauflösendes regionales gekoppeltes Atmosphären-Ozean-Modell (AORCM) entwickelt, um die Atmosphäre-Ozean-Rückkopplungsmechanismen zu simulieren. Dieses Modell beinhaltet die Kopplung von RCM COSMO-CLM (CCLM) und dem regionalen Ozeanmodell NEMO-MED12 für das Mittelmeer (MED) sowie NEMO-NORDIC für die Nord- und Ostsee (NORDIC). Die Entwicklung des AORCM dient den folgenden Zielen:

- bessere Darstellung der kleinräumigen, lokalen Prozesse und SST-Muster
- bessere Darstellung der Flüsse an der Meeresoberfläche durch Auflösung von kleinräumigen Atmosphäre-Ozean-Wechselwirkungen und Rückkopplungen
- Bessere Simulationen der Mittelmeer-Zyklonen (Medicanes und Vb-Zyklone)

Im Rahmen dieser Studie wurden mehrere Experimente mit gekoppelten und ungekoppelten Modellen durchgeführt, um die folgenden Schwerpunkte und diesbezügliche Fragen zu behandeln:

- Untersuchung der meeresoberflächennahen Wärmeflüsse und der Windgeschwindigkeit über dem Mittelmeer:
  - Welchen Einfluss haben kleinräumige Atmosphäre-Ozean-Wechselwirkungen und Rückkopplungen auf die Wärmeflüsse und die Windgeschwindigkeit des Meeres?
  - Wie wirkt sich die horizontale Gitterauflösung auf die Wärmeflüsse und die Windgeschwindigkeit über Meeresoberfläche aus?
  - Welchen Einfluss hat die tageszeitabhängige Variabilität der SST auf die Wärmeflüsse der Meeresoberfläche und die Windgeschwindigkeit auf stündlicher und längeren Zeitskalen?
- Untersuchung von Medicanes:
  - Welchen Einfluss haben kleinräumige Atmosphäre-Ozean-Wechselwirkungen und Rückkopplungen auf deren Intensität und Trajektorien?
  - Verbessert ein hochauflösendes horizontales atmosphärisches Gitter die Darstellung von Medicanes?
  - Wie wirkt sich die spektrale Nudging-Methode auf die Simulation aus?
- Untersuchung von Vb-Zyklonen:

– Wie wirken sich kleinräumige Atmosphäre-Ozean-Wechselwirkungen und Rückkopplungen über dem Mittelmeer bzw. über der Nord- und Ostsee auf die Intensität und die Trajektorien von Vb-Zyklonen aus?

S.2 Wissenschaftliche Ergebnisse

Im Rahmen dieser Studie wurden mehrere Experimente mit einem CCLM in ungekoppelter und gekoppelter Konfiguration durchgeführt. Sowohl die gekoppelten als auch die ungekoppelten Modelle konnten die Charakteristika des mediterranen Klimas reproduzieren. In Bezug auf die eingangs formulierten Themenschwerpunkte konnten mit dem hier entwickelten, hochauflösenden AORCM folgende Erkenntnisse erzielt werden.

S.2.1 Untersuchung der Wärmeflüsse und der Windgeschwindigkeit über dem Mittelmeer

Bei der Untersuchung des Einflusses der horizontalen atmosphärischen Gitterauflösung (0,08°∼9 km vs. 0,4°∼50 km) und der Kopplung der Ozeane auf die meeresoberflächennahen Wärmeflüsse und die Windgeschwindigkeit können folgende Schlussfolgerungen gezogen werden:

- Hochaufgelöste Simulationen führten im Gegensatz zu grobaufgelösten Simulationen zu einer besseren Darstellung der Winde, insbesondere in Küstennähe und im westlichen Mittelmeer. Folglich hat das feine atmosphärische Gitter einen positiven Einfluss auf turbulente Flüsse.
- Die Atmosphäre-Ozeankopplung führte zu einer Verbesserung bei den turbulenten Flüssen.
- Die Strahlungsflüsse sind in den grobaufgelösten Simulationen etwas besser dargestellt als in den hochaufgelösten Simulationen. Grund hierfür ist die etwas bessere Erfassung der Wolkenbedeckung. Schätzungen des Nettowärmeflusses (NH) sind jedoch in den gekoppelten Simulationen mit feinem Gitter realistischer.
- Das gekoppelte Modell simuliert sub-tägliche Variabilität der SST, die in der ERA-Interim-Reanalyse komplett fehlt. Die Ergebnisse zeigen, dass die sub-täglichen Schwankungen für den mittleren atmosphärischen Zustand im Mittelmeerraum von untergeordneter Bedeutung sind.

S.2.2 Untersuchung von Medicanes

Bei der Untersuchung der Auswirkungen der horizontalen atmosphärischen Gitterauflösung (0,44°∼50 km vs. 0,22°∼25 km vs. 0,08°∼9 km) und der Kopplung des Meeres auf die Zugbahnen der Medicanes und deren Intensität können folgende Schlussfolgerungen gezogen werden:

- Die Modellperformance hängt stark von der horizontalen atmosphärischen Gitterauflösung ab. Obwohl großräumige Störungen bei allen drei Auflösungen ziemlich gut simuliert werden, wurden charakteristische Merkmale der Medicanes bei der Auflösung von 0,44° nicht mehr detektiert.

- Der mittlere Luftdruck auf Meeresniveau und die warme Kernstruktur wurden in den 0,22°-Simulationen relativ gut erfasst, aber die Windgeschwindigkeit wurde stark unterschätzt. All diese Merkmale waren in den gekoppelten und ungekoppelten Simulationen von 0,08° tiefer und verfeinerter.

- Im Vergleich zu den ungekoppelten Simulationen zeigten die gekoppelten Simulationen beim Vergleich von 0,44° und 0,22° Auflösung keine signifikante Verbesserung.

- Bei der Auflösung von 0,22° waren Zugbahnen von Medicanes sowohl in den gekoppelten als auch in den ungekoppelten Simulationen nahezu identisch. Allerdings waren bei 0.08° Auflösung die Zugbahnen der Medicanes, die warme Kernstruktur und die Windgeschwindigkeit größtenteils besser erfasst als in den ungekoppelten Simulationen.

- In den meisten Fällen waren Zugbahnen der Medicaes in den gekoppelten Simulationen mit einer Auflösung von 0,08° länger und näher an den Beobachtungen. Diese Ergebnisse legen nahe, dass eine Rasterauflösung von 0,08° die Merkmale von Medicanes detaillierter erfasst, insbesondere mit einem gekoppelten Modell.

- Die spektrale Nudging-Technik erhöhte die Genauigkeit von Zeit und Ort von simulierten Medicanes. Beim mittleren Luftdruck auf Meeresniveau und der Windgeschwindigkeit wurde jedoch keine Verbesserung festgestellt.

- Ähnlich wie bei den Simulationen, die ohne spektrales Nudging durchgeführt wurden, waren in den gekoppelten Simulationen mit spektralem Nudging die Zugbahnen der Medicanes und diesbezügliche Windgeschwindigkeiten besser dargestellt als in den reinen Atmosphärensimulationen mit spektralen Nudging.

- Die Magnitude der latenten und fühlbaren Wärmeflüsse nahm mit der Ozeankopplung und der Erhöhung der atmosphärischen Gitterauflösung zu. Spektrales Nudging hatte jedoch keinen signifikanten Einfluss auf die latenten und fühlbaren Wärmeströme. Somit legen die Ergebnisse nahe, dass die Intensität von Medicanes stark verknüpft ist mit den oberflächennahen Wärmeflüssen und den kleinskaligen Merkmalen an der Grenzfläche zwischen Luft und Meer.

S.2.3 Untersuchung von Vb-Zyklonen

Vb-Zyklonen wurden untersucht anhand von Simulationen mit einer atmosphärischen Gitterauflösung von 0.22° und bei Verwendung eines gekoppelten AORCMs, welches das Mittelmeer (MED) und die Nord- und Ostsee einbezieht (NORDIC). Die Analyse der Auswirkungen der

Ozeankopplung auf die Zugbahnen und die Intensität der Vb-Zyklonen über dem Mittelmeer und Nord- und Ostsee führen zu folgenden Schlussfolgerungen:

- Die in MED+NORDIC simulierten durchschnittlichen saisonalen und jährlichen SSTs waren ähnlich wie MED für das Mittelmeer und NORDIC für die Nord- und Ostsee.
- Die Jahresmittelwerte und Trends der SST im Mittelmeer und in der Nord- und Ostsee stimmen gut mit den Beobachtungen überein.
- Im Vergleich zu den Beobachtungen zeigten die SSTs, die unter Verwendung der gekoppelten Konfigurationen simuliert wurden, eine BIAS von etwa 1 K über den Gebieten, in denen die Kopplung zum Einsatz kam. Der BIAS war insbesondere im Winter und Sommer sichtbar.
- Die gekoppelten Modellläufe waren stabil und robust, und die SST-Unsicherheiten des Modells sind angesichts der Beobachtungsunsicherheiten in den Randmeeren als gering einzuschätzen.
- Im Allgemeinen waren alle Modellkonfigurationen in der Lage, die Zugbahnen von Vb-Zyklonen und ihre hauptsächlichen Merkmale (wie z. B. die geopotentiellen Höhen) zu reproduzieren. Allerdings waren in den meisten Fällen die Position, Intensität und Lebensdauer von Vb-Zyklonen, die in den gekoppelten Modellen simuliert wurden, waren sehr nah oder sogar näher an den Observationen als jene Zyklonenmerkmale, die aus Reanalysedatensätzen abgeleitet wurden. Am schlechtesten schnitt diesbezüglich das ungekoppelte Modell ab.
- Die Positionen der Niederschlagsmaxima stimmten gut mit den entsprechenden Zyklonenzugbahnen überein.
- Die Evaluation simulierter Niederschlagsfelder ergab, dass alle Modellkonfigurationen in der Lage waren, intensive Niederschlagsmuster zu erfassen, die Muster jedoch unterschiedlich hoch und verschoben waren. Im Allgemeinen wurde der simulierte Niederschlag unterschätzt gegenüber den EOBS-Niederschlagsdaten. Dies ist möglicherweise verursacht durch das grobe Modellraster von 25 km, welches orographische Merkmale nicht ausreichend auflöst und die starke Konvektion bei intensiven Vb-Niederschlagsereignissen unterschätzt.
- Darüber hinaus zeigte allein die Kopplung der Nord- und Ostsee einen Vorteil bei der Simulation von Vb-Zyklonen, insbesondere für den Einzelfall im Juli 1997 (ebenfalls in Ho-Hagemann et al. 2015, diskutiert). Der Vorteil resultiert aus den Beiträgen unterschiedlicher Feuchtequellen und ist für jeden Einzelfall gesondert zu betrachten (vgl. Gimeno et al. 2010; Volosciuk et al. 2016; Messmer et al. 2017).

S.2.4 Abschließende Bewertung

Die in dieser Arbeit verwendeten Modelle waren allesamt in der Lage, die wichtigsten Eigenschaften jener physikalischer Prozesse zu reproduzieren, welche beteiligt sind an den oberflächennahen Wärmeflüssen über dem Mittelmeer, den Windgeschwindigkeiten, den Medicanes und den Vb-Zyklonen. Das gekoppelte Modell in Verknüpfung mit einer hohen Auflösung (< 10km) verbessert die Darstellung der oberflächennahen Wärmeflüsse, der Windgeschwindigkeit und der Medicanes. In Bezug auf die Vb-Zyklonen hat die Ozeankopplung einen generell positiven Einfluss auf die Zugbahnen und Intensitäten, obwohl es eine starke Variation von Fall zu Fall gibt (beispielsweise das Feuchtereservoir). Die Fähigkeit der AORCMs die SST explizit selbst aufzulösen, machen sie sehr wertvoll im Vergleich zu den ungekoppelten Atmosphärenmodellen. Diese Studie ist ein erster Schritt hin in Richtung der Verwendung von neuen, komplexeren Modellsystemen. Weitere Entwicklungen sind jedoch nötig, um noch auftretende Defizite zu überwinden.

S.3 Ausblick

Das vorliegende AORCM mit den an die Atmosphäre gekoppelten beiden Randmeeren (Mittelmeer und Nort-Ost-See) ist ein Schritt in Richtung zu einem hochauflösenden, vollständig gekoppelten regionalen Klimasystem, das für weitere Forschungen in diesem Gebiet genutzt werden kann. Im Rahmen dieser These werden nachfolgend einige Empfehlungen für zukünftige Untersuchungen vorgestellt.

- Angesichts der Unsicherheiten in den Strahlungsflüssen und der Befunde in der Literatur (Nabat et al. 2013) sollten die vorgegebenen optischen Aerosoldicken hinterfragt werden.
- Modellvergleiche innerhalb des Med-CORDEX- und EURO-CORDEX-Projekts könnten nützlich sein, um die Quelle der Unsicherheit in den verschiedenen physikalischen Parametrisierungen zu bewerten und die Vb-Zyklone zu untersuchen.
- Diese Studie könnte erweitert werden, um die Auswirkungen von sub-täglichen Schwankungen der SST auf extreme Ereignisse wie Starkniederschläge und Medicanes zu untersuchen.
- Das hier vorgestellte numerische Werkzeug mit einer hochfrequenten Kopplung zwischen Atmosphäre und Ozean über zwei europäischen Hauptmeere kann nützlich sein, um hochaufgelöst SSTs vorherzusagen und zukünftige Klimabedingungen zu untersuchen.
- Ähnlich wie bei Medicanes, könnten die Auswirkungen verschiedener atmosphärischer Gitterauflösungen auf Vb-Zyklone untersucht werden.
- Abflussmodelle mit realistischer Abflusssimulation wurden in dieser Arbeit nicht berücksichtigt, sollten jedoch zukünftig zur Anwendung kommen. Simulationen einschließlich

Abflussmodelle können nützlich sein, um die oberflächennahen turbulenten Flüsse und den mediterranen Wasserkreislauf zu untersuchen.

- Gegenwärtig verwendet das gekoppelte Modell klimatologische Werte der Meeresoberflächenhöhe. Experimente mit realistischeren Jahreswerten der Meeresspiegelhöhe bringen wahrscheinlich einen Mehrwert im Hinblick auf die Untersuchung des mediterranen Wasserkreislaufs.

- Das vorgestellte gekoppelte Modell kann in Zukunft auch verwendet werden, um den Einfluss der Atmosphäre-Ozean-Wechselwirkung auf der konvektiven Skala zu untersuchen.